OPTIMAL TIRE FORCE ALLOCATION FOR AUTONOMOUS TRAJECTORY TRACKING

A DISSERTATION
SUBMITTED TO THE DEPARTMENT OF MECHANICAL ENGINEERING
AND THE COMMITTEE ON GRADUATE STUDIES
OF STANFORD UNIVERSITY
IN PARTIAL FULFILLMENT OF THE REQUIREMENTS
FOR THE DEGREE OF
DOCTOR OF PHILOSOPHY

Hyungchai Park
March 2017

I certify that I have read this dissertation and that, in my opinion, it is fully adequate in scope and quality as a dissertation for the degree of Doctor of Philosophy.

J Gerdes, Primary Adviser

I certify that I have read this dissertation and that, in my opinion, it is fully adequate in scope and quality as a dissertation for the degree of Doctor of Philosophy.

Paul Mitiguy

I certify that I have read this dissertation and that, in my opinion, it is fully adequate in scope and quality as a dissertation for the degree of Doctor of Philosophy.

Stephen Rock

Approved for the Stanford University Committee on Graduate Studies.

Patricia J. Gumport, Vice Provost for Graduate Education

This signature page was generated electronically upon submission of this dissertation in electronic format. An original signed hard copy of the signature page is on file in University Archives.

Abstract

The advent of a hydraulic modulator, which is the automotive part that can control brake pressure on the wheels individually, gives a vehicle an additional authority to control its yaw motion, and this additional control authority enables active safety systems like Electronic Stability Control (ESC). ESC has been proven to be effective in avoiding a large number of car crashes, but advances that can further reduce the number are underway: recent developments in actuator technology for steering, driving, and braking dramatically improve the performance of individual actuators and expand the boundary of vehicle control authority achieved by the coordinated actions of these actuators. This expanded control authority can serve as a physical base to enable many new vehicle control systems that will further improve automobile safety and performance than ESC.

This dissertation presents a method that utilizes expanded control authority for allocating tire forces optimally with a convex optimization formulation. If a vehicle has all three actuators (steering, driving, and braking) on all four wheels, each tire ideally can generate any force within the tire's maximum available friction capability through combined actions of these actuators. The basic objective of the optimal tire force allocation is to find a set of tire forces that keeps the usage of tire friction capability equal over the four wheels and minimizes that usage as much as possible. Achieving this objective has the advantage of preventing some tires from reaching saturation before other tires, thereby keeping the vehicle from sideway skidding or spinning out and enhancing automobile safety near the limits of handling.

However, actually implementing all three actuators at all four wheels is technically challenging and costly. If there are any limits on actuation for a wheel, the feasible

tire force region is restricted to a certain area in the entire area within the tire's maximum friction capability. To be practical, the formulation for the optimal tire force allocation has to handle the situation of limited actuation by finding a set of tire forces only within the feasible tire force regions. This dissertation shows that the boundary of the feasible tire force region can be approximated by an ellipse and circle for a wheel with steering and braking actuators. By simply taking these approximations as constraints, the formulation for the optimal tire force allocation gives a feasible set of tire forces for a given actuation layout.

Actual roads are not perfectly flat and usually have some non-zero degrees of bank and grade. Even under these conditions, operating a vehicle with the basic objective of the optimal tire force allocation—keeping the same and minimal friction usage over the four wheels—has the same advantage of preventing some tires' earlier saturation. To achieve this objective, this dissertation presents a revised formulation for the optimal tire force allocation that can handle the effects of non-zero bank angles and grades of the road on the vehicle's motion.

Experimental trajectory tracking demonstrates the advantages of the optimal tire force allocation, especially near the limits of handling.

Acknowledgements

I look back on the path I have taken on my journey to the PhD with great gratitude for all the people who have encouraged and supported me. I would like to take a moment to thank some of these people that made this dissertation possible.

First of all, I would like to thank my adviser, Chris Gerdes. If I had to express all the things that he has provided for me in only one word, the word would be "opportunity." He offered me the opportunity to join the Dynamic Design Lab (DDL), which is headed by him and has great resources, an impassioned atmosphere, and enthusiastic colleagues for research. He offered me the opportunity to explore the world of automotive research as much as I wished to by supporting me with research guidance, technical expertise, and encouragement. Being a student of his gave me many opportunities to personally talk with distinguished people in the automotive world. Thanks to all of these great opportunities, I have grown personally and intellectually.

I would like to thank my Reading Committee members, Stephen Rock and Paul Mitiguy. I took control and dynamics classes from them, respectively, and the knowledge I acquired from these classes has served as a solid base to formulate the ideas I explored in my research. Even though I had taken undergraduate control and dynamics courses that covered similar course materials, these professors provided fresh insights into these materials and helped me discover new perspectives on them. Stephen Rock and Paul Mitiguy were also members of my PhD qualifying examination committee, which means that they approved the start of my PhD work as well as its end.

I would like to thank the people who had a huge impact on my daily life at Stanford. The DDL is the institution to which I have belonged for more years than

any other institution, and the members of this lab are the people with whom I have spent most of my time in the United States. My years in the DDL were made great by their companionship. Also, they are great colleagues who are always ready to discuss automotive research together and willing to help each other. All of the research and social activities in the DDL have been supported by the wonderful administrators Erina, Adele, Jo, Elizabeth, and Jennifer, and the technical support of Godwin. I would also like to thank Evelin Sullivan of the School of Engineering's Technical Communication Program, who has given me feedback on every piece of academic writing I have done at Stanford.

As an international student, I sometimes long for home. Even though I cannot frequently go back to my home country, still I get great consolation from friends at Stanford who have the same cultural background: friends from the same high school and university, the members of the Korean Mechanical Engineer Group and the members of the Korean Swimming Club, Water Hyacinth. Thanks also goes to Samsung Foundation for financially supporting my PhD and providing networking opportunities with great students in a wide range of research areas.

Finally, I would like to thank my family. My parents and sisters have dedicated lots of their time and resources to my education. Thanks to their dedication, I always have taken the best educational opportunities and focused on what I want to achieve. In the path of my life journey, I was very fortunate to find my wife, Jihyun. Since we started our PhD studies in the same year, we have been on all of the journey to the PhD together. During this period, she has been my friend, love, adviser, and supporter. Now she is also the mother of our first daughter, Yunna. I am really looking forward to the rest of my life journey together with Jihyun and Yunna.

Contents

Abstract **iv**

Acknowledgements **vi**

1 Introduction **1**

1.1 Motivation 1

1.2 State of the art 3

1.2.1 Developments of actuating technology 4

1.2.2 Automotive control using over-actuation capability 6

1.3 Dissertation contributions and outline 11

2 Optimal Tire Force Allocation **15**

2.1 Controller architecture 15

2.2 Total demands for trajectory tracking 18

2.2.1 Vehicle and tracking error dynamics 19

2.2.2 Feedforward and feedback demands 22

2.2.3 Total demands in the vehicle-fixed coordinate frame 23

2.3 Optimal tire force allocation 23

2.3.1 Requirements for optimal tire forces 24

2.3.2 Weight transfer model 25

2.3.3 Finding minimum common friction usage 27

2.4 Actuator commands 28

2.4.1 Coupled brush tire model 30

2.4.2 Steering commands 31

2.4.3 Driving and braking commands 32
2.5 Experiments 32
2.5.1 Trajectory description 33
2.5.2 Tire force allocation by interpolation 35
2.5.3 Results 36

3 Handling Limited Actuation **39**
3.1 Feasible tire force region for limited actuation 40
3.1.1 Issues of simple constraints on general axle forces 41
3.1.2 Feasible tire force region 43
3.1.3 Considering the change of tire's velocity vector 48
3.2 Optimization formulation considering feasible tire force region 49
3.2.1 Calculating normal forces 50
3.2.2 Optimization formulation 51
3.2.3 Considering different friction usages between tires 52
3.3 Torque vectoring for the rear axle 53
3.4 Experiments 55
3.4.1 Trajectory description 56
3.4.2 Tire force allocation by interpolation 56
3.4.3 Results 58

4 Force Allocation on an Uneven Road **63**
4.1 Effects of driving on a non-level road 64
4.1.1 Components of the gravitational acceleration 65
4.1.2 Equations of longitudinal, lateral, and yaw motion 66
4.1.3 Equations of vertical, pitch and roll motion 67
4.1.4 Optimization formulation with topographical considerations . 69
4.2 Interpolation for optimal allocation on a three-dimensional road . . . 70
4.2.1 Vertical scaling factor 71
4.2.2 Similarity between optimized solutions 72
4.2.3 Interpolation using similarity 75
4.3 Experiments 78

4.3.1 Test site and trajectory descriptions 78
4.3.2 Handling total demands exceeding vehicle's friction capability 80
4.3.3 Results 82

5 Conclusion **88**
5.1 Future work 89
5.1.1 Solving the optimization problem in real time 90
5.1.2 Identifying each tire's friction limit in real time 90
5.2 Outlook 91

Bibliography **92**

List of Tables

2.1 X1's parameters 33

List of Figures

1.1 Vehicle's behaviors near the limits of handling: (a) Understeer and (b) Oversteer [14]. 4

2.1 Equivalent relationship between actuator command, tire forces, and resultant forces/moment 16
2.2 Overall controller structure 17
2.3 Planar vehicle diagram 19
2.4 Vehicle diagram on path 20
2.5 A slip angle and tire forces of a single tire 29
2.6 The X1 research vehicle 33
2.7 Test trajectory with two turns structured from straight lines (a and e), transition curves (b and d), and a constant radius curve (c) 34
2.8 Experimental results from X1 with the controller: (a) tracking errors, (b) friction usage, (c) longitudinal force demand, (d) lateral force demand, and (e) yaw moment demand 37

3.1 A problem of the simple constraint on general axle forces, $F_{\mathrm{x}} < 0$. (a) The optimized general axle force demands satisfy the constraint, but (b) the transformed tire forces are not in the region described by the constraint. 43
3.2 Tire forces as braking torque increases at the following fixed slip angles: (a) $\alpha = 0$, (b) $0 < \alpha < \alpha_{\mathrm{sl}}$, and (c) $\alpha = \alpha_{\mathrm{sl}}$. 45
3.3 Feasible tire force region for a wheel with steering and braking actuators. 46
3.4 Lateral tire force curve when $\kappa = 0$. 46

3.5 Comparison between the exact boundary calculated from the tire model and the ellipse-approximated boundary. 47
3.6 New feasible force region rotated by δ_0. 48
3.7 Test trajectory with a single turn structured from straight lines (a and e), transition curves (b and d), and a constant radius curve (c) 57
3.8 Tire force commands for the front left (up) and front right (down) tires. (a) From the force allocation with simple constraints. (b) From the force allocation with ellipse constraints. 59
3.9 Steering angle commands for the four tires. (a) From the force allocation with simple constraints. (b) From the force allocation with ellipse constraints. 60
3.10 Lateral, speed, and heading tracking errors. (a) From the force allocation with simple constraints. (b) From the force allocation with ellipse constraints. 61

4.1 The proportional relationship (i.e. similarity) between the optimal solutions to the proportional inputs 73
4.2 Interpolation for the optimal tire force allocation on a three-dimensional road by using the reference map when $w = 1$. 77
4.3 Test trajectory with a single turn structured from straight lines (a and e), transition curves (b and d), and a constant radius curve (c) 79
4.4 Scaling down general axle forces that exceed tire's estimated friction capability 81
4.5 Lateral, speed, and heading tracking errors from the force allocation without topographical considerations 82
4.6 Lateral, speed, and heading tracking errors. (a) From the force allocation without topographical considerations. (b) From the force allocation with topographical considerations. 84
4.7 Total force and moment demands from the two different force allocations, one without and one with topographical considerations. 85

4.8 Friction usages from the two different force allocations, one without and one with topographical considerations. (a) Front left tire. (b) Front right tire. (c) Rear left tire. (d) Rear right tire. 87

Chapter 1

Introduction

1.1 Motivation

Safety is one of the key values by which customers judge cars. To make cars safer, engineers and researchers have devoted extensive effort to the development of vehicle safety technologies. As a result, automotive manufacturers equip modern vehicles with many safety features: besides passive safety such as seat belts and air bags, active safety systems like Antilock Braking System (ABS) and Electronic Stability Control (ESC) [67], [34] have also been widely adopted in passenger vehicles. In addition, more advanced safety technologies, such as front-crash prevention, lane departure warning, park assist, etc., are being introduced to the market.

Several recent studies have shown ESC to be effective in avoiding car crashes. Starnes [60] stated in a NHTSA report that ESC saved an estimated 1,144 lives among passenger vehicle occupants in 2012. Sivinski [57] in another NHTSA report evaluated the effect of the installation of ESC on reducing single-vehicle crashes, finding that crashes of cars and SUVs were reduced by 32 percent and 57 percent, respectively. Wang [69] assessed the effectiveness of ESC on large trucks, and found that ESC could prevent 40 to 56 percent of rollovers and 14 percent of loss-of-control crashes. Owing to this effectiveness, ESC became a standard feature on 2012 and later models of cars, SUVs, pickups and minivans in the United States.

One of the key physical components of ESC is an hydraulic modulator, which can

control brake pressures on the wheels individually. Before the advent of the hydraulic modulator, the vehicle could only brake all wheels simultaneously according to the driver's pedal input, and the brake actuation in this way could not affect vehicle yaw motion. With the hydraulic modulator, however, ESC selectively brakes some wheels to control vehicle yaw motion and counteract sideways skidding and loss of control of the vehicle. From the viewpoint of overall vehicle actuation, implementing the hydraulic modulator gives the vehicle an additional degree of freedom for controlling the vehicle's yaw motion, and this additional actuating capability makes ESC possible.

However, current ESC systems cannot eliminate all fatal accidents. The referenced studies above show not only the effectiveness of ESC but also that there is still room for new active safety systems to further lower the fatal accident rates. Production ESC systems also have some technological limitations. The ESC systems rely on a small set of sensors that yield only limited vehicle state information to determine when they activate. In addition, the current working principle of ESC is designed to operate the hydraulic modulator as a main actuator and is difficult to extend to the situation in which the vehicle has additional available actuators other than the hydraulic actuator to correct the vehicle's yaw motion.

Recent advances in actuator technology promise to dramatically change the way in which individual actuators can be operated and coordinated. New drive systems with in-wheel or multiple driving motors will make true all-wheel drive possible, while current all-wheel drive systems split the power from a single source into four wheels. By adopting a powerful electro-hydraulic or electro-mechanical brake system and individual steering motors at each wheel, the vehicle can fully modulate braking torques and steering angles of all four wheels individually. Additionally, these new actuating systems are inherently associated with by-wire technology, which replaces direct mechanical linkages from driver's inputs to actuators with electro-mechanical control systems using human-machine interfaces. By-wire technology brings great flexibility in implementing new actuator control strategies to complement human driver's operations.

As these technologies are being applied to vehicles, they are gaining more actuating authority. This expanded actuating capability will serve as a physical base to enable

many new vehicle control systems that will further improve automobile safety and performance, as the capability to rapidly modulate brake pressures individually and therefore control the vehicle's yaw motion makes ABS and ESC possible.

However, implementing new, separate controllers for these additional actuators individually or in some combinations can result in actuator fighting, lack of transparency, and impairment of the overall vehicle performance. Therefore, an algorithm is required to operate all available actuators in an integrated fashion in order to achieve a specific vehicle-motion-control objective.

1.2 State of the art

The most popular actuating layout for passenger vehicles is front-wheel steering, front-wheel drive, and four-wheel brakes with a predefined brake-pressure proportion between the front and rear axles. These actuating capabilities are controlled by the following input devices: a steering wheel, gas pedal, and brake pedal. By operating these input devices and therefore regulating three actuating capabilities, the driver performs the basic functions of a vehicle for normal driving: cornering, accelerating, and stopping.

However, there are situations in which operating the vehicle with only these basic actuators is not enough for safe driving. For example, when the driver drives on an icy or wet road or executes an emergency maneuver, a slight mistake in controlling the actuators can lead to a fatal accident. Under these driving circumstances, the vehicle operates near the limits of handling, which means that the finite available traction between the vehicle's tires and road is almost completely utilized.

If the vehicle reaches this status while driving on a straight line, excessive acceleration or braking can cause some wheels to completely lose their grip on the road and can eventually make the vehicle impossible to accelerate or stop as intended. Once the vehicle reaches this limited traction situation while turning, there is a high probability that the vehicle shows either of the following behaviors depending on which tires reach full saturation first: the vehicle skids sideways if the front tires reach saturation first, while the vehicle loses control and spins out if the rear tires reach saturation

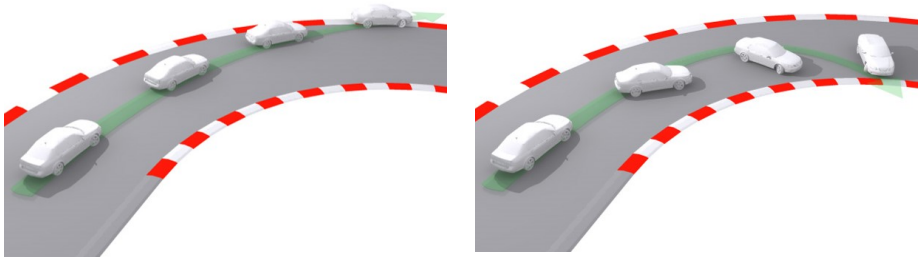

(a) (b)

Figure 1.1: Vehicle's behaviors near the limits of handling: (a) Understeer and (b) Oversteer [14].

first. These situations are referred to as understeer and oversteer, respectively, and shown in Figure 1.1.

Racecar or skillful drivers may recover from these adverse situations by carefully controlling only the given basic actuators, but average drivers are unlikely to handle these critical situations correctly. At the same situations, however, having more actuators on a vehicle can be greatly beneficial in preventing the vehicle from losing stability or controllability. Combining additional physical actuating capabilities with smart control strategies gives the vehicle the ability to manage the traction of the four wheels in a way that makes the vehicle safer. Several actuating technologies have been introduced to the market already, and control schemes utilizing these actuators are being actively investigated in both industry and academia.

1.2.1 Developments of actuating technology

Steering, driving, and braking are the three actuating capabilities that control traction of a tire for passenger vehicles. While steering and braking are easily associated with the corresponding actuator actions on a tire, driving is rather ambiguous. In the context of this dissertation, driving mainly indicates the actuator action that generate positive longitudinal force on a tire. There has been continual effort to apply these actuating capabilities to all four wheels. This section lists some of the existing technologies on the market and upcoming technologies under development for passenger cars.

For four-wheel drive, several car manufacturers have developed their own systems. Audi introduced a four-wheel drive system named "quattro" in 1980 [38, 4], and the system is well known for its operation mainly with mechanical components in some versions. Mercedes-Benz has developed "4Matic," which divides the engine torque between the front and rear axles using a computer-controlled traction system [37]. These systems and most other four-wheel drive systems on the market distribute the power from a single combustion engine to four wheels and have a limited range of the torque-split ratio. For hybrid or electric vehicles, the four-wheel-drive function can be achieved by implementing multiple driving actuators. Tesla offers the option of a dual-driving-motor configuration, which enables completely independent control over the driving torque on each axle [62]. A more progressive approach for four-wheel drive is also under development: in-wheel motors at four wheels. Protean Electric, one of the companies that develop an in-wheel electric drive system, demonstrated the actual application of its in-wheel motors on a standard passenger vehicle [20].

Four-wheel steering has also been explored by several car companies. Since Honda introduced the "Prelude" in 1987 with a mechanical four-wheel-steering system [56], the four-wheel-steering function has continued to be applied to some passenger car models. Recently, luxury sedans have widely adopted this function as part of the available options. For the current four-wheel-steering systems, however, front-wheel steering is still the major means of steering action while rear-wheel steering remains as an auxiliary means to support the front-wheel steering. Therefore, the range of the rear-steering angle is limited to just a few degrees. Acura's "Precision All-wheel Steer" employs a separate steering actuator for each wheel of the rear axle, which enables a car to steer the rear wheels independently [2].

As mentioned in Section 1.1, the hydraulic modulator on the brake system has become a standard component for passenger vehicles. Even with the hydraulic modulator, however, the major portion of brake pressure is still provided by the driver's pedal pressure most of the time. "Sensotronic Brake Control," which is an electro-hydraulic brake system developed by Bosch and Daimler [48, 31], has no direct hydraulic connection between the driver's pedal pressure and the actual brake pressure application. This system enables fully independent regulation of the hydraulic brake

pressure at each wheel. Brembo, a brake-solution provider, also announced its own brake-by-wire system, which could adopt an electro-mechanical brake for the rear wheels [71].

1.2.2 Automotive control using over-actuation capability

As steering, driving, and braking of each wheel are being independently actuated, vehicles are becoming over-actuated. This means that the number of available control inputs to influence the vehicle motion exceeds the number of vehicle states to be controlled. For example, a vehicle with independent four-wheel braking can regulate its longitudinal speed using only either the front brakes or the rear brakes.

In line with the trend of vehicles becoming over-actuated, considerable research effort has been devoted to the development of integrated chassis control systems that coordinate multiple actuators of different over-actuated configurations. The major objective of these control systems is to expand the margins of stability and enhance maneuverability of the vehicle to a level that conventionally actuated vehicles cannot achieve. More specifically, the controllers manipulate the dynamics of vehicle states closely related to stability and maneuverability by using an over-actuation capability. These controllers are grouped into two categories according to their choice of major control inputs: controllers in the first category allocate actuator commands, and controllers in the second category allocate tire forces.

Actuator command allocation

The formulation of the control systems in the first category starts with assigning control input variables specific to a given over-actuation layout. Some researchers adopt a control variable directly corresponding to each physical actuator command: for example, a torque variable is assigned to every driving motor or brake actuator [27]. Others replace the lumped effect from combined actions of some actuators with one control variable: for example, the effect of differential braking can be described by one variable that equals a yaw moment generated by differential braking [6]. The common benefit of these approaches is that the physical limits of actuators can be

easily taken into account by directly imposing constraints on control input variables. Once the control input variables are established, various control techniques can be applied to determine the values of these control inputs that are necessary to achieve a given control objective.

A number of control systems have been proposed for the control objective of regulating vehicle states in a desired way or within a stable region. Carlson and Gerdes [7] developed a model predictive control (MPC) scheme that coordinates active front steering and differential braking to track a driver's intent and prevent a vehicle rollover. They chose a front steering angle and four longitudinal tire forces generated by differential braking as their control inputs. For the same actuation layout, Di Cairano et al. [6] also adopted an MPC technique to design a controller that improves vehicle yaw stability. For their MPC formulation, they built a piecewise-affine vehicle dynamics model that has a front steering angle and a yaw moment from differential braking as control inputs. Nam et al. [43] designed a controller regulating body sideslip angle and yaw rate using a vehicle with active front steering and independent rear driving motors. Although they, too, adopted a front steering angle and a yaw moment from independent rear driving motors as control inputs, they used an adaptive feedforward-feedback controller structure to regulate the sideslip angle and yaw rate. Kang et al. [27] proposed a driving control algorithm that prevents rollover and improves vehicle maneuverability and lateral stability by coordinating independent front- and rear-drive motors and four-wheel independent braking modules. In this work, desired total longitudinal force and yaw moment at and around the center of gravity of the vehicle were calculated and then realized by two driving torque inputs from the front and rear axles and four braking torque inputs from the four wheels. De Novellis et al. [10] implemented a torque-vectoring controller for a four-wheel-drive vehicle to improve vehicle handling characteristics. Once total force and moment demands at and around the center of gravity of the vehicle were calculated to achieve a set of reference understeer characteristics, the optimal allocation of longitudinal tire forces was determined after the performance of different optimization objective functions were compared.

Another control objective that can benefit from the over-actuation capability is

trajectory tracking. For conventionally actuated vehicles, the number of tracking errors that can be regulated is reduced to the number of available actuators by ignoring one of the tracking errors or adopting a new variable that lumps together some tracking-error terms [22]. Over-actuated vehicles, in contrast, can utilize their expanded control authority to regulate more tracking errors individually. Falcone et al. [13] used MPC to optimize multiple actuator inputs, a front steering angle and longitudinal tire slips of the four wheels, and thereby achieved high performance in tracking reference path, heading, and speed profiles.

Tire force allocation

The control systems in the second category specifically focus on allocation of tire forces among the four wheels. Because handling and stability of a vehicle are directly dictated by tire forces and their saturation [16, 46], explicitly handling tire forces in automotive control system design is greatly beneficial to anticipate and prevent undesirable situations—for example, understeer and oversteer—especially at the limits of handling.

The basic assumption in this category is that having all three actuators for steering, driving, and braking enables a tire to deploy any set of tire forces within its friction or actuators' physical limits [46]. As a result, approaches in this category adopt longitudinal and lateral tire forces of the wheels as major control input variables, while the control systems in the first category directly relate control objectives to physical actuator commands specific to a given actuation layout. If the vehicle is equipped with active suspension, normal tire forces can also be regarded as controllable variables. This expanded capability for the deployment of tire forces enables an over-actuated vehicle to allocate tire forces among the four wheels in ways that a vehicle with a conventional actuation layout cannot achieve.

Most approaches in the tire force allocation category start by calculating total force and yaw moment at and around the center of gravity of a vehicle that regulate planar motion of the vehicle to achieve any given vehicle control objective. Once these total demands are calculated, the optimal set of individual tire forces achieving the total demands are obtained by solving an optimization problem that minimizes

a specific cost function in terms of tire forces. To parameterize the level of tire force saturation, the friction usage of each tire is defined as the ratio of actual tire force usage to maximum available friction capability and therefore frequently used in cost function expressions.

A number of cost functions have been proposed to achieve desired characteristics of tire force allocation. Mokhiamar and Abe [41, 1] took a weighted sum of each tire's friction usage as their cost function. The authors investigated how different sets of weighting coefficients affect vehicle handling performance [42]. While Kim et al. [29] adopted the same cost function, they applied an optimal tire force allocation method to control a six-wheel-drive and six-wheel-steer vehicle. Suzuki et al. [64] suggested two cost functions: one is identical to Mokhiama and Abe's cost function; the other is a sum of each tire's energy dissipation. Roshanbin and Naraghi [51], Naraghi et al. [44] and Tavasoli et al. [65] proposed a cost function that consists of two terms: the first term is a sum of each tire's friction usage; the second is a sum of each tire's longitudinal tire force usage. By adjusting the relative weight between the two terms according to the tires' friction usage levels, the contribution of longitudinal tire forces toward total demands is changed. The purpose of this cost function is to suppress excessive use of longitudinal tire forces at a low friction usage level because changes in longitudinal acceleration can be uncomfortable for passengers.

The optimization problems of these approaches adopt cost functions with only squared tire force terms and linear equality constraints that relate total demands and individual tire forces. Therefore, the optimization can be formulated as a convex optimization problem. There exist variations of this formulation. Song et al. [59] adopted additional linear inequality constraints that approximate the tires' friction circles by simplifying them with octagons. Instead of using the equality constraints, Wang et al. [70] and Li et al. [33] added to the cost function—which is the sum of each tire's friction usage—a term that represents the difference between the total force and moment that are demanded and those that are realized by tire forces. Then the optimization becomes an unconstrained convex optimization problem.

A few approaches have focused on balanced distribution of tire forces among the wheels because minimizing the total sum does not guarantee that some tires

do not reach saturation before other tires do. This consideration for saturation of individual tires becomes important as a car approaches the limits of handling. Ono et al. [45] developed a special optimization formulation with the assumption that the four wheels have equal friction usage. With this formulation, an optimized set of tire forces naturally resulted in equal friction usage over the four wheels. Peng et al. [49] proposed a cost function intended to achieve the same objective—equal friction usage over the four wheels—and explicitly adopted friction circles of the four tires as quadratic inequality constraints. Luo et al. [35] and Dai et al. [9] employed a cost function that is a weighted sum of the variance and mean of the tires' friction usages, which also tries to achieve equal friction usage over the four wheels.

These approaches can achieve equal friction usage over the four wheels and therefore help to enhance vehicle stability especially near the limits of handling, but they require special optimization solving techniques to treat the non-convexity of their cost functions. Therefore, the optimization in the approaches for balanced tire force allocation lacks two major benefits of a convex optimization formulation: a guarantee that any local minimum found is a global minimum, and existing tools that can solve a convex optimization problem efficiently for real-time automotive control applications.

These two properties become essential when optimization-based control is applied to the operation of a vehicle near the limits of handling, which is often tied to imminent emergency situations. If the convergence to a global minimum is not guaranteed, the optimization solver can generate quite different sets of control inputs to closely spaced sets of optimization parameters. This difference will cause large fluctuation in actuator commands between adjacent time steps and therefore can result in undesirable vehicle behaviors. Also, in a real emergency, the optimization must be calculable in real-time. Otherwise, the vehicle could be too late responding to a threat.

Most of the approaches above presuppose that the vehicle has steering, driving, and braking actuators, in some cases including active suspension, at all four wheels. However, because actually implementing all these actuators at all four wheels is technically challenging and costly, it is necessary to consider situations in which the vehicle remains over-actuated even though some of the actuators are not implemented. Roshanbin and Naraghi [51], Naraghi et al. [44], and Tavasoli et al. [65] assumed that

their controllers do not utilize a driving capability. To impose this physical limit on their optimization formulations, they adopted linear inequality constraints that limit positive longitudinal tire forces of the four wheels by assuming a simplified relationship between actuator actions and resulting tire forces. Andreasson [3] and Jonasson et al. [25] analyzed a number of differently actuated vehicles and presented key findings on how tire forces are generated with each actuation layout when steering angles are given.

1.3 Dissertation contributions and outline

This dissertation presents a controller that aims to optimally allocate tire forces over all four wheels for an over-actuated vehicle. The basic objective of this optimal allocation is to keep the usage of total tire friction capability equal over the four wheels. By achieving this objective, the controller can prevent some tires from reaching saturation before other tires, which can prohibit understeer and oversteer. While the optimal tire force allocation can be combined with any high-level vehicle motion control objective, the task of trajectory tracking near the limits of handling is chosen as the high-level objective in order to operate a vehicle near the limits constantly and show the performance of the optimal tire force allocation in this operating regime. Also, tracking a trajectory near the limits itself is one of the important vehicle control objectives as some of approaches for executing emergency maneuver has focused on developing trajectory tracking controllers [52, 58, 66, 28].

The three key contributions of this dissertation are presented below, each contribution corresponding to one chapter.

Chapter 2, Optimal Force Allocation for Trajectory Tracking:
Formulating a tire force allocation algorithm as a convex optimization problem

The objective of the controller is to utilize the over-actuation capability for allocating tire forces optimally while tracking a desired trajectory on a flat road. Chapter 2 presents how the controller is designed to achieve this objective.

The controller is structured hierarchically to treat the trajectory tracking problem and the optimal tire force allocation problem separately. The trajectory tracking problem is handled by a feedforward-feedback control technique to calculate the total force and moment demands at and about the center of gravity of the vehicle that are required to make the vehicle follow a given trajectory.

For the optimal tire force allocation problem, the objective is to keep the usage of tire friction capability equal over the four wheels and minimize that usage as much as possible. Based on the assumption that a vehicle is over-actuated and has full control of all three actuators (steering, driving, and braking) at all four wheels, 12 actuators in total, an algorithm is formulated as a convex optimization problem. In contrast, other allocation algorithms for the same allocation objective in the literature are often formulated as a non-convex optimization problem.

Experimental results demonstrate the controller's tracking performance for a trajectory that demands using up to 90% of the vehicle's maximum friction capability. In the experiment, solving the convex optimization problem was replaced by interpolation using a map, which relates a set of discrete total demands to the corresponding tire forces by solving the optimization off-line. Though this replacement does not take one of the benefits of a convex optimization formulation, which is to be suitable for real-time implementation, the other benefit of the convergence to a global minimum guarantees the strict one-to-one relationship between total demands and tire forces.

Chapter 3, Handling Limited Actuation:
Identifying feasible tire force regions for a limited-actuation layout
Developing constraints to express these regions in the allocation algorithm

The allocation algorithm in Chapter 2 assumes that each wheel of a vehicle has all three actuators (steering, driving, and braking), and that the feasible force region of the wheel is the entire area within the tire's friction limit. If a wheel lacks one of the three actuators for practical reasons, however, the feasible tire force region of the wheel is restricted to a certain range.

Chapter 3 explains how to handle this situation by using the allocation algorithm

in Chapter 2 with slight modifications. The first necessary modification is to add new constraints that can describe the feasible tire force regions for a given limited-actuation layout. By making some reasonable assumptions, these new constraints can be expressed in a concave form with measurable parameters alone. As a result, the allocation algorithm with the new constraints for feasible tire force regions keeps the form of a convex optimization formulation.

With the limited actuation, a new situation can occur in which it is no longer possible to achieve the original force allocation objective, which was to keep the usage of tire friction capability equal over the four wheels. In this situation, some tires have to use more of their friction capability than others to compensate for the restricted tire force generation of those other tires due to the limited actuation. The second necessary modification is to implement an additional algorithm that handles different friction usages.

The new allocation algorithm with the modifications above results in a feasible set of tire forces that can be generated by the given limited-actuation layout. Experimental results validate that the controller achieves this goal while tracking a trajectory.

Chapter 4, Force Allocation on a Road with Changing Geometry: **Integrating the effects of driving on an uneven road into the allocation algorithm**

A vehicle is assumed to drive on a level road in Chapter 2 and Chapter 3. All of the approaches to optimal tire force allocation in Section 1.2.2 also assume a level motion of the vehicle. However, actual roads are not perfectly flat and usually involve non-zero bank angles and grades. Because these road geometry components can greatly affect the vehicle's motion [61, 68, 32], the optimal tire force allocation also needs to take into account the effects of driving on a road with changing geometry.

Driving on these uneven roads particularly affects the vehicle's motion in the following two ways: the arrangement of the vehicle frame is changing with respect to the direction of the gravitational force, and the normal force distribution becomes different from that on a flat road.

Even with these changes, the objectives of the optimal force allocation in Chapter 2

and Chapter 3 are still valid for preventing the vehicle from encountering understeer or oversteer near the limits of handling. Chapter 4 describes how to take the effects of non-zero bank angles and grades of the road into account using the existing structure of the optimal force allocation algorithm. After an analysis of what changes happen to the normal force distribution when the vehicle is driving on a three-dimensional road, those changes are modeled in a form that can be incorporated into the allocation formulation.

Actual driving on an uneven road with these two different algorithms demonstrates that force allocation that considers non-zero bank and grade of the road exhibits better tracking performance than force allocation assuming a level motion.

Chapter 2

Optimal Tire Force Allocation

In this chapter, it is assumed that a vehicle is over-actuated and has full control of all three actuators (steering, driving, and braking) over four wheels, 12 actuators in total. Based on this assumption, a controller utilizes this over-actuating capability for allocating tire forces optimally while tracking a desired trajectory on a flat road. The basic objective of this optimal allocation is to keep the usage of tire friction capability equal over the four wheels and minimize that usage as much as possible. Achieving this goal has the advantage of preventing some tires from reaching saturation before other tires. An algorithm for the optimal tire force allocation is formulated as a convex optimization problem and combined with trajectory tracking to follow the desired speed, heading, and lateral position of a vehicle.

2.1 Controller architecture

As assumed in Chapter 1, combined actions of three actuators (steering, driving and braking) can generate any tire force within the friction limit. In other words, for a given tire force, there is always a matching set of actuator commands. This premise enables tire forces instead of actuator commands to be used as variables for analysis. Moreover, if the vehicle is assumed to be a rigid body, the tire forces of the four wheels can be replaced by total force and total yaw moment applied at and around the center of gravity of the vehicle. Then the motion of the vehicle and the trajectory tracking

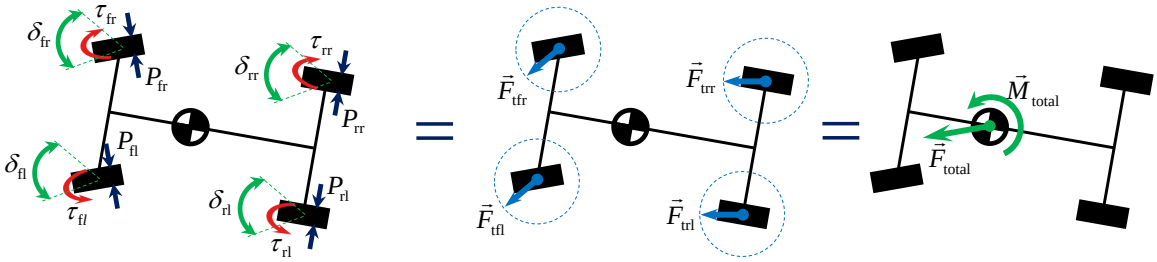

Figure 2.1: Equivalent relationship between actuator command, tire forces, and resultant forces/moment

problem can be analyzed with these resultant total force and moment instead of with the individual tire forces.

Figure 2.1 shows this equivalence between the actuator commands, the tire forces, and the total force and moment at and about the center of gravity of the vehicle. δ_{i}, τ_{i} and P_{i} are the steering angle, driving torque, and brake pressure at each wheel, respectively ($\mathrm{i} \in [\mathrm{fl}, \mathrm{fr}, \mathrm{rl}, \mathrm{rr}]$, where fl, fr, rl, and rr refer to the front left, front right, rear left, and rear right wheel, respectively). These terms are defined in Section 2.4. $\vec{F}_{\mathrm{ti}}$ is the tire force at each wheel while the dotted circle represents the friction limit, and $\vec{F}_{\mathrm{total}}$ and $\vec{M}_{\mathrm{total}}$ are the total force and moment at and about the center of gravity of the vehicle.

The goal of the controller is to calculate physical actuator commands of the four wheels (steering angles, driving torques, and brake pressures) that achieve the two control objectives of tracking a trajectory and optimally allocating tire forces concurrently. Owing to the equivalence shown in Figure 2.1, the controller can be structured to treat trajectory tracking, optimal tire force allocation and actuator command calculation separately in the order shown in Figure 2.2.

This separation has two major advantages. The first is the lack of the need to linearize system dynamics for a controller formulation. There is a non-linear relationship between physical actuator commands and the corresponding tire force generated from those actuator actions. To incorporate actuator commands as control variables directly into the controller formulation, one usually has to linearize the non-linear

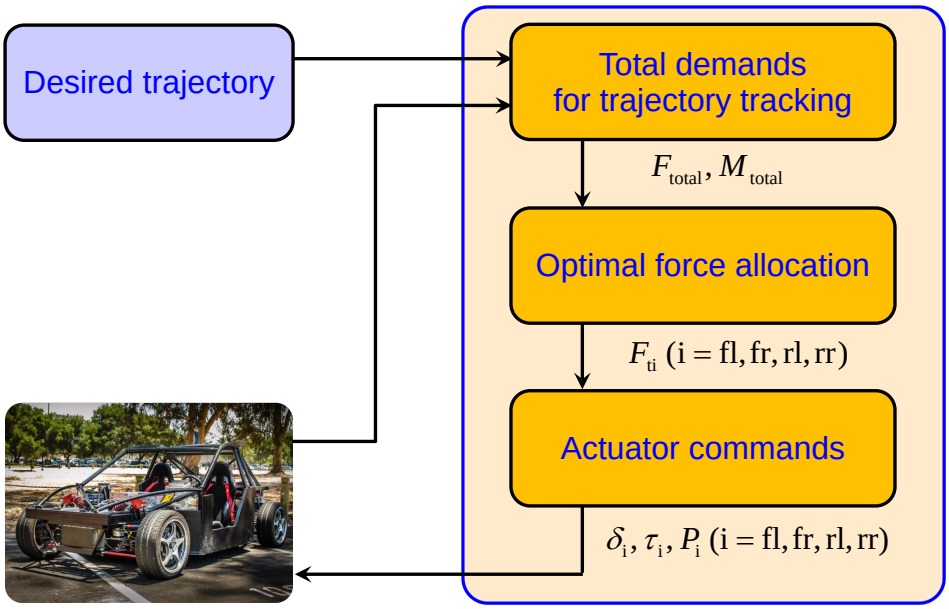

Figure 2.2: Overall controller structure

relationship, which can result in the loss of some of the characteristics of the relationship. By assigning tire forces as control variables and calculating actuator commands from those forces later, however, it is not necessary to adopt any linearization in the controller formulation.

The second advantage is that each part of the controller can behave like a module and be replaced by another module to handle different situations and control objectives. By making trajectory tracking independent of tire force allocation, the trajectory tracking module can be generically applied to any actuating configurations of the vehicle because the difference in actuating configuration can be handled by merely adopting a different tire force allocation module without changing the trajectory tracking module and the entire controller architecture. Therefore, it becomes easy to treat different actuator layouts with one controller structure. In turn, the tire force allocation module can be combined with different total demand calculation modules that adopt other control objectives or control techniques. Harkegard and Glad [21] and Johanssen and Fossen [23] listed additional advantages of this type of separation for over-actuated nonlinear systems.

The rest of this chapter describes each part of the controller in detail. Section 2.2 explains how to calculate the total force and moment demands at and about the center of gravity of the vehicle that are required to make the vehicle follow a given trajectory. After interpreting the information of the given trajectory as desired vehicle states, the controller calculates the feedforward portion of the total demands from the desired vehicle states while minimizing tracking errors by applying the feedback portion of the total demands. Section 2.3 describes how to distribute these total demands to individual tire forces optimally. The goal of the optimal allocation is to achieve equal friction usage among the four wheels while minimizing that friction usage. The algorithm to achieve this goal is formulated with an intuitive convex optimization problem. Section 2.4 shows the conversion from the optimized tire forces to actuator commands through a coupled tire force model. Section 2.5 presents experimental results demonstrating the controller's tracking performance for a trajectory that demands using up to 90% of the vehicle's maximum friction capability.

2.2 Total demands for trajectory tracking

This section explains how to calculate total force and moment demands at and about the center of gravity of the vehicle that are necessary for tracking a desired trajectory on a flat road. The equations for vehicle and tracking error dynamics are derived. Based on the analysis of these dynamics, the total force and moment demands are calculated by dividing them into two components: a feedforward part and a feedback part.

The feedforward force and moment demands are calculated with the assumption that a vehicle exactly follows the desired trajectory. The information of the desired trajectory is converted into the desired translational and yaw accelerations of the vehicle, and multiplying these accelerations by the vehicle's mass and inertia produces the feedforward force and moment demands, respectively. But in real situations, applying only the feedforward demands cannot ensure that the vehicle will follow the profiles of the given trajectory due to external disturbances, modeling errors, etc. To correct the vehicle's departure from the trajectory, the feedback force and moment

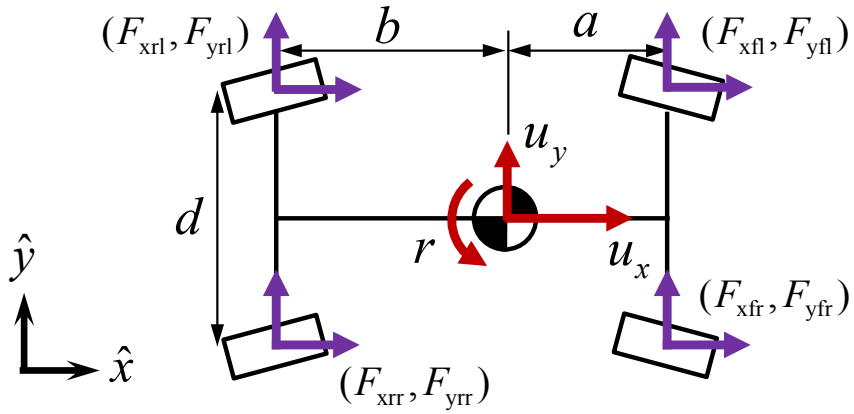

Figure 2.3: Planar vehicle diagram

demands are calculated with the purpose of minimizing lateral departure from the desired path and deviations from the desired speed and heading profiles.

2.2.1 Vehicle and tracking error dynamics

In order to describe the vehicle dynamics, a planar four-wheel vehicle model with three states is adopted. The three states are the vehicle's longitudinal speed u_{x}, lateral speed u_{y}, and yaw rate r, and these variables are referenced to the vehicle-fixed coordinate frame in which the axes $\hat{x}$ and $\hat{z}$ lie along the forward longitudinal direction of the vehicle and the upward nomal direction to the ground, respectively, as shown in Figure 2.3.

In Figure 2.3, a force generated at each wheel are replaced by the equivalent set of longitudinal and lateral forces at each wheel F_{xi} and F_{yi} ($\mathrm{i} \in [\mathrm{fl}, \mathrm{fr}, \mathrm{rl}, \mathrm{rr}]$) along the x and y axes of the vehicle-fixed coordinate frame. For the rest of this dissertation, these forces are referred to as the general axle forces. This replacement is useful in formulating a force allocation algorithm in the following section without having advance knowledge of the directions of wheel heading.

The sum of the general axle forces and the yaw moment by these forces about the center of gravity can be replaced by the longitudinal and lateral resultants and

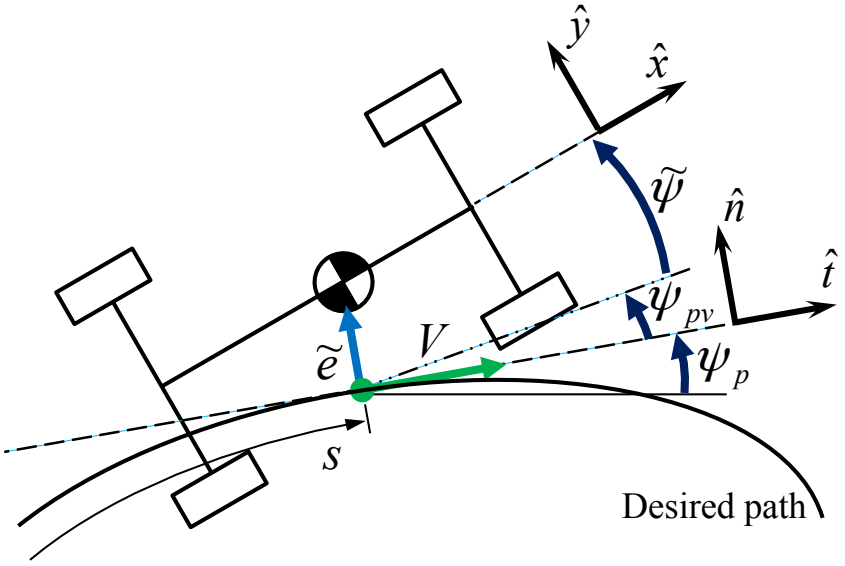

Figure 2.4: Vehicle diagram on path

moment at and about the center of gravity $F_{\mathrm{x,total}}$, $F_{\mathrm{y,total}}$, and $M_{\mathrm{z,total}}$:

$$\begin{aligned} F_{\mathrm{x,total}} &= F_{\mathrm{xfl}} + F_{\mathrm{xfr}} + F_{\mathrm{xrl}} + F_{\mathrm{xrr}} \\ F_{\mathrm{y,total}} &= F_{\mathrm{yfl}} + F_{\mathrm{yfr}} + F_{\mathrm{yrl}} + F_{\mathrm{yrr}} \\ M_{\mathrm{z,total}} &= a(F_{\mathrm{yfl}} + F_{\mathrm{yfr}}) - b(F_{\mathrm{yrl}} + F_{\mathrm{yrr}}) \\ &\quad + d/2(F_{\mathrm{xfr}} + F_{\mathrm{xrr}}) - d/2(F_{\mathrm{xfl}} + F_{\mathrm{xrl}}). \end{aligned} \tag{2.1}$$

where a and b are the distances from the vehicle's center of gravity to the front and rear axles, respectively, and d is the track width, as shown in Figure 2.3.

With these parameters, the equations of motion are as follows:

$$\begin{aligned} ma_{\mathrm{x}} &= m(\dot{u}_{\mathrm{x}} - ru_{\mathrm{y}}) = F_{\mathrm{x,total}} \\ ma_{\mathrm{y}} &= m(\dot{u}_{\mathrm{y}} + ru_{\mathrm{x}}) = F_{\mathrm{y,total}} \\ I_z\dot{r} &= M_{\mathrm{z,total}}. \end{aligned} \tag{2.2}$$

where m and I_z are the mass and the yaw inertia, respectively; and a_{x} and a_{y} are the vehicle's longitudinal and lateral accelerations at the center of gravity, respectively.

In this dissertation, a desired trajectory is described by its geometric path, a speed

profile tangent to the path, and a heading profile of the vehicle relative to the tangent of the path. Defining these elements of the trajectory gives the heading of the path ψ_{p}, the desired speed of the vehicle tangent to the path V, and the desired heading of the vehicle relative to the heading of the path ψ_{pv} at a specific point on the desired path, as depicted in Figure 2.4. These terms are defined as functions of the path length s.

Figure 2.4 also shows the situation in which the vehicle deviates from the desired trajectory. The departure from the trajectory is defined by the differences between the desired trajectory and the actual vehicle states and is quantified as three scalar terms for lateral, speed, and heading tracking errors. These errors are referenced to an instantaneous coordinate frame in which the axis $\hat{t}$ lies along the tangent of the path at the minimum distance point from the vehicle's center of gravity. The axis $\hat{n}$ is the dot product of $\hat{z}$ and $\hat{t}$. The lateral error $\tilde{e}$ is that minimum distance between the desired path and the vehicle's center of gravity. The speed error $\tilde{V}$ is the difference between the desired speed at the minimum distance point and the vehicle's actual speed along the direction parallel to the tangent of the path. The heading error $\tilde{\psi}$ is the difference between the desired heading of the vehicle at the minimum distance point and the vehicle's actual heading. According to these definitions, the derivatives of the lateral error $\dot{\tilde{e}}$, $\tilde{V}$, and $\tilde{\psi}$ are as follows:

$$\begin{aligned}
\dot{\tilde{e}} &= u_{\mathrm{x}} \sin(\tilde{\psi} + \psi_{\mathrm{pv}}) + u_{\mathrm{y}} \cos(\tilde{\psi} + \psi_{\mathrm{pv}}) \\
\tilde{V} &= [u_{\mathrm{x}} \cos(\tilde{\psi} + \psi_{\mathrm{pv}}) - u_{\mathrm{y}} \sin(\tilde{\psi} + \psi_{\mathrm{pv}})] - V \\
\tilde{\psi} &= \psi_{\mathrm{act}} - \psi_{\mathrm{des}} = \psi_{\mathrm{act}} - (\psi_{\mathrm{p}} + \psi_{\mathrm{pv}})
\end{aligned} \tag{2.3}$$

where ψ_{act} and ψ_{des} are the vehicle's actual and desired heading angles, respectively.

The vehicle's actual states can be described by the tracking errors and the desired trajectory descriptions by reformulating (2.3):

$$\begin{aligned}
u_{\mathrm{x}} &= (\tilde{V} + V) \cos(\tilde{\psi} + \psi_{\mathrm{pv}}) + \dot{\tilde{e}} \sin(\tilde{\psi} + \psi_{\mathrm{pv}}) \\
u_{\mathrm{y}} &= -(\tilde{V} + V) \sin(\tilde{\psi} + \psi_{\mathrm{pv}}) + \dot{\tilde{e}} \cos(\tilde{\psi} + \psi_{\mathrm{pv}}) \\
r &= \dot{\psi}_{\mathrm{act}} = \dot{\tilde{\psi}} + \dot{\psi}_{\mathrm{p}} + \dot{\psi}_{\mathrm{pv}}.
\end{aligned} \tag{2.4}$$

Because the tracking errors are referenced to the instantaneous coordinate frame normal and tangential to the path, transforming the total forces $F_{\mathrm{x,total}}$ and $F_{\mathrm{y,total}}$ in (2.2) into forces in this frame $F_{\mathrm{t,total}}$ and $F_{\mathrm{n,total}}$ is beneficial for tracking error analysis. The transformation is performed by multiplying $F_{\mathrm{x,total}}$ and $F_{\mathrm{y,total}}$ by the rotation matrix that relates $(\hat{x}, \hat{y})$ to $(\hat{x}, \hat{y})$ as follows:

$$\begin{bmatrix} F_{\mathrm{t,total}} \\ F_{\mathrm{n,total}} \end{bmatrix} = \begin{bmatrix} \cos(\tilde{\psi} + \psi_{\mathrm{pv}}) & \sin(\tilde{\psi} + \psi_{\mathrm{pv}}) \\ -\sin(\tilde{\psi} + \psi_{\mathrm{pv}}) & \cos(\tilde{\psi} + \psi_{\mathrm{pv}}) \end{bmatrix} \begin{bmatrix} F_{\mathrm{x,total}} \\ F_{\mathrm{y,total}} \end{bmatrix}. \tag{2.5}$$

Substituting the vehicle states and the total forces in (2.2) for the expressions in (2.4) and (2.5) yields the equations of tracking error dynamics as follows:

$$\begin{aligned} m\dot{\tilde{V}} &= -m\dot{V} + m\dot{\tilde{e}}\dot{\psi}_{\mathrm{p}} + F_{\mathrm{t,total}} \\ m\ddot{\tilde{e}} &= -mV\dot{\psi}_{\mathrm{p}} - m\tilde{V}\dot{\psi}_{\mathrm{p}} + F_{\mathrm{n,total}} \\ I_{\mathrm{z}}\ddot{\tilde{\psi}} &= -I_{\mathrm{z}}(\ddot{\psi}_{\mathrm{p}} + \ddot{\psi}_{\mathrm{pv}}) + M_{\mathrm{z,total}}. \end{aligned} \tag{2.6}$$

2.2.2 Feedforward and feedback demands

$F_{\mathrm{t,total}}$, $F_{\mathrm{n,total}}$, and $M_{\mathrm{z,total}}$ in (2.6) become the total demands to control the tracking errors, and the total demands are separated into feedforward and feedback force and moment demands. The feedforward force and moment demands are calculated with the assumption that the vehicle exactly follows the desired trajectory. In other words, when all tracking error terms and their derivatives in (2.6) are set to zero, the remaining terms correspond to the feedforward demands:

$$\begin{aligned} F_{\mathrm{t,feedforward}} &= m\dot{V} \\ F_{\mathrm{n,feedforward}} &= mV\dot{\psi}_{\mathrm{p}} \\ M_{\mathrm{z,feedforward}} &= I_{\mathrm{z}}(\ddot{\psi}_{\mathrm{p}} + \ddot{\psi}_{\mathrm{pv}}). \end{aligned} \tag{2.7}$$

The feedback force and moment demands are calculated with the purpose of mitigating the tracking errors. Any control schemes that achieve this purpose can be applied. In this dissertation, proportional and proportional-derivative controls are

used after compensating for the remaining nonlinear terms in (2.6) that are not included in the feedforward demands. The resulting equations are:

$$\begin{aligned} F_{\mathrm{t,feedback}} &= -m\dot{\tilde{e}}\dot{\psi}_{\mathrm{p}} - K_{\mathrm{speed}}\tilde{V} \\ F_{\mathrm{n,feedback}} &= m\tilde{V}\dot{\psi}_{\mathrm{p}} - K_{\mathrm{d,lateral}}\dot{\tilde{e}} - K_{\mathrm{p,lateral}}\tilde{e} \\ M_{\mathrm{z,feedback}} &= -K_{\mathrm{d,heading}}\dot{\tilde{\psi}} - K_{\mathrm{p,heading}}\tilde{\psi}. \end{aligned} \tag{2.8}$$

2.2.3 Total demands in the vehicle-fixed coordinate frame

Adding the feedforward and feedback demands in (2.7) and (2.8) results in the total demands $F_{\mathrm{t,total}}$, $F_{\mathrm{n,total}}$, and $M_{\mathrm{z,total}}$ in the instantaneous coordinate frame that is normal and tangential to the path. Among these demands, the total force demands $F_{\mathrm{t,total}}$ and $F_{\mathrm{n,total}}$ are transformed back to the total force demands $F_{\mathrm{x,total}}$ and $F_{\mathrm{y,total}}$ in the vehicle-fixed coordinate frame by inverting the relationship in (2.5). In addition to this transformation, a drag compensation force F_{drag} is added to $F_{\mathrm{x,total}}$ to offset rolling resistance, aerodynamic force, etc. The total force demands in the vehicle-fixed coordinate frame are as follows:

$$\begin{aligned} F_{\mathrm{x,total}} &= F_{\mathrm{t,total}}\cos(\tilde{\psi} + \psi_{\mathrm{pv}}) + F_{\mathrm{n,total}}\sin(\tilde{\psi} + \psi_{\mathrm{pv}}) + F_{\mathrm{drag}} \\ F_{\mathrm{y,total}} &= -F_{\mathrm{t,total}}\sin(\tilde{\psi} + \psi_{\mathrm{pv}}) + F_{\mathrm{n,total}}\cos(\tilde{\psi} + \psi_{\mathrm{pv}}). \end{aligned} \tag{2.9}$$

2.3 Optimal tire force allocation

This section presents the algorithm for allocating the total force and moment demands $F_{\mathrm{x,total}}$, $F_{\mathrm{y,total}}$, and $M_{\mathrm{z,total}}$ to general axle forces at each wheel. If the four wheels with all three actuators (steering, driving, and braking) can achieve any force within the friction limit at each tire as assumed in Chapter 1, F_{xi} and F_{yi} ($\mathrm{i} \in [\mathrm{fl}, \mathrm{fr}, \mathrm{rl}, \mathrm{rr}]$) in (2.1) become eight independent control variables.

Because the number of variables exceeds the number of equations in (2.1), an optimization technique is adopted to determine a unique set of general axle forces at the tires among multiple solutions. The criterion for the optimal set of general axle forces is to achieve equal friction usage among the four wheels and minimize the usage

of available friction as much as possible. To find the optimal solution that satisfies this criterion, the algorithm is formulated as quasiconvex optimization with a convex feasibility problem. In this way, the resulting formulation avoids using a complex non-convex cost function that is able to achieve the same criterion but makes the entire formulation non-convex. Because the friction capability of each tire is directly determined by its normal force, the optimization formulation also takes into account the effect of weight transfer on the normal forces.

2.3.1 Requirements for optimal tire forces

When a conventionally actuated vehicle tracks a trajectory near the limits of handling, some tires reach saturation while others are not saturated and retain available friction capability. This results in understeer or oversteer. If an over-actuated vehicle can allocate tire forces in a way that prevents some of the tires from using their friction capability more than the other tires do while minimizing the usage of available friction, the over-actuated vehicle can successfully track the same trajectory without saturating any tires. Furthermore, there is room to push the vehicle closer to the limits of handling because all four tires retain some available friction.

The friction usage of each wheel is defined as the ratio of actual tire force usage to maximum available friction capability. This quantity is described by the variable k_{i} ($\mathrm{i} \in [\mathrm{fl}, \mathrm{fr}, \mathrm{rl}, \mathrm{rr}]$) for each tire, and the value of k_{i} exists only within a certain interval as follows:

$$k_{\mathrm{i}} = \frac{\sqrt{{F_{\mathrm{xi}}}^2 + {F_{\mathrm{yi}}}^2}}{\mu F_{\mathrm{zi}}}, \quad 0 \leq k_{\mathrm{i}} \leq 1 \tag{2.10}$$

where μ is the effective friction coefficient and F_{zi} is the normal force of each tire. The minimum magnitude of tire force is zero when no force is utilized while the maximum is μF_{zi} because the tire cannot generate more force than its friction capability. Therefore, k_{i} exists only within [0,1].

For a given set of total force and moment demands, different solutions to (2.1) result in different combinations of the friction usage over the four wheels. The optimal approach for preventing some tires from saturating earlier than others is to keep the

friction usages of the four tires equal or, in other words, to make the four tires have a common friction usage value. At the same time, minimizing the usage of available friction can be achieved by keeping the common friction usage as low as possible. Therefore, the above explanation of the requirements for a set of optimal tire forces is mathematically described as having the minimum common friction usage, $k_{\min}$, over the four wheels.

2.3.2 Weight transfer model

When a vehicle is highly accelerated and operates near the limits of handling, it experiences significant weight transfer, and the weight transfer directly affects the normal forces of the tires. Because the normal force term is included in (2.10), it is important to consider the effect of the weight transfer on the normal forces for the accurate friction usage calculation.

Several analytic models have been proposed to quantify weight transfer [5, 54, 55, 11]. In this dissertation, a model assuming a quasi-static independent weight transfer along the longitudinal and lateral directions is adopted.

If the total force demands $F_{\mathrm{x,total}}$ and $F_{\mathrm{y,total}}$ are assumed to be fully and instantaneously realized by tire forces, the longitudinal and lateral accelerations a_{x} and a_{y} of the vehicle can be calculated as follows:

$$\begin{aligned} a_{\mathrm{x}} &= F_{\mathrm{x,total}}/m \\ a_{\mathrm{y}} &= F_{\mathrm{y,total}}/m. \end{aligned} \tag{2.11}$$

The normal loads of the front and rear axles F_{zf} and F_{zr}, which take into account longitudinal weight transfer due to a_{x}, are determined from D'Alembert principal [39]. By treating the effective force ma_{x} as a force in the opposite direction and assuming that the vehicle behaves like a rigid body along the longitudinal direction, the equations of quasi-static equilibrium are formulated. Solving these equations for F_{zf} and

F_{zr} gives the following expressions:

$$\begin{aligned} F_{\mathrm{zf}} &= m\left(\frac{bg - h_{\mathrm{cg}}a_{\mathrm{x}}}{L}\right) \\ F_{\mathrm{zr}} &= m\left(\frac{ag + h_{\mathrm{cg}}a_{\mathrm{x}}}{L}\right) \end{aligned} \tag{2.12}$$

where g is the magnitude of the gravitational acceleration, h_{cg} is the vertical distance from the center of gravity of the vehicle to the ground, and L is the wheelbase, which is the sum of a and b.

The equations for lateral weight transfer due to a_{y} are derived from a static roll model that considers the vehicle's suspension characteristics using a roll axis [16]. First, the static body-roll angle ϕ_{v} is determined as follows:

$$\phi_{\mathrm{v}} = \frac{m_{\mathrm{s}}h_{\mathrm{l}}a_{\mathrm{y}}}{k_{\phi} - m_{\mathrm{s}}h_{\mathrm{l}}g} \tag{2.13}$$

where m_{s} is the sprung mass of the vehicle, h_{l} is the vertical distance from the center of gravity of the vehicle to the roll axis, and k_{ϕ} is the total roll stiffness, which is the sum of $k_{\phi\mathrm{f}}$ and $k_{\phi\mathrm{r}}$, the roll stiffness of the front and rear axles, respectively.

Then the amount of the lateral weight transfer on each axle is derived as follows:

$$\begin{aligned} \Delta F_{\mathrm{zf}} &= \frac{1}{d}\{k_{\phi\mathrm{f}}\phi_{\mathrm{v}} + h_{\mathrm{f}}(F_{\mathrm{yfl}} + F_{\mathrm{yfr}})\} \\ \Delta F_{\mathrm{zr}} &= \frac{1}{d}\{k_{\phi\mathrm{r}}\phi_{\mathrm{v}} + h_{\mathrm{r}}(F_{\mathrm{yrl}} + F_{\mathrm{yrr}})\} \end{aligned} \tag{2.14}$$

where h_{f} and h_{r} are the heights of the front and rear roll centers from the ground, respectively.

Finally, the normal force of each wheel is described with the derived terms in

(2.12) and (2.14):

$$\begin{aligned} F_{\mathrm{zfl}} &= F_{\mathrm{zf}}/2 - \Delta F_{\mathrm{zf}} \\ F_{\mathrm{zfr}} &= F_{\mathrm{zf}}/2 + \Delta F_{\mathrm{zf}} \\ F_{\mathrm{zrl}} &= F_{\mathrm{zr}}/2 - \Delta F_{\mathrm{zr}} \\ F_{\mathrm{zrr}} &= F_{\mathrm{zr}}/2 + \Delta F_{\mathrm{zr}}. \end{aligned} \tag{2.15}$$

2.3.3 Finding minimum common friction usage

If the value of the minimum common friction usage $k_{\min}$ is known, a set of general axle forces corresponding to that $k_{\min}$ satisfies (2.1) and the following equation:

$$\sqrt{{F_{\mathrm{xi}}}^2 + {F_{\mathrm{yi}}}^2} = k_{\min}\,\mu\,F_{\mathrm{zi}} \quad (\mathrm{i} \in [\mathrm{fl}, \mathrm{fr}, \mathrm{rl}, \mathrm{rr}]) \tag{2.16}$$

where μ is assumed to be known and F_{zi} is from (2.15).

Because $k_{\min}$ in (2.16) is assumed to be the smallest common friction usage, any common friction usage smaller than this value does not produce a feasible solution to (2.1) and (2.16). It is, therefore, possible to formulate an optimization feasibility problem that checks whether a specific common friction usage k_0 results in a feasible solution to both (2.1) and (2.16):

$$\begin{aligned} \text{find} \quad & \{(F_{\mathrm{xi}}, F_{\mathrm{yi}}) \,|\, \mathrm{i} = \mathrm{fl}, \mathrm{fr}, \mathrm{lr}, \mathrm{rr}\} \\ \text{subject to} \quad & \sqrt{{F_{\mathrm{xi}}}^2 + {F_{\mathrm{yi}}}^2} \leq k_0\,\mu\,F_{\mathrm{zi}} \\ & \sum\nolimits_i F_{\mathrm{xi}} = F_{\mathrm{x,total}} \\ & \sum\nolimits_i F_{\mathrm{yi}} = F_{\mathrm{y,total}} \\ & \sum\nolimits_i M_{\mathrm{zi}} = M_{\mathrm{z,total}}. \end{aligned} \tag{2.17}$$

The inequality constraints are convex, and the equality constraints are affine. Accordingly, (2.17) becomes a convex feasibility problem. If the problem is feasible for a given k_0, there exists a set of tire forces that makes all constraints consistent. However, if the problem is infeasible, no set of general axle forces satisfies all the

constraints in (2.17) with a given k_0.

Because the friction usage of a single tire has a value between 0 and 1, the value of the common friction usage also exists in [0,1]. Using this fact, the minimum common friction usage can be found by solving a quasiconvex optimization. The algorithm to solve a quasiconvex optimization via the bisection method is as follows:

Algorithm 1 Quasiconvex optimization via bisection method

given initial search interval $[k_{\text{low}}, k_{\text{high}}] = [0,1]$, tolerance $k_{\text{tol}} > 0$

repeat

1. $k_0 = (k_{\text{high}} + k_{\text{low}})/2$
2. solve the convex feasibility problem (2.17) for k_0
3. **if** the problem is feasible, $k_0 \geq k_{\text{min}}$. set $k_{\text{high}} = k_0$;
   else set $k_{\text{low}} = k_0$

until $k_{\text{high}} - k_{\text{low}} \leq k_{\text{tol}}$

Once Algorithm 1 with the convex feasibility problem in (2.17) stops at a specific k_0, that k_0 is the minimum common friction usage. The values of general axle forces corresponding to k_{min} are a set of optimal and desired general axle forces that satisfies the requirements in Section 2.3.1.

2.4 Actuator commands

This section explains how to convert desired general axle forces at a single tire into commands for the three actuators (a steering angle, driving torque, and braking pressure) by relating the general axle forces to these physical actuator commands through a coupled tire force model. For the rest of this dissertation, the subscript i is dropped from variable descriptions when a single tire is discussed. The basic idea is to invert the tire model in order to calculate the desired longitudinal and lateral tire slips and then to calculate the actuator commands that achieve the desired slips.

The optimal force allocation in Section 2.3 gives a solution in terms of the general axle forces F_{x} and F_{y} referenced in the vehicle-fixed coordinate frame. A Force generated by the combined actions of actuators at a tire, however, is usually described

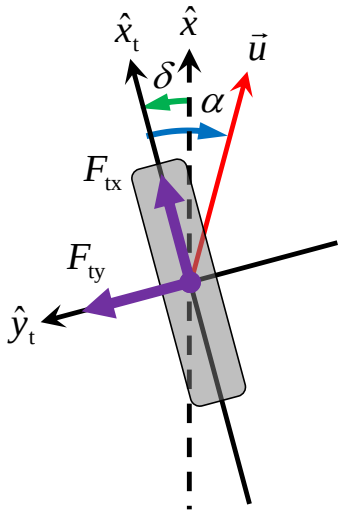

Figure 2.5: A slip angle and tire forces of a single tire

by the tire forces F_{tx} and F_{ty}, as shown in Figure 2.5. These scalar force terms are referenced in each tire's tire-fixed coordinate frame, whose x-axis $\hat{x}_t$ lies along the direction of the wheel's heading.

The actuator actions are described by the following three terms: the steering angle δ is the angle between the two x-axes $\hat{x}$ and $\hat{x}_t$, as shown in Figure 2.5; the driving torque τ is the torque around the spin axis of the wheel $\hat{y}_t$; and the braking pressure P is the hydraulic pressure that is applied to calipers of the wheel.

Because the tire force model describes the relationship between tire slips and tire forces, the desired general axle forces have to be transformed to the tire forces before the tire model inversion. As the tire-fixed coordinate frame rotates from the vehicle-fixed coordinate frame by the steering angle δ, the steering angle is necessary for this transformation. However, this angle is not a known value but a variable that has to be solved for. To overcome this issue, the tire model is reformulated to directly relate the steering angle and longitudinal slip to the desired general axle forces. Once the steering angle is determined by inverting the modified tire model, the driving torque and brake pressure are calculated from the transformed longitudinal tire force by assuming a static relationship between longitudinal tire force and driving torque or braking pressure.

2.4.1 Coupled brush tire model

The model adopted in this dissertation is a modified version of Pacejka's combined-slip brush tire model [46]. The tire slips are represented by the following two terms: the tire slip angle α is the angle between the tire's heading $\hat{x}_{\mathrm{t}}$ and the tire's velocity vector $\vec{u}$, as shown in Figure 2.5; and the longitudinal slip κ is calculated by the equation $(R\omega - \vec{u} \cdot \hat{x}_{\mathrm{t}})/(\vec{u} \cdot \hat{x}_{\mathrm{t}})$, where R is the wheel radius and ω is the wheel speed along $\hat{y}_{\mathrm{t}}$. For given α and κ, longitudinal and lateral theoretical slip quantities σ_{x} and σ_{y} are defined as follows:

$$\sigma_{\mathrm{x}} = \frac{\kappa}{1+\kappa} \tag{2.18}$$

$$\sigma_{\mathrm{y}} = \frac{-\tan\alpha}{1+\kappa}. \tag{2.19}$$

The weighted vector norm of the theoretical slip quantities f is defined as follows:

$$f = \sqrt{(C_{\mathrm{x}}\sigma_{\mathrm{x}})^2 + (C_{\alpha}\sigma_{\mathrm{y}})^2} \tag{2.20}$$

where C_{x} and C_{α} are the longitudinal and lateral tire stiffness, respectively.

Before the tire reaches saturation, the magnitude of the total force vector on the tire F is a function of f, where the tire normal force F_{z} and the effective friction coefficient μ are parameters. After saturation, the total force simply equals the friction force:

$$F = \begin{cases} f - \frac{1}{3\mu F_z} f^2 + \frac{1}{27\mu^2 F_z^2} f^3, & f \le 3\mu F_z \\ \mu F_z & f > 3\mu F_z \end{cases} \tag{2.21}$$

where total sliding of the tire occurs at $f = 3\mu F_{\mathrm{z}}$.

Then the longitudinal and lateral tire forces F_{tx} and F_{ty} are the projections of the total force vector according to the ratio of the weighted longitudinal and lateral theoretical slip quantities. Because all quantities defined in this section are functions

of α and κ, F_{tx} and F_{ty} are also functions of α and κ:

$$\begin{aligned}(F_{\mathrm{tx}}, F_{\mathrm{ty}}) &= \left(\frac{C_{\mathrm{x}}\sigma_{\mathrm{x}}}{f}F, \frac{-C_{\alpha}\sigma_{\mathrm{y}}}{f}F\right) \\ &= \vec{f}_{\mathrm{tire}}(\alpha, \kappa).\end{aligned} \tag{2.22}$$

2.4.2 Steering commands

If F_{tx}, F_{ty} and F_{z} of the tire are given, the corresponding tire slip angle α and the longitudinal slip κ can be calculated by inverting the tire model above. To achieve this desired tire slip angle, the steering angle command δ is calculated using the kinematic relationship of the slip angle and the angle of the tire's velocity vector as follows:

$$\delta = \tan^{-1}\left(\frac{u_{\mathrm{y,tire}}}{u_{\mathrm{x,tire}}}\right) - \alpha. \tag{2.23}$$

where $u_{\mathrm{x,tire}}$ and $u_{\mathrm{y,tire}}$ are the longitudinal and lateral speeds at the center point of the tire in the vehicle-fixed coordinate frame, respectively.

The optimization in Sec. 2.3, however, gives not tire forces but general axle forces F_{x} and F_{y} in the vehicle-fixed coordinate frame. They, therefore, need to be transformed to tire forces F_{tx} and F_{ty} using the following relationship:

$$\begin{bmatrix} F_{\mathrm{tx}} \\ F_{\mathrm{ty}} \end{bmatrix} = \begin{bmatrix} \cos(\delta) & \sin(\delta) \\ -\sin(\delta) & \cos(\delta) \end{bmatrix} \begin{bmatrix} F_{\mathrm{x}} \\ F_{\mathrm{y}} \end{bmatrix}. \tag{2.24}$$

Because the tire forces are not the determined values but the variables as a function of δ, it is impossible to simply invert the tire model. By replacing α in (2.22) with δ using the relationship in (2.23), however, the tire model can be rewritten using δ and κ as variables instead of α and κ:

$$(\cos(\delta)F_{\mathrm{x}} + \sin(\delta)F_{\mathrm{y}}, -\sin(\delta)F_{\mathrm{x}} + \cos(\delta)F_{\mathrm{y}}) = \vec{f}_{\mathrm{tire}}\left(\tan^{-1}\left(\frac{u_{\mathrm{y,tire}}}{u_{\mathrm{x,tire}}}\right) - \delta, \kappa\right). \tag{2.25}$$

The steering angle δ can be found by solving nonlinear equations derived from (2.25).

2.4.3 Driving and braking commands

The longitudinal slip κ can also be found while solving (2.25). It can be controlled by torque applied to the tire and is governed by the wheel slip dynamics. In this dissertation, however, the wheel slip dynamics are ignored, and κ is not directly controlled. Instead, a static relationship is assumed between the longitudinal tire force and driving or braking torque. This is reasonable since the optimization produces only feasible longitudinal tire forces that are within the tire's friction limits and can be generated by given actuators. Using δ calculated in the previous section, the longitudinal force F_{tx} is found by (2.24). Then the commands for the driving torque τ and the brake pressure P are as follows:

$$\tau = \begin{cases} R_{\text{w}} F_{\text{tx}}, & F_{\text{tx}} > 0 \\ 0, & F_{\text{tx}} \leq 0 \end{cases} \tag{2.26}$$

$$P = \begin{cases} 0, & F_{\text{tx}} \geq 0 \\ \frac{R_{\text{w}} F_{\text{tx}}}{r_{\text{brake}}}, & F_{\text{tx}} < 0 \end{cases} \tag{2.27}$$

where R_{w} is the wheel effective radius and r_{brake} is the conversion coefficient from brake pressure to brake torque.

2.5 Experiments

The controller with the optimal tire force allocation was experimentally validated using the X1 research vehicle shown in Figure 2.6. The vehicle has four-wheel independent steering and braking capabilities and one electric driving motor connected to the rear axle through an open differential. Even though the front axle does not have a driving capability, X1 is highly over-actuated compared to production vehicles. The vehicle's parameters can be found in Table 2.1.

The task chosen for validating the controller was to track a racing line close to the limits of handling. Because the task demands a continuously-changing set of large total forces and moment, it requires all four tires to stay in the nonlinear region and

Table 2.1: X1's parameters

mass	m	2,009	kg
distance from CG to front axle	a	1.56	m
distance from CG to rear axle	b	1.18	m
distance from CG to ground	h_{cg}	0.47	m
yaw moment of inertia	I_{z}	2,000	$\mathrm{kg} \cdot \mathrm{m}^2$
track width	d	1.63	m
effective wheel radius	R_{w}	0.3	m

Figure 2.6: The X1 research vehicle

all three actuators at each wheel to be fully engaged and to cooperate. X1 was tested on a paved racing track at Thunderhill Raceway Park, Willows, California. During the entire maneuver, the controller drove X1 autonomously.

2.5.1 Trajectory description

Path and speed profile generation for a racing line follows the methodology proposed by Kritayakirana and Gerdes [30]. The geometric path is structured from three types of segments: a straight line, a constant radius curve, and a transition curve. For the transition curve, a clothoid geometry, which has linear variation of its curvature along

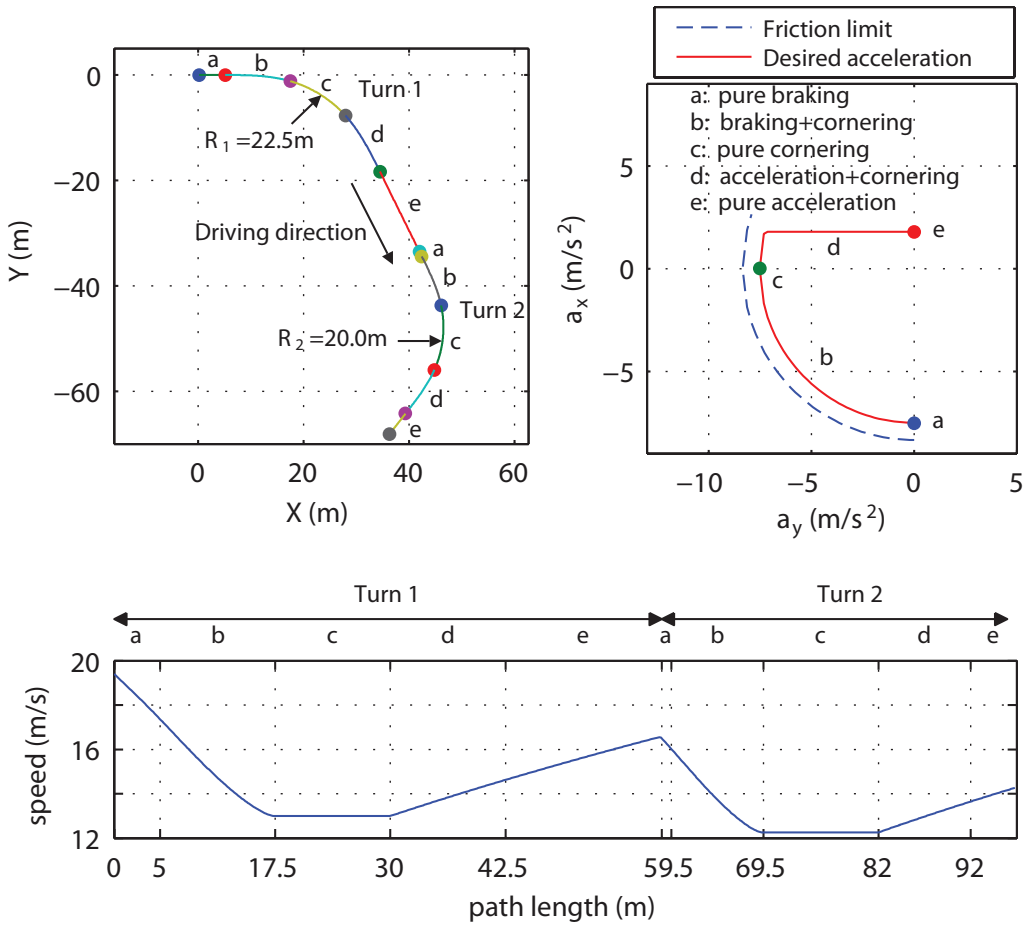

Figure 2.7: Test trajectory with two turns structured from straight lines (a and e), transition curves (b and d), and a constant radius curve (c)

its length, is adopted to connect the straight line and the constant radius curve that have zero and constant curvature, respectively.

Defining the geometric path gives the heading profile $\psi_{\mathrm{p}}(s)$. The speed profile $V(s)$ can be obtained by integrating the acceleration profile along the path length. The acceleration profile was designed so that X1 stays at 90 % of the vehicle's maximum acceleration, which is μg and μ was estimated to be 0.85 using the algorithm developed by Hsu et al. [26]. The maximum positive longitudinal acceleration, however, was limited to 1.8 m/s^2 due to the torque limit on the X1's driving motor. The geometric path, the acceleration profile, and the speed profile of the desired trajectory, which has two consecutive turns, are shown in Figure 2.7.

The driving sequences of one single turn are divided into the following five steps: pure braking in a straight line, combined braking and cornering in a transient curve, pure cornering in a constant radius curve, combined acceleration and cornering in a transient curve, and pure acceleration in a straight line. These five steps are labeled from a to e, respectively, in Figure 2.7.

The relative heading of the vehicle ψ_{pv} was set to zero in this experiment. In other words, the vehicle's desired heading was identical to the tangent of the path. Therefore, the tracking objectives are to keep X1's center of gravity on the desired path and make X1's heading and speed tangent to the path follow the heading and speed profiles of the desired trajectory, respectively.

2.5.2 Tire force allocation by interpolation

Ideally, the optimization in Section 2.3 can be solved in real time. But, generally, real-time optimization requires extensive computing power or some modifications to the original formulation to fit it into a solvable form for a real-time optimization program.

If one assumes that μ is constant and F_{zi} depends only on total force demands, as derived in Section 2.3.2, the optmization formulation in Section 2.3.3 can be viewed as having three inputs: total longitudinal/lateral force and yaw moment demands.

The maximum achievable total forces and moment of the vehicle are limited within

a certain range because tire forces are limited within the maximum friction capability of each tire. From this fact, it is possible to create a map relating a set of discrete total demands to the corresponding general axle forces at the tires by solving the optimization off-line by CVX, a package for specifying and solving convex programs [19],[18]. During the test, solving the optimization problem was replaced by interpolation using this map. This can greatly reduce the operation time of the controller.

2.5.3 Results

Figure 2.8a depicts the tracking errors for the entire path. The controller demonstrated its capability to follow all three tracking objectives by achieving very small errors: the lateral and speed errors were kept within ± 0.2 m and [-0.6 0] m/s, respectively, and the heading error did not exceed 0.02 rad ($\approx$1.15 °).

Even though the system dynamics are not linearized for the controller formulation, the model of the system is not perfect because there exist unmodeled physical effects. For example, there is a delay in tracking actuator commands. Including this actuation delay, several factors can affect the realization of desired tire forces: ignorance of the wheel dynamics, unmodeled tire dynamics such as transient force development and side-wall deformation, etc. The small tracking errors, however, suggest the impact of these adverse properties is small and easily handled with feedback. This experimentally supports the basic trajectory tracking approach with a simple feedforward-feedback structure.

Figure 2.8b illustrates the friction usage at each of the four wheels. Because actual tire forces were not directly measured in this test, the values of the friction usage were calculated from the commanded general axle forces and estimated normal tire forces. Up to the constant radius curve (the turn segments a, b, and c), all four tires showed almost equal friction usage. This is the result that is precisely intended by the optimization algorithm in Section 2.3.

During the corner exit (the turn segments d and e), which demands high positive longitudinal acceleration, however, the rear wheels had higher friction usage than the front wheels. This is because X1 can generate positive longitudinal force only at the

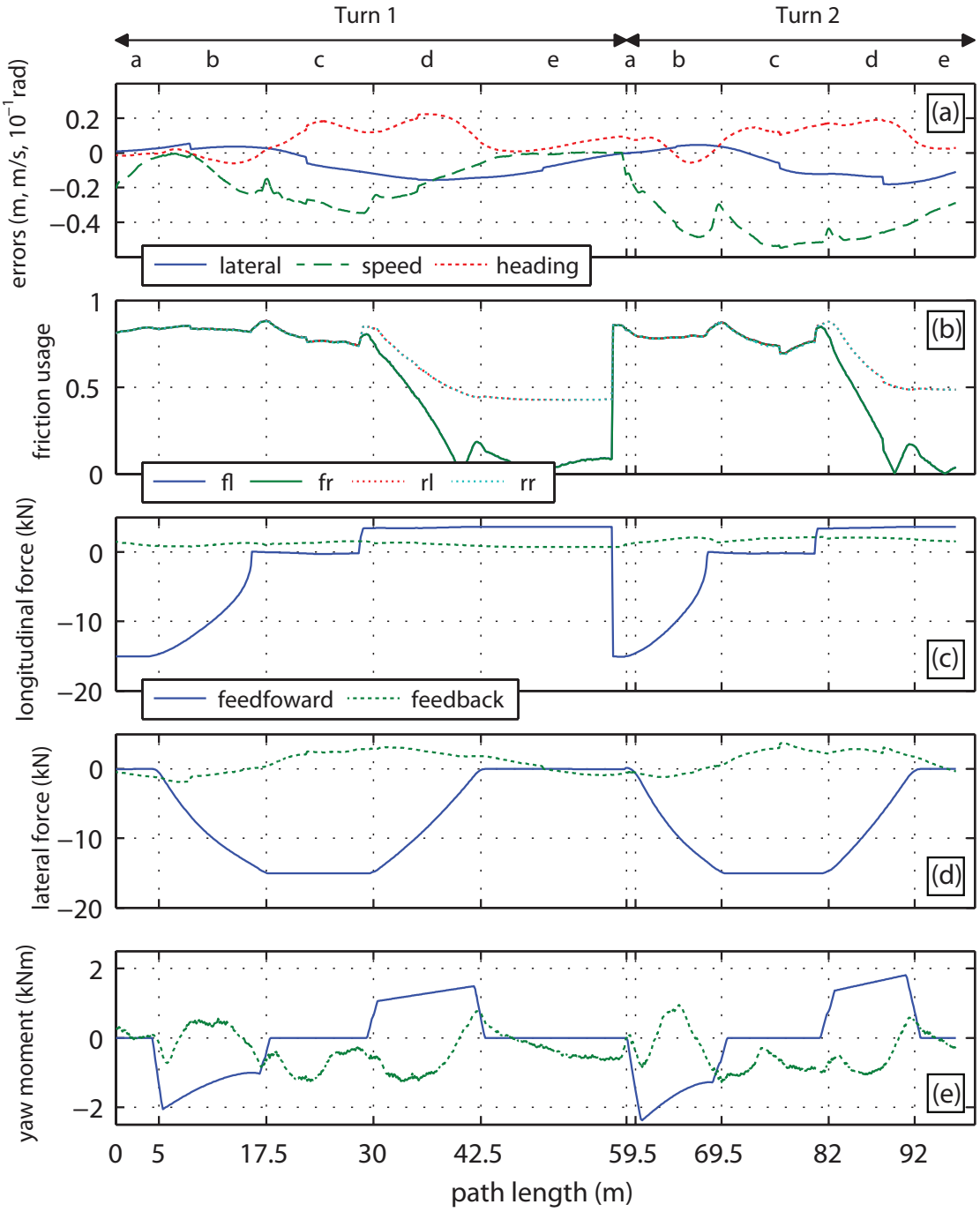

Figure 2.8: Experimental results from X1 with the controller: (a) tracking errors, (b) friction usage, (c) longitudinal force demand, (d) lateral force demand, and (e) yaw moment demand

rear axle. As a result, the rear tires must use more of their friction capability and have a higher friction usage than the front tires to achieve positive total longitudinal force.

Therefore, it is no longer possible for a vehicle with limited actuation to achieve the original objective of the optimal tire force allocation–keeping the same friction usage over the four wheels–for specific total force and moment demands. Therefore, the need for a new optimal tire force allocation algorithm arises to handle limited actuation properly. This is the topic of Chapter 3.

Chapter 3

Handling Limited Actuation

The analysis in Chapter 2 assumes that all four wheels of a vehicle have full control over all three actuators (steering, driving, and braking), and that the feasible force region of each tire is the entire area within a circle whose radius is μF_{zi} ($\mathrm{i} \in [\mathrm{fl}, \mathrm{fr}, \mathrm{rl}, \mathrm{rr}]$). However, actually implementing all three actuators at all four wheels is technically challenging and costly.

Even with some limited actuation, certain actuating configurations can emulate independent steering/driving/braking capabilities at a wheel. In this case, the assumptions still hold. However, if a wheel completely lacks one of the three actuators for practical reasons, feasible tire forces of that tire are restricted to a certain range from the entire area of its friction circle.

Because the controller in Chapter 2 calculates actuator commands using optimized general axle force commands for the wheels, it is important for the optimal tire force allocation algorithm to result in only a set of general axle forces that can actually be realized by a given actuation layout. In other words, the algorithm has to find a solution that lies only within feasible tire force regions. At the same time, the controller must handle the new situation in which it is no longer possible to achieve the original force allocation objective, which was keeping the usage of tire friction capability equal over the four wheels: some tires have to use more of their friction capability than others to compensate for the restricted tire force generation of those other tires due to the limited actuation.

In this chapter, these goals are achieved by applying new constraints and an additional algorithm to the existing optimization formulation. These constraints and algorithm are designed to take into account a situation in which some of the actuators are not implemented while the vehicle still remains over-actuated.

Developing new constraints requires transforming physical limits of a given actuation layout into the constraints on general axle forces. After carefully analyzing feasible tire force regions that can actually be generated by the given actuation layout at specific vehicle states, this chapter presents constraints that describe the feasible tire force regions and enable the entire allocation algorithm to keep the form of a convex optimization formulation. To solve for a unique set of general axle forces when the friction usage of each tire is different, an additional algorithm that supplements Algorithm 1 is also presented. Section 3.1 shows that some simple constraints trying to capture actuating limitations can fail to generate feasible tire forces for a given actuating configuration and explains how to correctly describe a feasible tire force region in a form suitable for convex optimization. Section 3.2 describes a new formulation for optimal force allocation that adopts the analysis of the feasible tire force region discussed in Section 3.1 and also presents the algorithm handling different friction usages. Section 3.3 explains how to emulate independent driving and braking capabilities at both rear wheels of the X1 research vehicle by using one driving motor and individual brakes on the rear axle. Doing so enables X1 to handle its limited actuation without imposing any constraint for the rear wheels in the optimal tire force allocation. Section 3.4 presents experimental results demonstrating the effectiveness of the new constraints by operating X1 with the controller that adopts the new optimization formulation.

3.1 Feasible tire force region for limited actuation

This section explains how to mathematically describe a feasible tire force region of a single tire when some limitations on actuation exist. Therefore, the subscript i is dropped from variable descriptions. The optimal force allocation is formulated and gives a solution in terms of general axle forces F_{x} and F_{y} in the vehicle-fixed

coordinate frame whereas a force generated by combined actions of actuators are usually described by tire forces F_{tx} and F_{ty} referenced to a tire-fixed coordinate frame, as shown in Figure 2.5. Therefore, a feasible tire force region that can be achieved by a given actuator configuration is easy to describe in terms of F_{tx} and F_{ty}.

Once a steering angle is given, the expression of a feasible force region in terms of F_{tx} and F_{ty} can be easily transformed to the expression of the same feasible tire force region in terms of F_{x} and F_{y} by changing force variables using the relationship in (2.24). For the controller in Chapter 2, however, the steering angle is not a known value at the stage of the optimal force allocation.

Therefore, the expression of the feasible tire force region has to be independent of the steering angle and written in terms of general axle forces while being accurate enough to capture the key characteristics of the feasible region, in order to allow its use in the formulation of the optimal force allocation.

In this section, the actuating configuration of interest is a wheel with steering and braking actuators but without a driving actuator as is the case for X1's front wheels. For a single tire with the fixed friction coefficient μ and normal force F_{z}, the analysis is concerned with how tire forces are generated with the combined actions of the steering and braking actuators. Based on this analysis, the shape of the feasible tire force region is identified. With a reasonable approximation, a set of convex equations can describe the boundary of this region in terms of general axle forces and given vehicle states.

3.1.1 Issues of simple constraints on general axle forces

For a wheel assembly with all three actuators, the feasible tire force region covers the entire area of a circle whose radius is μF_{zi}. In this case, the description of the feasible tire force region in terms of general axle forces is also the entire area of the tire's friction circle and is independent of a steering angle.

When a wheel assembly does not have all three actuators, the feasible tire force region of the tire no longer covers the entire area of the tire's friction circle. Therefore, the mathematical description of a new feasible tire force region has to be included

in the optimization formulation for tire force allocation as constraints. Because the variables of the optimization are the general axle forces, these constraints are also imposed on the general axle forces.

However, if those constraints are not carefully chosen, the feasible tire force region described in terms of general axle forces may not accurately represent the tire force region that can be generated by a given actuation layout. Especially, a constraint that is valid when the steering angle is small may become invalid as the steering angle increases because of the difference between the general axle forces and tire forces.

In other words, when the steering angle is small, the difference between the general axle forces and the transformed tire forces by (2.24) is also small. Therefore, it is acceptable to assume that those two force sets are equal and that the description of the feasible tire force region in terms of the tire forces can be converted to the description of the region in terms of the general axle forces by simply replacing force variables. As the steering angle increases, however, the difference between the two force sets can no longer be ignored, and simply replacing F_{tx} and F_{ty} with F_{x} and F_{y} in the description cannot represent the feasible tire force region properly. As a result, the tire forces transformed from the optimized general axle forces may not be in the feasible tire force region, and the tire cannot generate forces that match the optimized general axle forces.

One example is a wheel without a driving capability. Such a wheel cannot generate positive longitudinal tire force. This situation can be exactly described by an inequality that limits a longitudinal tire force to be equal to or less than zero, $F_{\mathrm{tx}} \leq 0$. By replacing a force variable, this inequality becomes $F_{\mathrm{x}} \leq 0$: the simple form that can be used as a constraint in the optimization formulation. The optimal tire force allocation for the experiments in Chapter 2 adopted this inequality constraint to take into account the X1's lack of a front-wheel-driving capability: two additional constraints on the front longitudinal general axle forces, $F_{\mathrm{xfl}} \leq 0$ and $F_{\mathrm{xfr}} \leq 0$, were added to the original feasibility problem (2.17).

If the optimization results in large pure lateral general axle force on the wheel, as shown in Figure 3.1a, which is totally feasible for general axle forces, a large tire slip angle is necessary to generate a large lateral tire force that matches the lateral

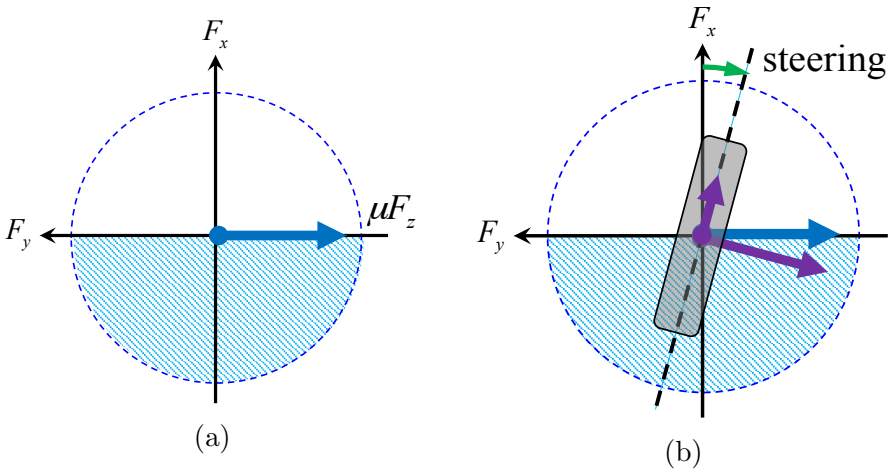

Figure 3.1: A problem of the simple constraint on general axle forces, $F_x < 0$. (a) The optimized general axle force demands satisfy the constraint, but (b) the transformed tire forces are not in the region described by the constraint.

general axle force. If the tire's velocity vector lies along the x-axis of the vehicle-fixed coordinate frame, the steering angle also has to be large to achieve the corresponding tire slip angle. In this situation, the transformed tire forces inevitably contain the portion of the positive longitudinal tire forces that cannot be generated by the wheel without a driving capability. This is shown in Figure 3.1b. In this case, the general axle force demand cannot be achieved, and new constraints are required to obtain a feasible set of general axle forces that can actually be generated by a given actuator configuration.

3.1.2 Feasible tire force region

To formulate the new constraints, it is necessary to understand how tire forces are generated when there are any limits on actuation at the tire. As mentioned above, the case in which the tire has steering and braking capabilities but not driving capability is investigated here because X1 lacks only a front-wheel-drive capability.

To simplify the analysis for now, it is assumed that the tire's velocity vector lies along the x-axis in the vehicle-fixed coordinate frame. Then the slip angle α, the angle between the tire's heading and the tire's velocity vector, has the same magnitude as

the steering angle δ but the opposite sign.

How tire forces are changing while braking torque increases at some fixed steering angles is investigated first. When δ is zero, α is also zero, and no lateral tire force is generated. The longitudinal tire force changes from zero to negative maximum available friction capability as braking torque increases. Figure 3.2a illustrates this case. When the tire is steered while the braking torque is zero, α has some non-zero value, and pure lateral tire force is generated in the tire-fixed coordinate frame, which is rotated from the vehicle-fixed coordinate frame by the steering angle. If the braking torque increases while δ is fixed, the lateral tire force decreases in magnitude while the magnitude of the longitudinal tire force increases, as shown in Figure 3.2b. If the tire's steering angle increases further, α finally reaches its sliding limit α_{sl}, which causes tire force saturation. This is shown in Figure 3.2c. Jonasson et al. [24] presented the detailed description of this tire force generation pattern.

If the area covered by the tire forces resulting from all combinations of the steering angle and the braking torque is plotted, this results in the shaded area in Figure 3.3. The boundary of the feasible tire force region in Figure 3.3 is defined by two parts: the lower boundary is described by a friction limit, which is the circle whose radius is μF_{z}, and the upper boundary is expressed by slip angles and pure lateral tire forces corresponding to those slip angles when longitudinal slip κ is zero. For a specific slip angle α_0, the coordinates of the point on the upper boundary corresponding to α_0 in the vehicle-fixed coordinate frame are written as follows:

$$\begin{pmatrix} F_{\mathrm{x}} \\ F_{\mathrm{y}} \end{pmatrix} = \begin{pmatrix} \sin(\alpha_0)\, F_{\mathrm{ty}}(\alpha_0)|_{\kappa=0} \\ \cos(\alpha_0)\, F_{\mathrm{ty}}(\alpha_0)|_{\kappa=0} \end{pmatrix}. \tag{3.1}$$

When α_0 reaches its sliding limit value, α_{sl}, the two boundaries intersect, and the coordinates of the intersecting point are

$$\begin{pmatrix} F_{\mathrm{x}} \\ F_{\mathrm{y}} \end{pmatrix} = \begin{pmatrix} \sin(\alpha_{\mathrm{sl}})\, \mu F_{\mathrm{z}} \\ \cos(\alpha_{\mathrm{sl}})\, \mu F_{\mathrm{z}} \end{pmatrix}. \tag{3.2}$$

Besides the brush tire model introduced in Section 2.4.1, there exist other tire

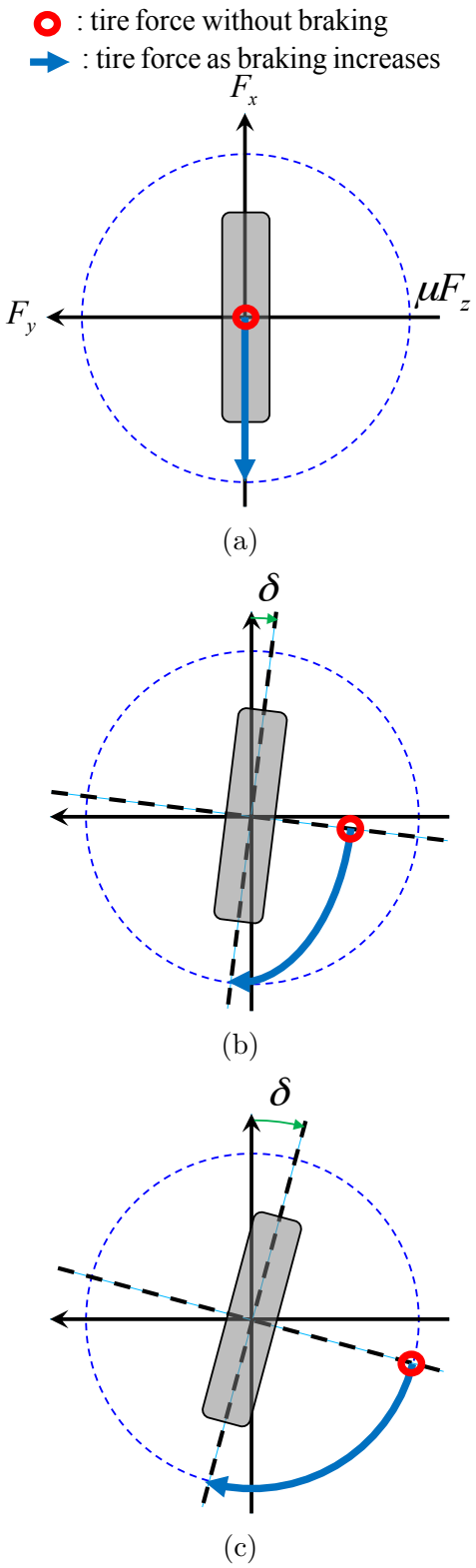

Figure 3.2: Tire forces as braking torque increases at the following fixed slip angles: (a) $\alpha = 0$, (b) $0 < \alpha < \alpha_{\text{sl}}$, and (c) $\alpha = \alpha_{\text{sl}}$.

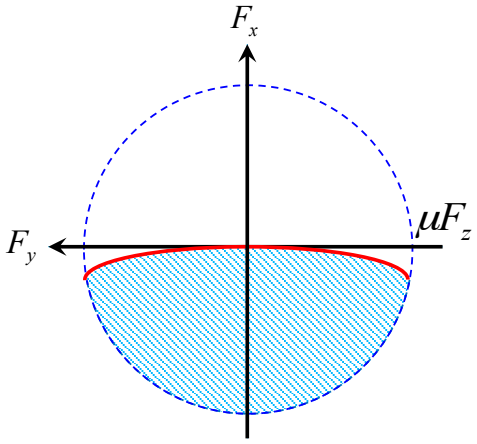

Figure 3.3: Feasible tire force region for a wheel with steering and braking actuators.

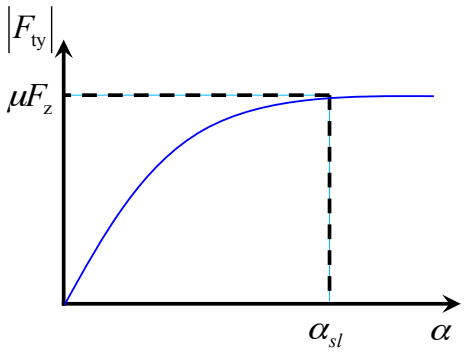

Figure 3.4: Lateral tire force curve when $\kappa = 0$.

models that can describe analytically how tire forces are generated at a tire [47, 15, 12]. Because the expression of $F_{\mathrm{ty}}(\alpha_0)|_{\kappa=0}$ is determined by which tire model is used, the exact mathematical representation of the upper boundary also depends on a specific tire model. However, for any tire model that exhibits a decreasing slope of lateral tire force as the slip angle increases, as shown in Figure 3.4, the upper boundary can be successfully approximated by the upper half of an ellipse that has a semi-major axis of $\mu F_{\mathrm{z}} \cos(\alpha_{\mathrm{sl}})$ and a semi-minor axis of $\mu F_{\mathrm{z}} \sin(\alpha_{\mathrm{sl}})$. The equation for the ellipse is as follows:

$$\left(\frac{F_{\mathrm{x}} + \mu F_{\mathrm{z}} \sin(\alpha_{\mathrm{sl}})}{\mu F_{\mathrm{z}} \sin(\alpha_{\mathrm{sl}})}\right)^2 + \left(\frac{F_{\mathrm{y}}}{\mu F_{\mathrm{z}} \cos(\alpha_{\mathrm{sl}})}\right)^2 = 1. \tag{3.3}$$

The upper boundary of the feasible tire force region corresponds to only the upper

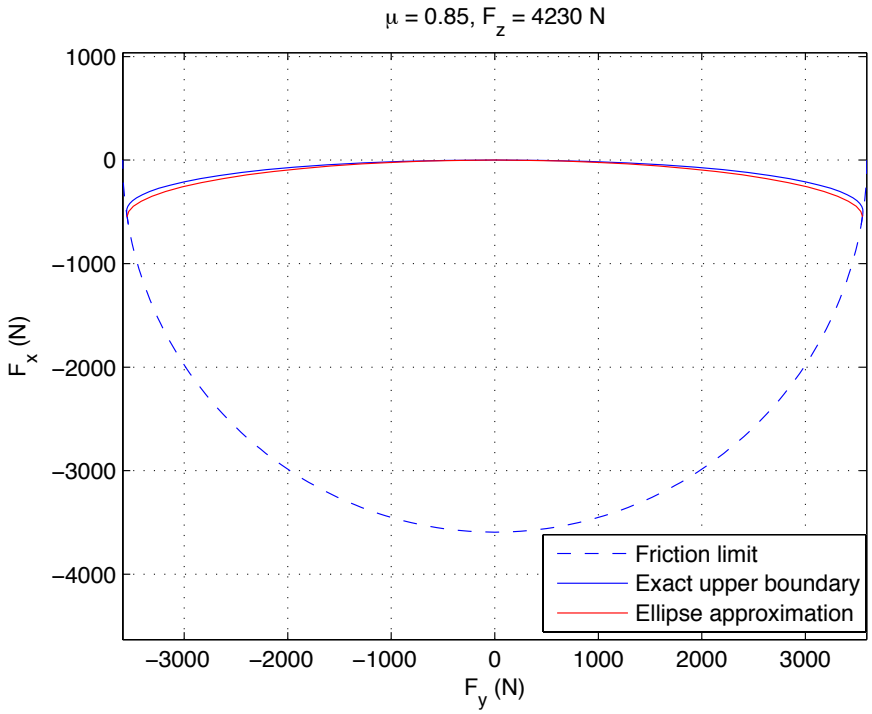

Figure 3.5: Comparison between the exact boundary calculated from the tire model and the ellipse-approximated boundary.

half of the ellipse and is expressed as follows:

$$F_{\mathrm{x}} = -\mu F_{\mathrm{z}} \sin(\alpha_{\mathrm{sl}}) + \mu F_{\mathrm{z}} \sin(\alpha_{\mathrm{sl}}) \sqrt{1 - \left(\frac{F_{\mathrm{y}}}{\mu F_{\mathrm{z}} \cos(\alpha_{\mathrm{sl}})} \right)^2}. \tag{3.4}$$

To validate the ellipse approximation, two different upper boundaries are plotted in Figure 3.5: one is the exact upper boundary calculated by (3.1) using the coupled brush tire model presented in Section 2.4.1, and the other is from the ellipse approximation in (3.4). Those two lines are almost identical, which justifies the use of the ellipse approximation to describe the boundary of feasible tire force region for a tire with steering and braking actuators. With (3.4) and the friction limit circle whose radius is μF_{z}, the boundary of the feasible tire force region can be fully described using only general axle force variables F_{x} and F_{y}.

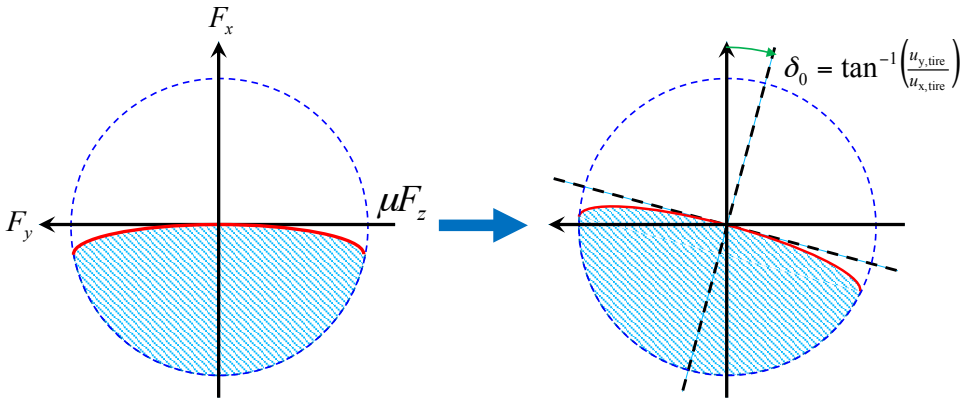

Figure 3.6: New feasible force region rotated by δ_0.

3.1.3 Considering the change of tire's velocity vector

In Section 3.1.2, the tire's velocity vector is assumed to lie along the x-axis in the vehicle-fixed coordinate frame. As the vehicle states keep changing while the vehicle is driving, however, the direction of the tire's velocity vector also keeps changing and deviates from the x-axis. Accordingly, the feasible tire force region has to be adjusted.

From the analysis in Section 3.1.2, the feasible tire force region is symmetric with respect to the axis at which the slip angle α is zero. For an arbitrary vector of the tire's velocity, α becomes zero when the tire steers through the angle of that velocity vector. In other words, the axis aligned with the tire's velocity vector is the axis of symmetry for a new feasible tire force region. Therefore, the new feasible tire force region for the arbitrary velocity vector can be found by simply rotating the original feasible region in Section 3.1.2 by the angle of the tire's velocity vector, as shown in Figure 3.6. This angle, δ_0, is calculated as follows:

$$\delta_0 = \tan^{-1}\left(\frac{u_{\mathrm{y,tire}}}{u_{\mathrm{x,tire}}}\right) \tag{3.5}$$

where $u_{\mathrm{x,tire}}$ and $u_{\mathrm{y,tire}}$ are the longitudinal and lateral velocities at the center point of a tire in the vehicle-fixed coordinate frame, respectively.

As the feasible tire force region rotates, the equation of the region's upper boundary needs to be transformed. This can be done by changing F_{x} and F_{y} in (3.4) with

the new force variables F_{cx} and F_{cy} in the coordinate frame that is rotated from the vehicle-fixed coordinate by the angle δ_0. F_{cx} and F_{cy} are the temporary variables adopted only to simplify the expression of the new constraints. Then, the relationship between $(F_{\mathrm{cx}}, F_{\mathrm{cy}})$ and $(F_{\mathrm{x}}, F_{\mathrm{y}})$ is as follows:

$$\begin{bmatrix} F_{\mathrm{cx}} \\ F_{\mathrm{cy}} \end{bmatrix} = \begin{bmatrix} \cos(\delta_0) & \sin(\delta_0) \\ -\sin(\delta_0) & \cos(\delta_0) \end{bmatrix} \begin{bmatrix} F_{\mathrm{x}} \\ F_{\mathrm{y}} \end{bmatrix} \tag{3.6}$$

The equation of the new upper boundary can be described using F_{cx} and F_{cy} as follows:

$$F_{\mathrm{cx}} = -\mu F_{\mathrm{z}} \sin(\alpha_{\mathrm{sl}}) + \mu F_{\mathrm{z}} \sin(\alpha_{\mathrm{sl}}) \sqrt{1 - \left(\frac{F_{\mathrm{cy}}}{\mu F_{\mathrm{z}} \cos(\alpha_{\mathrm{sl}})} \right)^2}. \tag{3.7}$$

3.2 Optimization formulation considering feasible tire force region

This section presents a new formulation for optimal force allocation that reflects the analysis of the feasible tire force region in Section 3.1. The expressions for feasible tire force regions in terms of general axle forces (3.7) are adopted as new constraints in the original feasibility problem (2.17). To maintain convexity of the formulation, the normal force F_{z} and the limit slip angle α_{sl} in the expression of the new constraint need to be determined in advance, and the necessary modification of the weight transfer model for the prior calculation of these values is proposed.

If the feasible tire force regions of some tires do not cover the entire area of the tires' friction circles, the situation can occur in which other tires have to use more of their fiction capability in order to compensate for the restricted tire force generation of those tires. Then, it becomes impossible to achieve the same friction usage over the four wheels. Because Algorithm 1 gives the minimum friction usage only for the most-used tires in this situation, an additional algorithm is presented to determine desired general axle forces of the less-used tires with the objective of keeping the friction usage of those less-used tires equal.

3.2.1 Calculating normal forces

According to the weight transfer model presented in Section 2.3.2, the normal tire forces are affine functions of lateral general axle forces for given total force demands and can be expressed simply as follows:

$$\begin{aligned} F_{\mathrm{zi}} &= C_{\mathrm{i},1}(F_{\mathrm{yfl}} + F_{\mathrm{yfr}}) + C_{\mathrm{i},2} \quad (\mathrm{i} \in [\mathrm{fl}, \mathrm{fr}]) \\ F_{\mathrm{zi}} &= C_{\mathrm{i},1}(F_{\mathrm{yrl}} + F_{\mathrm{yrr}}) + C_{\mathrm{i},2} \quad (\mathrm{i} \in [\mathrm{rl}, \mathrm{rr}]) \end{aligned} \tag{3.8}$$

where $C_{\mathrm{i},1}$ and $C_{\mathrm{i},2}$ are constants that can be determined from the given total force demands and the vehicle parameters.

This affine characteristic allows the normal force terms in (2.17) to be replaced with these expressions (3.8) without loss of the convexity of the optimization formulation. It is, therefore, unnecessary to calculate the normal forces in advance before solving (2.17).

In (3.7), however, the normal force term is included in the denominator, and replacing that term with the affine model makes (3.7) a neither convex nor concave expression for F_{cx} and F_{cy}. On the other hand, if μ, F_{z} and α_{sl} in (3.7) are known in advance, F_{cx} becomes a concave function of F_{cy}. Because F_{cx} and F_{cy} are linear functions of general axle forces F_{x} and F_{y} for a given δ_0 as shown in (3.6), (3.7) eventually becomes a concave expression for F_{x} and F_{y}.

To adopt (3.7) as a constraint while preserving convexity, the normal forces need to be determined before the optimization problem is solved. This is done by replacing the sums of the lateral general axle forces in (3.8) with the lateral forces at the front and rear axles from a steady-state force balance assumption on a planar bicycle model as follows:

$$\begin{aligned} F_{\mathrm{yfl}} + F_{\mathrm{yfr}} &= \frac{b}{L} m a_{\mathrm{y}} = \frac{b}{L} F_{\mathrm{y,total}} \\ F_{\mathrm{yrl}} + F_{\mathrm{yrr}} &= \frac{a}{L} m a_{\mathrm{y}} = \frac{a}{L} F_{\mathrm{y,total}}. \end{aligned} \tag{3.9}$$

Then the normal force F_{zi} of each tire becomes a function of only given total force demands and the vehicle parameters, and it can be determined before the optimization

problem is solved.

3.2.2 Optimization formulation

A new feasibility problem is derived with the more feasible force boundaries discussed above. The constraints of the new formulation are designed for the actuation layout of the X1 research vehicle, which lacks front-wheel-drive capability. To describe the feasible tire force regions of the front tires using (3.7), the angle of each tire's velocity vector δ_0, its normal force F_z and its sliding limit slip angle α_{sl} need to be calculated first.

The angles of the front tires' velocity vectors $\delta_{0,i}$ ($i \in [fl, fr]$) are derived by replacing the velocity terms in (3.5) with kinematic functions of the vehicle's geometry and states:

$$\delta_{0,fl} = \tan^{-1}\left(\frac{u_y + ar}{u_x - \frac{d}{2}r}\right) \qquad \delta_{0,fr} = \tan^{-1}\left(\frac{u_y + ar}{u_x + \frac{d}{2}r}\right) \tag{3.10}$$

where u_x and u_y are the vehicle's longitudinal and lateral velocities, respectively, and r is the yaw rate of the vehicle.

The normal forces F_{zi} ($i \in [fl, fr, rl, rr]$) are calculated as explained in Section 3.2.1. Once the normal forces are determined, $\alpha_{sl,i}$ ($i \in [fl, fr]$) can be calculated using the tire model presented in Section 2.4.1 as follows:

$$\alpha_{sl,i} = \tan^{-1}\left(\frac{3\mu F_{zi}}{C_{\alpha f}}\right) \quad (i \in [fl, fr]) \tag{3.11}$$

where $C_{\alpha f}$ is the lateral tire stiffness of the front tires.

Then the new convex feasibility problem is written as follows:

$$
\begin{aligned}
\text{find} \quad & \{(F_{\mathrm{xi}}, F_{\mathrm{yi}}) \,|\, \mathrm{i} = \mathrm{fl}, \mathrm{fr}, \mathrm{lr}, \mathrm{rr}\} \\
\text{subject to} \quad & \sqrt{{F_{\mathrm{xi}}}^2 + {F_{\mathrm{yi}}}^2} \leq k_0 \mu F_{\mathrm{zi}} \\
& \sum\nolimits_i F_{\mathrm{xi}} = F_{\mathrm{x,total}} \\
& \sum\nolimits_i F_{\mathrm{yi}} = F_{\mathrm{y,total}} \\
& \sum\nolimits_i M_{\mathrm{zi}} = M_{\mathrm{z,total}} \\
& F_{\mathrm{cxfl}} \leq -\mu F_{\mathrm{zfl}} \sin(\alpha_{\mathrm{sl,fl}}) + \mu F_{\mathrm{zfl}} \sin(\alpha_{\mathrm{sl,fl}}) \sqrt{1 - \left(\frac{F_{\mathrm{cyfl}}}{\mu F_{\mathrm{zfl}} \cos(\alpha_{\mathrm{sl,fl}})} \right)^2} \\
& F_{\mathrm{cxfr}} \leq -\mu F_{\mathrm{zfr}} \sin(\alpha_{\mathrm{sl,fr}}) + \mu F_{\mathrm{zfr}} \sin(\alpha_{\mathrm{sl,fr}}) \sqrt{1 - \left(\frac{F_{\mathrm{cyfr}}}{\mu F_{\mathrm{zfr}} \cos(\alpha_{\mathrm{sl,fr}})} \right)^2}
\end{aligned}
\tag{3.12}
$$

where

$$
\begin{bmatrix} F_{\mathrm{cxfl}} \\ F_{\mathrm{cyfl}} \end{bmatrix} = \begin{bmatrix} \cos(\delta_{0,\mathrm{fl}}) & \sin(\delta_{0,\mathrm{fl}}) \\ -\sin(\delta_{0,\mathrm{fl}}) & \cos(\delta_{0,\mathrm{fl}}) \end{bmatrix} \begin{bmatrix} F_{\mathrm{xfl}} \\ F_{\mathrm{yfl}} \end{bmatrix},
$$

$$
\begin{bmatrix} F_{\mathrm{cxfr}} \\ F_{\mathrm{cyfr}} \end{bmatrix} = \begin{bmatrix} \cos(\delta_{0,\mathrm{fr}}) & \sin(\delta_{0,\mathrm{fr}}) \\ -\sin(\delta_{0,\mathrm{fr}}) & \cos(\delta_{0,\mathrm{fr}}) \end{bmatrix} \begin{bmatrix} F_{\mathrm{xfr}} \\ F_{\mathrm{yfr}} \end{bmatrix}.
$$

3.2.3 Considering different friction usages between tires

Adding additional constraints on the front tires of X1 creates a situation in which the rear tires must use more of their friction capabilities than the front tires: for example, the rear tires become the most-used tires while X1 accelerates along a straight line because only the rear axle has driving capability. If (3.12) is used as the convex feasibility problem in Algorithm 1, the algorithm still gives the minimum friction usage. For specific total force and moment demands, however, the resulting k_0 is now no longer common for the four tires but is valid only for the most-used tires. Mathematically, this implies that only the friction limit inequality constraints of the most-used tires become active.

Because no set of tire forces can achieve a smaller friction usage for the most-used tires than the resulting k_0 from Algorithm 1, the tire forces corresponding to that k_0 can be regarded as the unique and final solution that makes the most-used tires achieve the minimum feasible friction usage. For the less-used tires, whose friction usage is smaller than the k_0, and whose friction limit inequality constraints are not active, however, there still could be several sets of tire forces that satisfy all the other constraints.

Among those possible sets of tire forces, the optimal set for the less-used tires can be chosen by applying the basic principle of the original requirements for the optimal tire forces over the four wheels to the less-used tires: keeping the friction usage of the less-used tires equal. This new requirement for the optimal tire forces can be realized by running Algorithm 1 again while the optimization variables in (3.12) are only the tire forces of the less-used tires, and the tire forces of the most-used tires determined from the first run of Algorithm 1 become constants. To execute this consecutive run automatically, Algorithm 2 is used:

Algorithm 2 Successive quasiconvex optimization

given $\mathrm{S} = \{\mathrm{i} \,|\, \mathrm{i} = \mathrm{fl}, \mathrm{fr}, \mathrm{rl}, \mathrm{rr}\}$
repeat
1. solve Algorithm 1 for $\{(F_{\mathrm{xi}}, F_{\mathrm{yi}}) \,|\, i \in \mathrm{S}\}$
2. calculate k_{i} in (2.10) for $\mathrm{i} \in \mathrm{S}$
3. $\mathrm{S} = \{\mathrm{i} \,|\, k_{\mathrm{i}} < k_0\}$

until $\mathrm{S} = \emptyset$

3.3 Torque vectoring for the rear axle

Because the constraints of the feasibility problem (3.12) do not specify the relationship between the longitudinal tire forces on the left and right wheels of the rear axle F_{txrl} and F_{txrr}, these forces can have different signs and/or magnitudes. If a vehicle drives and brakes the left and right wheels independently, the vehicle can achieve any set of longitudinal tire force commands.

X1, however, can brake the rear wheels independently but cannot drive them in

the same manner. The rear axle of X1 is driven by one electric motor through an open differential [8], which splits the torque from the motor almost equally into the left and right wheels. Assuming the static relationship between the driving torque at one wheel and the corresponding positive longitudinal tire force, the X1's driving capability on the rear axle can achieve only the same magnitude of positive longitudinal tire force on the both wheels.

To overcome this limitation and generate longitudinal tire forces that have different signs and/or magnitudes, X1 can regulate the driving torque from the motor at one wheel by applying one-sided braking simultaneously and therefore vary driving torque to each side of the rear wheels.

The driving motor commands a torque that can generate a positive longitudinal tire force at one wheel in larger magnitude. The excessive driving torque from the motor at the opposing wheel is counterbalanced by the brake action so that the net torque reaches the desired value to generate a longitudinal tire force at the opposing wheel. According to this operation, the torque command for the driving motor τ_{motor} and the brake pressure commands for the left and right rear wheels P_{rl} and P_{rr} are as follows:

$$
\begin{aligned}
F_{\text{txr,max}} &= \max(F_{\text{txrl}}, F_{\text{txrr}}) \\
\tau_{\text{motor}} &= \begin{cases} 2r_{\text{diff}} R_{\text{w}} F_{\text{tx}}, & F_{\text{txr,max}} > 0 \\ 0, & F_{\text{txr,max}} \leq 0 \end{cases} \\
P_{\text{rl}} &= \begin{cases} 0, & F_{\text{txr,max}} > 0 \text{ and } F_{\text{txrl}} > F_{\text{txrr}} \\ \frac{R_{\text{w}}(F_{\text{txrl}} - F_{\text{txrr}})}{r_{\text{brake}}}, & F_{\text{txr,max}} > 0 \text{ and } F_{\text{txrl}} \leq F_{\text{txrr}} \\ \frac{R_{\text{w}} F_{\text{txrl}}}{r_{\text{brake}}}, & F_{\text{txr,max}} \leq 0 \end{cases} \\
P_{\text{rr}} &= \begin{cases} \frac{R_{\text{w}}(F_{\text{txrr}} - F_{\text{txrl}})}{r_{\text{brake}}}, & F_{\text{txr,max}} > 0 \text{ and } F_{\text{txrl}} > F_{\text{txrr}} \\ 0, & F_{\text{txr,max}} > 0 \text{ and } F_{\text{txrl}} \leq F_{\text{txrr}} \\ \frac{R_{\text{w}} F_{\text{txrr}}}{r_{\text{brake}}}, & F_{\text{txr,max}} \leq 0 \end{cases}
\end{aligned}
\tag{3.13}
$$

where R_{w} is the wheel effective radius, r_{diff} is the gear ratio of the open differential,

and r_{brake} is the mapping from brake pressure to brake torque.

The principal of this operation is one way to realize a technology called torque vectoring [36]. Several automotive suppliers and manufacturers have developed their own systems to realize torque vectoring technology [40, 50, 17].

3.4 Experiments

The effectiveness of new constraints taking into account feasible tire force regions was experimentally validated using the X1 research vehicle. This was done by operating X1 using the controller with the optimal tire force allocation module that adopts the new constraints. While constructing this controller, the other modules of the controller for trajectory tracking and actuator command calculation remained intact, and only the optimal tire force allocation module was replaced. The feasibility problem (3.12) was used for the optimal tire force allocation because its constraints match the actuation layout of X1: four-wheel independent steering/braking and rear-wheel driving.

The task chosen for the validation was to track a given trajectory while X1 remained close to the limits of handling, as it was in Chapter 2. At some parts of the trajectory, especially while cornering, this task demands large lateral general axle forces, and these demands require large tire slip angles in the opposite sign. According to the angles of the tires' velocity vectors at a certain moment and the relationship in (2.23), some tires may have to be steered to large angles to achieve the corresponding tire slip angles. Then, as explained in Section 3.1.1, the difference between the general axle forces and the transformed tire forces also becomes apparent. If the optimization algorithm does not handle the limited actuation properly, some portions of the transformed tire forces may not be realized by the given actuation layout. Therefore, this task can show the effectiveness of the new constraints to incorporate feasible tire force regions into the optimal tire force allocation. X1 was tested on a paved paddock at Thunderhill Raceway Park, Willows, California. During the entire maneuver, the controller drove X1 autonomously.

Two optimization algorithms were compared that account differently for X1's

lack of front driving capability in their constraints of the convex feasibility problem: one uses simple inequality constraints on front longitudinal general axle forces, as explained in Section 3.1.1, and the other uses inequality constraints approximated by ellipses to describe feasible tire force regions, as in Section 3.2.2. For the rest of this chapter, the former is identified as the force allocation algorithm with simple constraints, and the latter as the force allocation algorithm with ellipse constraints.

3.4.1 Trajectory description

The structure of the trajectory for the test is identical to the structure of the trajectory in Chapter 2. However, to clearly investigate the effects of the simple and ellipse constraints on the optimal tire force allocation and the vehicle motion, the length of a constant radius curve was extended because the controller would likely command large steering angles in the constant radius curve.

Figure 3.7 shows the geometric path, the acceleration profile, and the speed profile of the desired trajectory that has a single turn. As it was in Chapter 2, the acceleration profile was designed so that X1 stays at 90 % of the vehicle's maximum acceleration.

3.4.2 Tire force allocation by interpolation

Solving the optimization in Section 3.2.2 in real time during the test was replaced by interpolation using a map that was calculated off-line, as it was in Chapter 2. Instead, the number of inputs for the interpolation map increases to five. In addition to the existing three inputs of total force and moment demands ($F_{\mathrm{x,total}}$, $F_{\mathrm{y,total}}$, and $M_{\mathrm{z,total}}$), the angles of the front tires' velocity vectors $\alpha_{\mathrm{sl,fl}}$ and $\alpha_{\mathrm{sl,fr}}$ are also necessary to specify all constraints in the feasibility problem (3.12).

Using the fact that the difference between $\alpha_{\mathrm{sl,fl}}$ and $\alpha_{\mathrm{sl,fr}}$ is small when the longitudinal velocity of the vehicle is large, it is possible to assume a single angle for both front tires' velocity vectors by taking the average of both. Therefore, the number of inputs for the interpolation map can be reduced by four instead of five. Reducing one dimension of the map lowers the size of the map significantly.

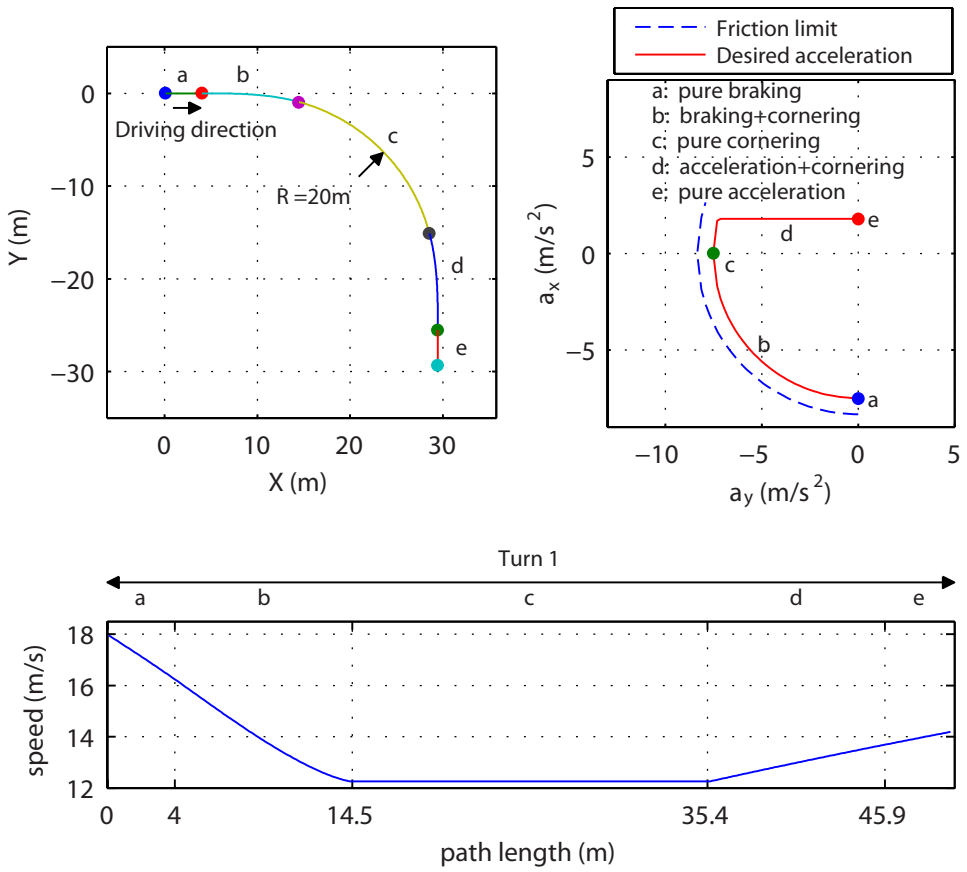

Figure 3.7: Test trajectory with a single turn structured from straight lines (a and e), transition curves (b and d), and a constant radius curve (c)

3.4.3 Results

The two different controllers operated X1 while it was tracking the same trajectory: one controller adopted the force allocation algorithm with simple constraints, and the other controller adopted the force allocation algorithm with ellipse constraints. Figure 3.8 shows the two sets of longitudinal and lateral tire force commands for the front tires from these two controllers: the tire forces in Figure 3.8a were acquired from the former controller, while the tire forces in Figure 3.8b were acquired from the latter controller.

While X1 was driven for experiments, the controllers calculated general axle force demands at the tires and then steering angle commands. From these values, tire force commands can be calculated by (2.24). In Figure 3.8a, the longitudinal tire forces for the front tires F_{txfl} and F_{txfr} become positive at the following regions: from the end of the transient entry curve (the path segment b), through the entire constant radius curve (the path segment c), and to the beginning of the transient exit curve (the path segment d), where the traveled distance is about from 11.3 m to 41.4 m for the front left tire and from 13.0 m to 41.0 m for the front right tire. When F_{txfl} and F_{txfr} reach a steady state in the constant radius curve, their values are about 550 N and 180 N, respectively.

At the regions above, the controller demanded large negative lateral general axle forces at the tires to make a right turn at high acceleration. To achieve large positive tire slip angles that match the large negative lateral force demands, the steering angle commands for the front tires had to be also large as shown in Figure 3.9. Therefore, the difference between the general axle forces and the transformed tire forces became apparent. The existence of positive longitudinal tire forces indicates that the simple inequality constraints on longitudinal general axle forces were not effective in preventing positive longitudinal tire forces at a large steering angle.

On the contrary, in Figure 3.8b, the controller did not command positive longitudinal tire forces for the front tires at any segment of the trajectory. This demonstrates the effectiveness of the force allocation algorithm with ellipse constraints.

Figure 3.10 depicts the tracking errors along the path. Both controllers demonstrated its capability to follow all three tracking objectives by exhibiting only small

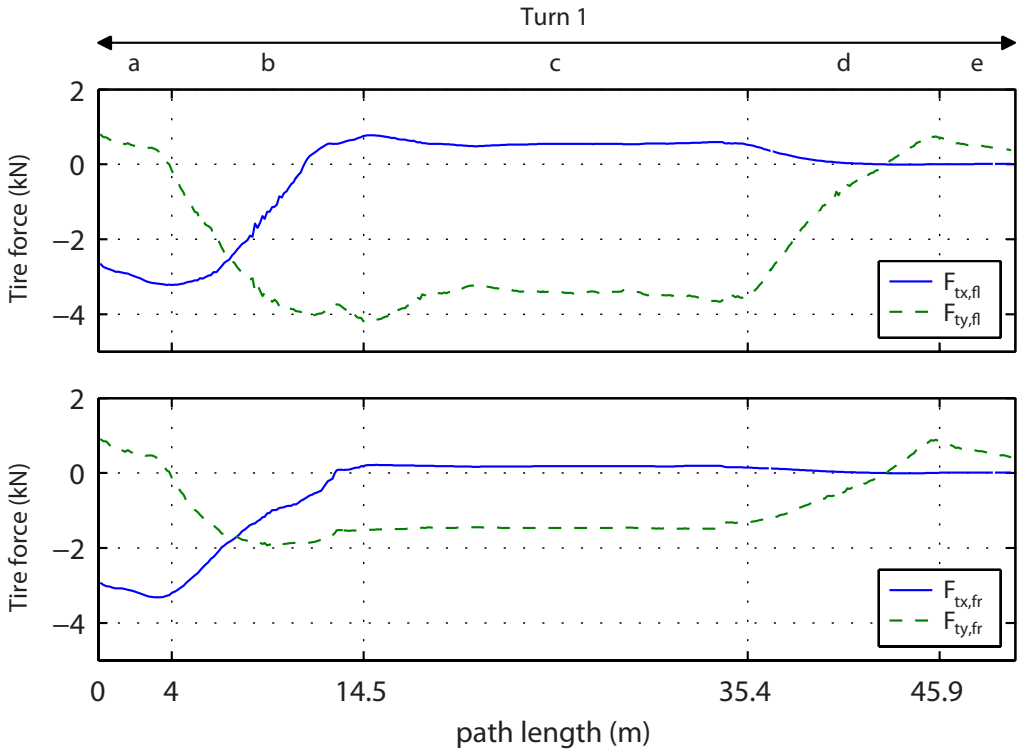

(a)

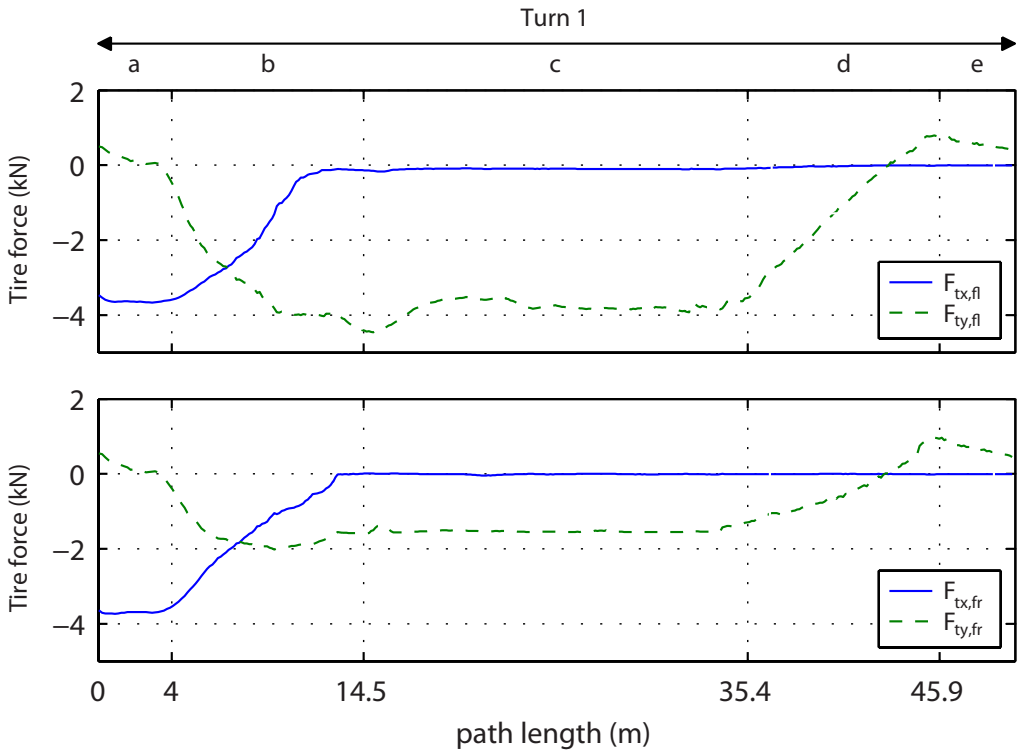

(b)

Figure 3.8: Tire force commands for the front left (up) and front right (down) tires. (a) From the force allocation with simple constraints. (b) From the force allocation with ellipse constraints.

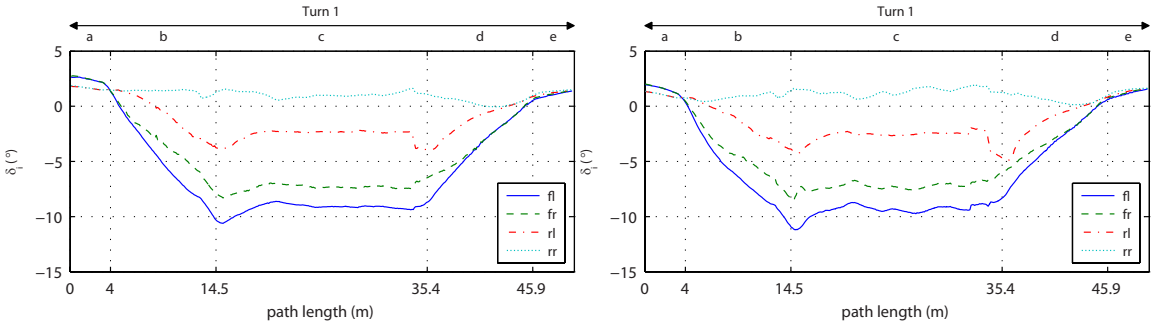

(a) (b)

Figure 3.9: Steering angle commands for the four tires. (a) From the force allocation with simple constraints. (b) From the force allocation with ellipse constraints.

errors. In the path segment c (the constant radius curve), the speed and heading errors were kept within 0.42 m/s and 0.72 °, respectively, for the controller that adopted the force allocation algorithm with simple constraints and within 0.22 m/s and 0.33 °, respectively, for the controller that adopted the force allocation algorithm with ellipse constraints. The lateral errors did not exceed 19 cm for both controllers.

Even though both experimental results showed a similarly small level of tracking errors, the patterns and magnitudes of the errors along the path differed for the two controllers. The controller that adopted the force allocation algorithm with simple constraints exhibited specific patterns in the tracking errors, as shown in Figure 3.10a and also in Figure 2.8: the heading error became positive, and the speed error became negative approximately in the regions where the longitudinal tire force commands were positive. The pattern for the speed error is more clearly observable in Figure 2.8.

On the other hand, for the controller that adopted the force allocation algorithm with ellipse constraints, the heading errors were oscillating around zero without a specific pattern, and the magnitudes of both speed and heading errors were smaller for the most of the traveled distance as shown in Figure 3.10.

This result can be explained by the effects of positive longitudinal tire force commands at the front tires. The commands for driving and braking actuators are calculated from the longitudinal part of tire force commands. Because the front tires do not have a driving actuator, any positive longitudinal tire force commands for the

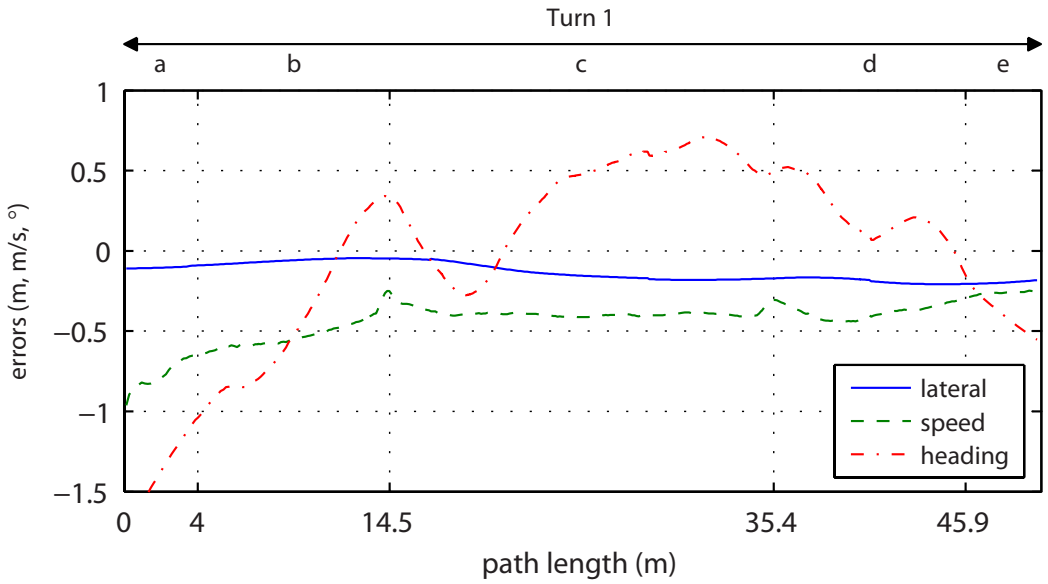

(a)

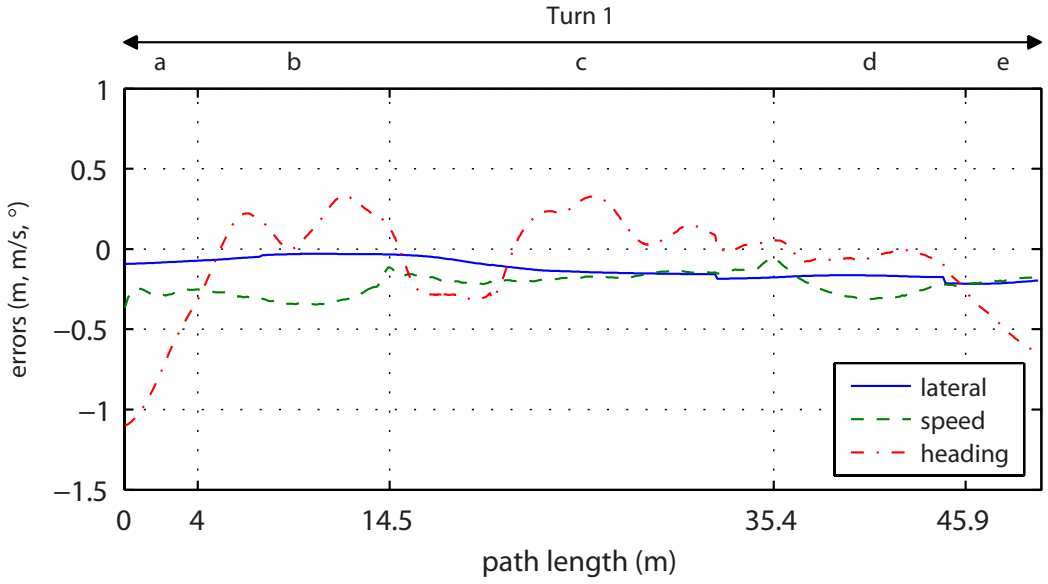

(b)

Figure 3.10: Lateral, speed, and heading tracking errors. (a) From the force allocation with simple constraints. (b) From the force allocation with ellipse constraints.

front tires cannot be realized and actually was ignored in the experiments.

In Figure 3.8a, the controller demanded positive longitudinal tire forces on both front tires while the magnitude of longitudinal tire force at the left tire was larger than that at the right tire. Therefore, the contributions of these longitudinal tire forces toward the total force and moment demands were a positive longitudinal force and a negative yaw moment at and around the center of gravity, which would make X1 accelerating and turning right.

However, because these commands of positive longitudinal tire force could not actually be realized due to the lack of a driving actuator, their contributions toward the total force and moment demands were also not realized. In other words, some positive portion of the total longitudinal force demand and some negative portion of the total yaw moment demand were not realized. One can expect that these ignored portions of total demands makes X1 accelerate less and turn less to the right than desired, which leads to negative speed errors and positive heading errors. In Figure 3.10a, the speed and heading errors from the controller that adopted the force allocation algorithm with simple constraints are shown to become negative and positive, respectively, at the onset of the constant radius curve, as expected.

The controller that adopted the force allocation algorithm with ellipse constraints commands only the tire forces that can be realized by the given actuation layout. Therefore, tracking errors from this controller are not expected to show the specific patterns explained above. While there is no guarantee that the wheels can realize the desired tire force commands exactly due to several factors such as actuator delays, the tracking errors in Figure 3.10b exhibits the expected behavior compared to the tracking errors in Figure 3.10a: the heading errors were oscillating around zero without a specific pattern, and the magnitudes of both speed and heading errors were smaller for the most of the traveled distance. It must be noted that the controller achieved these improvements in tracking errors not by modifying the trajectory tracking control law or adjusting controller parameters but by only taking into account feasible tire force regions in the optimal tire force allocation.

Chapter 4

Force Allocation on an Uneven Road

Until now, the optimal tire force allocation has been discussed in a situation of driving on a level road. However, actual roads are not perfectly flat and usually have some non-zero degrees of bank and grade. Racing tracks sometimes introduce significantly greater bank angles and steeper grades than public roads to challenge professional drivers. Some parts of public roads also present relatively high levels of bank and grade: for example, at highway entrance or exit ramps or on roads in hilly terrains. Driving on these uneven roads affects the vehicle's motion, mainly because the relative direction of the gravitational force with respect to the vehicle-fixed coordinate frame is changing and the normal force distribution becomes different from what it is on a flat road.

Even under these conditions, operating a vehicle with the primary objective of the optimal tire force allocation–keeping the same and minimal friction usage over the four wheels–has the same advantage of preventing some tires' earlier saturation. To achieve this objective, this chapter presents a revised optimal tire force allocation algorithm that can handle the effects of non-zero bank angles and grades of the road on the vehicle's motion. Section 4.1 analyzes what changes happen to the vehicle dynamics and the normal force distribution when the vehicle is driving on a three-dimensional road. Based on this analysis, a new formulation for optimal tire force

allocation that takes into account topographical effects is presented. Section 4.2 explains how to create and use a map to allocate tire forces by interpolation when a vehicle is driving on an uneven road. Under reasonable assumptions, a single map can handle an arbitrary combination of non-zero bank angles and grades. Section 4.3 presents experimental results demonstrating the performance of the optimal tire force allocation with topographical considerations when X1 is operated on a slanted surface.

4.1 Effects of driving on a non-level road

The assumption of a perfectly flat road results in no pitch/roll motions and no height change of the vehicle-fixed coordinate frame relative to an inertial earth-fixed coordinate frame. Therefore, the vehicle's motion in Chapters 2 and 3 can be described by the equations of planar motion: only three equations for longitudinal, lateral, and yaw motions. In these equations, the only external forces except the drag force are longitudinal and lateral general axle forces of the four wheels as shown in (2.1) and (2.2). The gravitational force acts only along the z axis; therefore, it does not appear in the equations of motion.

If the vehicle is driving on a non-level road while all its tires are in contact with the road, however, the vehicle-fixed coordinate frame experiences three-dimensional motion. To describe this motion exactly, six equations of motion for full translational and rotational movements of the vehicle are required along the x, y, and z axes of the vehicle-fixed coordinate frame. Subosits and Gerdes [63] present these full equations of motion for a bicycle model when the vehicle tracks a given path on a three-dimensional road.

When the vehicle experiences three-dimensional motion, the gravitational force is split into three components along the x, y, and z axes of the vehicle-fixed coordinate frame. Accordingly, these components affect the vehicle's motion and appear in the equations of motion not only along the z axis but along the x and y axes as well.

This section shows how to calculate each component of the gravitational force and derive the equations of motion and the expressions of the normal tire forces for a four-wheel vehicle model on a non-level road. A new formulation for optimal tire

force allocation using these equations is also presented.

4.1.1 Components of the gravitational acceleration

Because the components of the gravitational force are given by multiplying the components of the gravitational acceleration by the vehicle mass, this section calculates the components of the gravitational acceleration. The direction of the gravitational acceleration lies along the z axis of an inertial earth-fixed coordinate frame. If this direction does not align with the z axis of the vehicle-fixed coordinate frame due to the vehicle's three-dimensional motion, the expression of the gravitational acceleration in the vehicle-fixed coordinate frame has non-zero components along the x and y axes. To calculate the component of the gravitational acceleration along each axis of the vehicle-fixed coordinate frame, the orientation of one frame with respect to the other needs to be defined first.

In this section, the orientation of one frame with respect to the other is described by a rotation matrix which, in turn, is defined by a set of Euler angles for a body-fixed zyx rotation. These Euler angles are denoted by (ψ, θ, ϕ), where ψ is the yaw angle for the rotation about the z axis, θ is the pitch angle for the rotation about the y axis, and ϕ is the roll angle for the rotation about the x axis.

The rotation matrix from the inertial earth-fixed coordinate frame N to the vehicle-fixed coordinate frame V, ${}^{\mathrm{V}}R^{\mathrm{N}}$, is given by the multiplication of the three matrices as follows:

$$ {}^{\mathrm{V}}R^{\mathrm{N}} = {}^{\mathrm{V}}R^{\mathrm{B}} * {}^{\mathrm{B}}R^{\mathrm{A}} * {}^{\mathrm{A}}R^{\mathrm{N}} \tag{4.1} $$

where the three matrices on the right side of the equation describe the body-fixed rotations along $\hat{x}$, $\hat{y}$, and $\hat{z}$, respectively. Then these matrices are:

$$ {}^{\mathrm{V}}R^{\mathrm{B}} = \begin{bmatrix} 1 & 0 & 0 \\ 0 & \cos\phi & \sin\phi \\ 0 & -\sin\phi & \cos\phi \end{bmatrix} \tag{4.2} $$

$$ {}^{\mathrm{B}}R^{\mathrm{A}} = \begin{bmatrix} \cos\theta & 0 & -\sin\theta \\ 0 & 1 & 0 \\ \sin\theta & 0 & \cos\theta \end{bmatrix} \tag{4.3} $$

$$ {}^{\mathrm{A}}R^{\mathrm{N}} = \begin{bmatrix} \cos\psi & \sin\psi & 0 \\ -\sin\psi & \cos\psi & 0 \\ 0 & 0 & 1 \end{bmatrix} \tag{4.4} $$

where A and B are intermediate coordinate frames after each successive rotation.

Once the rotation matrix is determined, the scalar components of the gravitational acceleration g_{x}, g_{y}, and g_{z} are calculated by multiplying the rotation matrix by the gravitational acceleration in the inertial earth-fixed coordinate frame as follows:

$$ \begin{bmatrix} g_{\mathrm{x}} \\ g_{\mathrm{y}} \\ g_{\mathrm{z}} \end{bmatrix} = {}^{\mathrm{V}}R^{\mathrm{N}} \begin{bmatrix} 0 \\ 0 \\ -g \end{bmatrix} \tag{4.5} $$

where g is the magnitude of the gravitational acceleration.

4.1.2 Equations of longitudinal, lateral, and yaw motion

In this section, all the tires of the vehicle are assumed to stay in contact with the road, and all the contact points between the tires and the road are assumed to be on the plane that is parallel to the xy-plane of the vehicle-fixed coordinate frame. These assumptions are reasonable because the scale of the topographical changes in public roads is generally much larger than the wheelbase and the track width of the vehicle.

Longitudinal and lateral general axle forces at each contact point are also assumed to be on the xy-plane of the vehicle-fixed coordinate frame. Under this assumption, only longitudinal and lateral (not normal) general axle forces are involved in the new equations of longitudinal, lateral, and yaw motions in three-dimensional space as they are in the equations in two-dimensional space (2.1) and (2.2). Unlike these equations, however, the new equations for longitudinal and lateral motions have extra terms to reflect non-zero components of the gravitational force along the x and y axes of

the vehicle-fixed coordinate frame. The equations of longitudinal, lateral, and yaw motions in three-dimensional space are as follows:

$$ {}^{N}\mathbf{F}^{V} \cdot \mathbf{v}_{\mathrm{x}} = F_{\mathrm{xfl}} + F_{\mathrm{xfr}} + F_{\mathrm{xrl}} + F_{\mathrm{xrr}} + mg_{\mathrm{x}} \tag{4.6} $$

$$ {}^{N}\mathbf{F}^{V} \cdot \mathbf{v}_{\mathrm{y}} = F_{\mathrm{yfl}} + F_{\mathrm{yfr}} + F_{\mathrm{yrl}} + F_{\mathrm{yrr}} + mg_{\mathrm{y}} \tag{4.7} $$

$$ \begin{aligned} {}^{N}\mathbf{M}^{V/V_{cg}} \cdot \mathbf{v}_{\mathrm{z}} = {} & a(F_{\mathrm{yfl}} + F_{\mathrm{yfr}}) - b(F_{\mathrm{yrl}} + F_{\mathrm{yrr}}) \\ & + d/2(F_{\mathrm{xfr}} + F_{\mathrm{xrr}}) - d/2(F_{\mathrm{xfl}} + F_{\mathrm{xrl}}) \end{aligned} \tag{4.8} $$

where ${}^{N}\mathbf{F}^{V}$ and ${}^{N}\mathbf{M}^{V/V_{cg}}$ are the effective force and moment about the center of gravity of the vehicle, respectively, and $\mathbf{v}_{\mathrm{i}}$ ($\mathrm{i} \in [\mathrm{x}, \mathrm{y}, \mathrm{z}]$) is a unit vector along each axis of the vehicle-fixed coordinate frame.

4.1.3 Equations of vertical, pitch and roll motion

Because all the tires of the vehicle are assumed to stay in contact with the road, the pitch and roll motions of the vehicle-fixed coordinate frame are mainly induced by the changes of bank and grade of the road. If the changes of bank and grade along a given path are gradual, which is true for public roads, angular velocities and accelerations for the pitch and roll motions can be assumed to be zero. In other words, the pitch and roll motions can be assumed to be in quasi-static equilibrium.

Under this assumption, the angular velocity of the vehicle becomes simply $r\mathbf{v}_{\mathrm{z}}$, and the moment of effective force of the vehicle about the center of gravity is as follows:

$$ {}^{N}\mathbf{M}^{V/V_{cg}} = I_{\mathrm{z}}\dot{r}\mathbf{v}_{\mathrm{z}}. \tag{4.9} $$

Also, the effective force of the vehicle can be expressed as follows:

$$ {}^{N}\mathbf{F}^{V} = ma_{\mathrm{x}}\mathbf{v}_{\mathrm{x}} + ma_{\mathrm{y}}\mathbf{v}_{\mathrm{y}} + ma_{\mathrm{z}}\mathbf{v}_{\mathrm{z}} \tag{4.10} $$

where a_{i} ($\mathrm{i} \in [\mathrm{x}, \mathrm{y}, \mathrm{z}]$) is the vehicle's acceleration at the center of gravity along each axis of the vehicle-fixed coordinate frame. Substituting the effective force and moment terms in (4.6), (4.7), and (4.8) for the expressions in (4.9) and (4.10) makes the left

sides of the equations ma_{x}, ma_{y}, and $I_{\mathrm{z}}\dot{r}$, respectively

For the vertical and pitch motions, normal tire forces as well as longitudinal general axle forces are involved in the equations of motion. Therefore, solving these equations for the normal forces and applying the solution to a weight transfer model gives the expressions for normal tire forces on three-dimensional roads. The effect of weight transfer is modeled in the same way as it was in Section 2.3.2: the vehicle is assumed to behave like a rigid body along the longitudinal direction and to act according to the static roll model along the lateral direction.

The equations of vertical and pitch motions are as follows:

$$ {}^{N}\mathbf{F}^{V} \cdot \mathbf{v}_{\mathrm{z}} = F_{\mathrm{zfl}} + F_{\mathrm{zfr}} + F_{\mathrm{zrl}} + F_{\mathrm{zrr}} + mg_{\mathrm{z}} \tag{4.11} $$

$$ {}^{N}\mathbf{M}^{V/V_{cg}} \cdot \mathbf{v}_{\mathrm{y}} = a(F_{\mathrm{zfl}} + F_{\mathrm{zfr}}) - b(F_{\mathrm{zrl}} + F_{\mathrm{zrr}}) + h_{\mathrm{cg}}(F_{\mathrm{xfl}} + F_{\mathrm{xfr}} + F_{\mathrm{xrl}} + F_{\mathrm{xrr}}). \tag{4.12} $$

Applying (4.9) and (4.10) to the effective force and moment terms in (4.11) and (4.12) makes the left sides of the above equations ma_{z} and 0, respectively. By replacing two individual normal tire force variables on the same axle with one combined normal tire force variable on that axle, and replacing the sum of the longitudinal tire forces in (4.12) with the expression in (4.6), equations (4.11) and (4.12) can be solved for the normal tire forces of the front and rear axles F_{zf} and F_{zr} as follows:

$$ \begin{aligned} F_{\mathrm{zf}} &= m\left\{\frac{b(a_{\mathrm{z}} - g_{\mathrm{z}}) - h_{\mathrm{cg}}(a_{\mathrm{x}} - g_{\mathrm{x}})}{L}\right\} \\ F_{\mathrm{zr}} &= m\left\{\frac{a(a_{\mathrm{z}} - g_{\mathrm{z}}) + h_{\mathrm{cg}}(a_{\mathrm{x}} - g_{\mathrm{x}})}{L}\right\}. \end{aligned} \tag{4.13} $$

For the analysis of roll motion, the vehicle-body roll and the resulting lateral weight transfer are considered together through the static roll model. Under the assumption of quasi-static equilibrium, the static vehicle-body roll angle ϕ_{v} on a three-dimensional road is derived as follows:

$$ \phi_{\mathrm{v}} = \frac{m_{\mathrm{s}}h_{\mathrm{l}}(a_{\mathrm{y}} - g_{\mathrm{y}})}{k_{\phi} - m_{\mathrm{s}}h_{\mathrm{l}}(a_{\mathrm{z}} - g_{\mathrm{z}})}. \tag{4.14} $$

While (4.13) and (4.14) have a form similar to (2.12) and (2.13), the vehicle

and gravitational acceleration terms in (2.12) and (2.13) are adjusted to account for the changes in the components of the gravitational acceleration and the vertical acceleration of the vehicle.

Once the static roll angle is determined, the amount of the lateral weight transfer on each axle is derived as follows:

$$\begin{aligned} \Delta F_{\mathrm{zf}} &= \frac{1}{d}\{k_{\phi \mathrm{f}}\phi_{\mathrm{v}} + h_{\mathrm{f}}(F_{\mathrm{yfl}} + F_{\mathrm{yfr}})\} \\ \Delta F_{\mathrm{zr}} &= \frac{1}{d}\{k_{\phi \mathrm{r}}\phi_{\mathrm{v}} + h_{\mathrm{r}}(F_{\mathrm{yrl}} + F_{\mathrm{yrr}})\}. \end{aligned} \tag{4.15}$$

Finally, the normal force of each wheel is described with the derived terms in (4.13) and (4.15):

$$\begin{aligned} F_{\mathrm{zfl}} &= F_{\mathrm{zf}}/2 - \Delta F_{\mathrm{zf}} \\ F_{\mathrm{zfr}} &= F_{\mathrm{zf}}/2 + \Delta F_{\mathrm{zf}} \\ F_{\mathrm{zrl}} &= F_{\mathrm{zr}}/2 - \Delta F_{\mathrm{zr}} \\ F_{\mathrm{zrr}} &= F_{\mathrm{zr}}/2 + \Delta F_{\mathrm{zr}}. \end{aligned} \tag{4.16}$$

4.1.4 Optimization formulation with topographical considerations

Rearranging (4.6), (4.7), and (4.8) gives the sum of general axle forces and the yaw moment by these forces about the center of gravity as follows:

$$\begin{aligned} F_{\mathrm{x,total}} &= ma_{\mathrm{x}} - mg_{\mathrm{x}} \\ F_{\mathrm{y,total}} &= ma_{\mathrm{y}} - mg_{\mathrm{y}} \\ M_{\mathrm{z,total}} &= I_z\dot{r}. \end{aligned} \tag{4.17}$$

For trajectory tracking, a_{x}, a_{y}, and $\dot{r}$ can be regarded as the desired linear and angular accelerations of the vehicle that are necessary to track a desired trajectory at a certain instance. Then ma_{x}, ma_{y}, and $I_z\dot{r}$ become control forces and moment at and around the center of gravity for trajectory tracking. In Section 2.2, these control forces and moment are calculated by the feedforward-feedback control scheme using

the vehicle states and the trajectory information.

For planar motion, the control forces and moment equal the sum of the general axle forces and the yaw moment by these forces about the center of gravity $F_{\mathrm{x,total}}$, $F_{\mathrm{y,total}}$, and $M_{\mathrm{z,total}}$. However, (4.17) indicates that the x and y components of the gravitational force have to be compensated for by forces on the tires to achieve the desired linear accelerations for the vehicle's three-dimensional motion.

Once the values of the vertical acceleration of the vehicle a_{z} and g_{i} ($\mathrm{i} \in [\mathrm{x}, \mathrm{y}, \mathrm{z}]$) are measured or calculated, (4.17) and (4.16) give $F_{\mathrm{x,total}}$, $F_{\mathrm{y,total}}$, $M_{\mathrm{z,total}}$ and the normal tire forces F_{zi} ($\mathrm{i} \in [\mathrm{fl}, \mathrm{fr}, \mathrm{rl}, \mathrm{rr}]$) for the vehicle driving on a three-dimensional road. Then the convex feasibility problem (3.12) and Algorithm 2 can be used without any changes for the optimal tire force allocation on a road with changing geometry.

4.2 Interpolation for optimal allocation on a three-dimensional road

In the experiments discussed in Chapters 2 and 3, solving an optimization problem in real time is replaced by an interpolation using a single map that is calculated off-line. What makes this replacement possible is that the dimension and size of the map are kept in reasonable ranges for the actual implementation of the control system because the number of inputs for the interpolation is relatively small and the values of those inputs are constrained in certain ranges.

To apply the same interpolation technique for optimal tire force allocation on a three-dimensional road, it is necessary to calculate a new map by solving the optimization formulation in Section 4.1.4. As explained in that section, the vertical acceleration of the vehicle-fixed coordinate frame a_{z} and the three components of the gravitational acceleration g_{i} ($\mathrm{i} \in [\mathrm{x}, \mathrm{y}, \mathrm{z}]$) are necessary to determine the terms in the constraints of the optimization: the total longitudinal/lateral forces $F_{\mathrm{x,total}}/F_{\mathrm{y,total}}$, the total yaw moment $M_{\mathrm{z,total}}$, and the normal tire forces F_{zi} ($\mathrm{i} \in [\mathrm{fl}, \mathrm{fr}, \mathrm{rl}, \mathrm{rr}]$).

A straightforward way to handle this situation is to create a map that adopts a_{z} and g_{i} ($\mathrm{i} \in [\mathrm{x}, \mathrm{y}, \mathrm{z}]$) as the additional four inputs for the interpolation. Including the

existing four inputs for the interpolation map explained in Section 3.4.2, the total number of inputs for the interpolation becomes eight. This increase of inputs results in a large map that will consume significant memory of the control system. To make the interpolation technique practical, it is necessary to keep the size of the map used for the interpolation as small as possible. Through the analysis of this section, the total number of inputs is reduced to five.

The rest of this section presents how to replace solving an optimization problem with an interpolation for the situation in which the vehicle is driving on a three-dimensional road. Owing to the characteristics of the equations in Section 4.1, it is possible to consider the topographical effects on the vehicle dynamics with a reduced number of variables. Moreover, the optimized solutions for different inputs are proportional to each other if those inputs are proportional to each other. Using these characteristics, the optimal tire force allocation on a three-dimensional road can be handled by the interpolation using a map with a reduced number of inputs.

4.2.1 Vertical scaling factor

On a flat road, the sum of the normal tire forces equals the multiplication of the vehicle's mass by the gravitational acceleration. On a three-dimensional road, however, the sum of the normal tire forces equals the multiplication of the vehicle's mass by the sum of the component of the gravitational acceleration and the vehicle's acceleration along the z axis of the vehicle-fixed coordinate frame as in (4.11).

The vertical scaling factor w is defined as the ratio of the sum of the normal tire forces on a three-dimensional road to the sum of the normal tire forces on a flat road as follows:

$$\begin{aligned} w &= \frac{m(a_{\mathrm{z}} - g_{\mathrm{z}})}{mg} \\ &= \frac{a_{\mathrm{z}} - g_{\mathrm{z}}}{g}. \end{aligned} \tag{4.18}$$

4.2.2 Similarity between optimized solutions

To simplify the analysis for now, the convex feasibility problem without limited-actuation constraints (2.17) is considered here. In the optimization with this feasibility problem, only total force and moment demands are regarded as three inputs as explained in Section 2.5.2, and a body-roll angle ϕ_{v} is assumed to be a dependent variable that is determined from a given total lateral force as in (2.13). However, it is possible to treat the body-roll angle as an independent variable and an additional input. Then the set of inputs for the convex feasibility problem becomes $(F_{\mathrm{x,total}}, F_{\mathrm{y,total}}, M_{\mathrm{z,total}}, \phi_{\mathrm{v}})$.

When $w = 1$, a specific set of total demands and a body-roll angle is denoted with the superscript 0 as follows:

$$(F^0_{\mathrm{x,total}}, F^0_{\mathrm{y,total}}, M^0_{\mathrm{z,total}}, \phi^0_{\mathrm{v}}),$$

and the corresponding set of optimized general axle forces at the tires is also denoted with the superscript 0 as follows:

$$\{(F^0_{\mathrm{xi}}, F^0_{\mathrm{yi}}) | \, \mathrm{i} = \mathrm{fl}, \mathrm{fr}, \mathrm{lr}, \mathrm{rr}\}.$$

In contrast, when $w \neq 1$, the value of w is denoted as w^*, and a set of the inputs is denoted with the same superscript as follows:

$$(F^*_{\mathrm{x,total}}, F^*_{\mathrm{y,total}}, M^*_{\mathrm{z,total}}, \phi^*_{\mathrm{v}}).$$

The hypothesis is that the optimized solution for $(F^*_{\mathrm{x,total}}, F^*_{\mathrm{y,total}}, M^*_{\mathrm{z,total}}, \phi^*_{\mathrm{v}})$ is $\{w^*(F^0_{\mathrm{xi}}, F^0_{\mathrm{yi}}) | \, \mathrm{i} = \mathrm{fl}, \mathrm{fr}, \mathrm{lr}, \mathrm{rr}\}$ if there is the following proportional relationship between the two sets of inputs:

$$(F^*_{\mathrm{x,total}}, F^*_{\mathrm{y,total}}, M^*_{\mathrm{z,total}}, \phi^*_{\mathrm{v}}) = w^*(F^0_{\mathrm{x,total}}, F^0_{\mathrm{y,total}}, M^0_{\mathrm{z,total}}, \phi^0_{\mathrm{v}}). \tag{4.19}$$

If this hypothesis is true, it is not necessary to solve the optimization problem for the

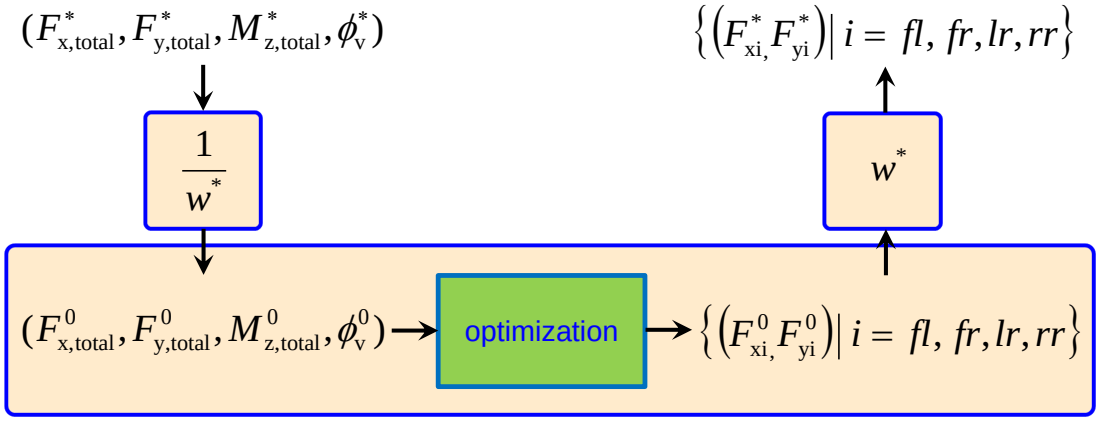

Figure 4.1: The proportional relationship (i.e. similarity) between the optimal solutions to the proportional inputs

case when $w \neq 1$. Once the optimized solutions for the case when $w = 1$ are calculated, an optimized solution for a set of inputs when $w \neq 1$ can be simply determined by finding the optimized solution when $w = 1$ for the set of inputs multiplied by $\frac{1}{w^*}$ and multiplying that solution by w^*. Figure 4.1 graphically shows this process.

The proof of this hypothesis can be done by showing that the optimized solutions for the two sets of inputs with the relationship in (4.19) actually have the proportional relationship. The feasibility problem for the set of inputs $(F^*_{x,total}, F^*_{y,total}, M^*_{z,total}, \phi^*_v)$ is as follows:

$$\begin{aligned} \text{find} \quad & \{(F_{xi}, F_{yi}) \,|\, i = fl, fr, lr, rr\} \\ \text{subject to} \quad & \sqrt{{F_{xi}}^2 + {F_{yi}}^2} \leq k_0 \mu F^*_{zi} \\ & \sum\nolimits_i F_{xi} = F^*_{x,total} \\ & \sum\nolimits_i F_{yi} = F^*_{y,total} \\ & \sum\nolimits_i M_{zi} = M^*_{z,total} \end{aligned} \tag{4.20}$$

where F^*_{zi} is the normal tire force for the given body-roll angle ϕ^*_v.

F^*_{zi} can be expanded using the equations for longitudinal and lateral weight transfer in (4.13) and (4.15). For example, the normal tire force for the front left tire is as

follows:

$$\begin{aligned} F^*_{\text{zfl}} &= F^*_{\text{zf}} - \Delta F^*_{\text{zf}} \\ &= m\left\{\frac{b(a_{\text{z}}-g_{\text{z}})-h_{\text{cg}}(a_{\text{x}}-g_{\text{x}})}{L}\right\} - \frac{1}{d}\{k_{\phi\text{f}}\phi^*_{\text{v}} + h_{\text{f}}(F_{\text{yfl}}+F_{\text{yfr}})\} \\ &= -\frac{mb}{L}(g_{\text{z}}-a_{\text{z}}) - \frac{h_{\text{cg}}}{L}F^*_{\text{x,total}} - \frac{k_{\phi\text{f}}}{d}\phi^*_{\text{v}} - \frac{h_{\text{f}}}{d}(F_{\text{yfl}}+F_{\text{yfr}}) \end{aligned} \tag{4.21}$$

Here, new optimization variables $(F'_{\text{xi}}, F'_{\text{yi}})$ are defined as follows:

$$(F'_{\text{xi}}, F'_{\text{yi}}) = \frac{1}{w^*}(F_{\text{xi}}, F_{\text{yi}}). \tag{4.22}$$

By replacing the variables in (4.21) with the relationships between variables in (4.18), (4.19) and (4.22), the normal tire force for the front left tire is re-written as follows:

$$\begin{aligned} F^*_{\text{zfl}} &= -\frac{mb}{L}w^*g - \frac{h_{\text{cg}}}{L}w^*F^0_{\text{x,total}} - \frac{k_{\phi\text{f}}}{d}w^*\phi^0_{\text{v}} - \frac{h_{\text{f}}}{d}w^*(F'_{\text{yfl}}+F'_{\text{yfr}}) \\ &= w^*\left\{-\frac{mb}{L}g - \frac{h_{\text{cg}}}{L}F^0_{\text{x,total}} - \frac{k_{\phi\text{f}}}{d}\phi^0_{\text{v}} - \frac{h_{\text{f}}}{d}(F'_{\text{yfl}}+F'_{\text{yfr}})\right\} \\ &= w^*F^0_{\text{zfl}}. \end{aligned} \tag{4.23}$$

where F^0_{zfl} is the normal tire force of the front left tire for the given body-roll angle ϕ^0_{v}. The same relationship can be found for the normal tire forces of the other three tires. This result means that the normal tire forces for the two sets of inputs also have the same proportional relationship.

After replacing the optimization and input variables using (4.19), (4.22) and

(4.23), the feasibility problem can be re-written as follows:

$$\begin{aligned} \text{find} \quad & \{(F'_{\text{xi}}, F'_{\text{yi}}) \,|\, \text{i} = \text{fl}, \text{fr}, \text{lr}, \text{rr}\} \\ \text{subject to} \quad & \sqrt{{F'_{\text{xi}}}^2 + {F'_{\text{yi}}}^2} \leq k_0 \mu F^0_{\text{zi}} \\ & \sum\nolimits_i F'_{\text{xi}} = F^0_{\text{x,total}} \\ & \sum\nolimits_i F'_{\text{yi}} = F^0_{\text{y,total}} \\ & \sum\nolimits_i M'_{\text{zi}} = M^0_{\text{z,total}}. \end{aligned} \tag{4.24}$$

The inputs for (4.24) are now $(F^0_{\text{x,total}}, F^0_{\text{y,total}}, M^0_{\text{z,total}}, \phi^0_{\text{v}})$. Therefore, the corresponding solution for the optimization variables $(F'_{\text{xi}}, F'_{\text{yi}})$ is $\{(F^0_{\text{xi}}, F^0_{\text{yi}})|\text{i} = \text{fl}, \text{fr}, \text{lr}, \text{rr}\}$. From the relationship in (4.22), the optimized solution for the optimization variables $(F_{\text{xi}}, F_{\text{yi}})$ becomes $\{w^*(F^0_{\text{xi}}, F^0_{\text{yi}})|\text{i} = \text{fl}, \text{fr}, \text{lr}, \text{rr}\}$. In other words, when the set of inputs for optimization is $(F^*_{\text{x,total}}, F^*_{\text{y,total}}, M^*_{\text{z,total}}, \phi^*_{\text{v}})$, the optimized solution is $\{w^*(F^0_{\text{xi}}, F^0_{\text{yi}})|\text{i} = \text{fl}, \text{fr}, \text{lr}, \text{rr}\}$. This completes the proof of the hypothesis.

4.2.3 Interpolation using similarity

In the previous section, the proportional relationship (i.e. similarity) between the solutions to the proportional inputs is proved only for the convex feasibility problem without limited-actuation constraints. Therefore, it is necessary to check whether the same similarity holds true for the convex feasibility problem with limited-actuation constraints (3.12).

For a tire with the normal force F_{z} and the tire's velocity vector along the x axis of the vehicle-fixed coordinate frame, the ellipse approximation for the upper boundary of the feasible tire force region is given by (3.4). The check for the similarity can be done by comparing the following two upper boundaries of the feasible tire force regions for a tire with the normal force F^*_{z}, which equals w^*F_{z}: the first upper boundary is formed by the scaled general axle force $(w^*F_{\text{x}}, w^*F_{\text{y}})$, which is denoted by $(F'_{\text{x}}, F'_{\text{y}})$; the second is formed by the ellipse approximation for F^*_{z} and the corresponding limit slip angle α^*_{sl}. If these two expressions are equal or nearly equal to each other, $(w^*F_{\text{x}}, w^*F_{\text{y}})$ becomes the feasible solution for the tire without the steering actuator.

The equation for the first boundary is derived by replacing $(F_{\mathrm{x}}, F_{\mathrm{y}})$ in (3.4) with $(\frac{F'_{\mathrm{x}}}{w^*}, \frac{F'_{\mathrm{y}}}{w^*})$ and rearranging (3.4) gives

$$F'_{\mathrm{x}} = -\mu F^*_{\mathrm{z}} \sin(\alpha_{\mathrm{sl}}) + \mu F^*_{\mathrm{z}} \sin(\alpha_{\mathrm{sl}}) \sqrt{1 - \left(\frac{F'_{\mathrm{y}}}{\mu F^*_{\mathrm{z}} \cos(\alpha_{\mathrm{sl}})} \right)^2}. \tag{4.25}$$

The equation for the second boundary is derived by replacing F_{z} and α_{sl} in (3.4) with F^*_{z} and α^*_{sl} as follows:

$$F_{\mathrm{x}} = -\mu F^*_{\mathrm{z}} \sin(\alpha^*_{\mathrm{sl}}) + \mu F^*_{\mathrm{z}} \sin(\alpha^*_{\mathrm{sl}}) \sqrt{1 - \left(\frac{F_{\mathrm{y}}}{\mu F^*_{\mathrm{z}} \cos(\alpha^*_{\mathrm{sl}})} \right)^2}. \tag{4.26}$$

The only difference between (4.25) and (4.26) is the limit slip angle. To give a sense of how different the boundaries given by (4.25) and (4.26) are, the coordinates of the right vertices on the semi-major axes of these two boundaries are compared. These coordinates are $(-\mu F^*_{\mathrm{z}} \sin(\alpha_{\mathrm{sl}}), \mu F^*_{\mathrm{z}} \cos(\alpha_{\mathrm{sl}}))$ and $(-\mu F^*_{\mathrm{z}} \sin(\alpha^*_{\mathrm{sl}}), \mu F^*_{\mathrm{z}} \cos(\alpha^*_{\mathrm{sl}}))$, respectively. Using the example values for $F_{\mathrm{z}} = 5000N$ and $w^* = 0.75$ and (3.11), the values of the coordinates become about (-577N, 3135N) and (-634N, 3127N), respectively. Compared to the length of the semi-major axis, the difference between these two points is very small even when $w^* = 0.75$, i.e. when the total normal force is reduced by 25%. As a result, the proportional relationship between the solutions to the proportional inputs can be assumed to be valid also for the convex feasibility problem with limited-actuation constraints.

The diagram in Figure 4.2 shows how the optimal set of general axle forces are calculated by the interpolation using the proof for the similarity in Section 4.2.2 and this section. The measurements of Euler angles (ψ, θ, ϕ) and the vehicle's vertical acceleration a_{z} give the components of the gravitational acceleration $(g_{\mathrm{x}}, g_{\mathrm{y}}, g_{\mathrm{z}})$ and the vertical scaling factor w using (4.5) and (4.18). The total force demands from the trajectory tracking module $F_{\mathrm{x,total}}$ and $F_{\mathrm{y,total}}$ are adjusted to compensate for the components of the gravitational force. The body roll angle ϕ_{V} can be calculated by (4.14) or estimated real-time [53].

Once all the inputs for the interpolation are determined, these inputs except the

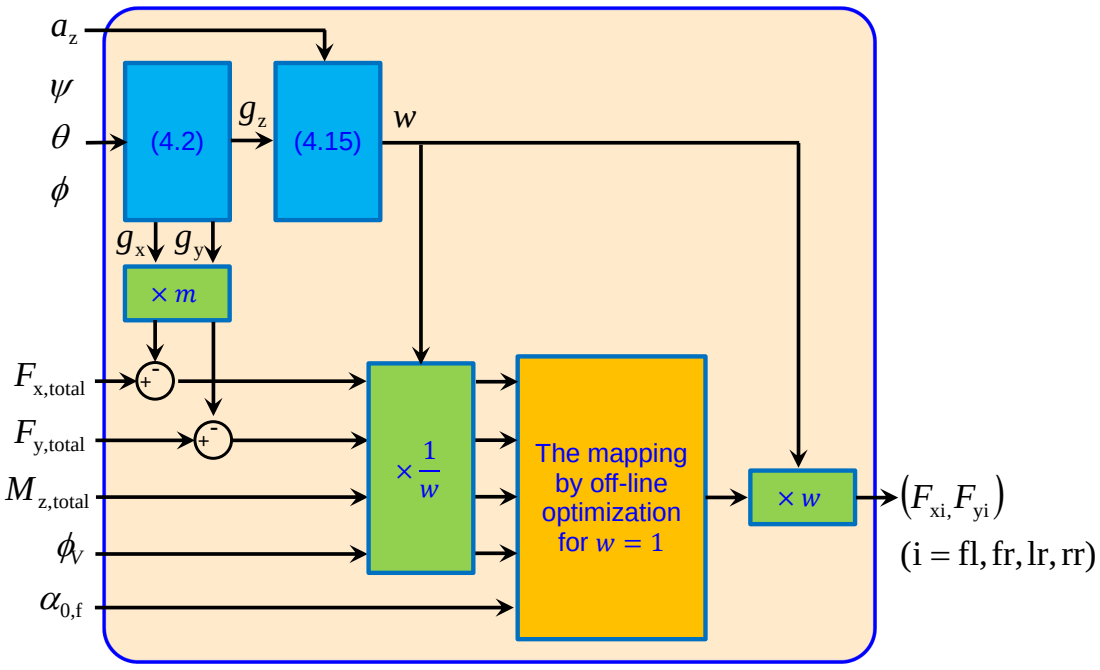

Figure 4.2: Interpolation for the optimal tire force allocation on a three-dimensional road by using the reference map when $w = 1$.

angle of the front tires' velocity vector $\alpha_{0,\mathrm{f}}$ are scaled by $1/w$. Then, the solution from the interpolation using the reference map is scaled by w, and this scaled solution becomes the optimal set of general axle forces on a three-dimensional road.

4.3 Experiments

Experiments using the X1 research vehicle were conducted to validate the performance of optimal tire force allocation in which topographic effects are taken into account. In this chapter, the task chosen for the validation was to track a given trajectory near the limits of handling on an uneven surface. The trajectory was constructed in the same manner as it was in the experiments discussed in Chapter 2 and Chapter 3: the path profile gives only desired x and y positions of a vehicle. However, unlike in the experiments discussed in the previous chapters–which were conducted on relatively flat surfaces–the new test site exhibits topographic characteristics that cannot be ignored. If X1 drives on this site, this road topography affects X1's motion as explained in Section 4.1.

While trying to track the same trajectory designed for a flat road, one of the two controllers that operated X1 during the experiment adopted a new module for the optimal tire force allocation which accounts for the topographic effects, whereas the other controller continued to use the optimal tire force allocation module developed in Chapter 3. Comparing trajectory tracking performances from the two controllers demonstrated the effectiveness of the optimal tire force allocation accounting for the topographic effects.

4.3.1 Test site and trajectory descriptions

The test site was a skidpad at Thunderhill Raceway Park. This skidpad is a paved rectangular open area that has an overall constant slope of about 2.5 degrees.

The geometric path was constructed to have the same three segments of a racing line as the trajectories in Chapter 2 and Chapter 3 had. However, the path used in this chapter had a longer constant radius curve segment, as shown in Figure 4.3. The

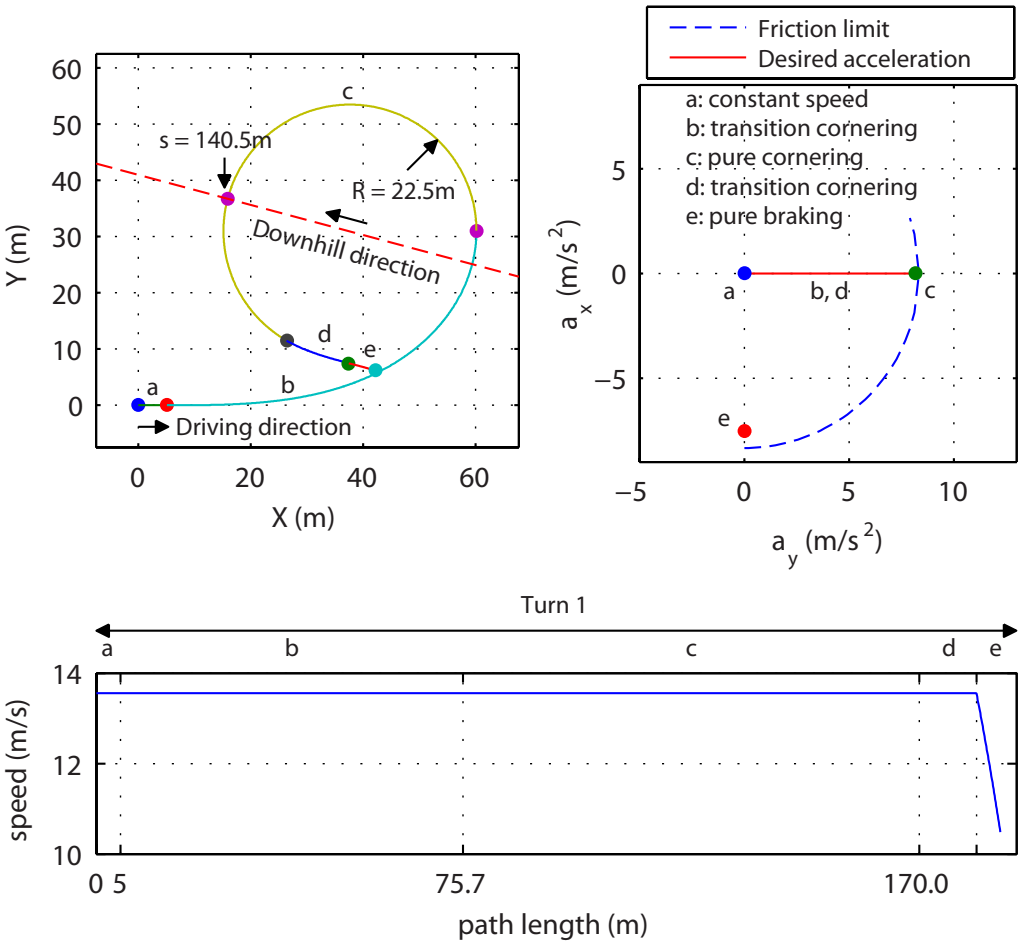

Figure 4.3: Test trajectory with a single turn structured from straight lines (a and e), transition curves (b and d), and a constant radius curve (c)

desired speed was set to be constant (13.6 m/s) for the entire path except for the segment e, and this resulted in the desired lateral acceleration of X1 in the constant radius (22.5 m) curve at 0.98 μg, which made X1 operate almost at the limits of handling. In other words, X1 drove a long constant radius and speed curve.

The purpose of this trajectory design is to make X1 experience various combinations of bank angles and grades as it tries to maintain the constant radius turn at high acceleration. Even though the skidpad has a constant slope, the bank angle and grade vary according to X1's relative heading with respect to the downhill direction.

When the path length is 140.5 m, the tangent of the constant radius curve becomes perpendicular to the downhill direction. This point is the lowest point of the curve, and the bank angle reaches its maximum at this point and equals the slope angle if X1's heading tracks the tangent of the path.

4.3.2 Handling total demands exceeding vehicle's friction capability

In the feasibility problem equations (2.17) and (3.12) for the optimal tire force allocation, the equality equations between total demands and general axle forces (2.1) are set as hard constraints. In other words, the optimal tire force allocation assumes that total demands can always be achieved by a set of general axle forces within the tires' friction limits and feasible force regions.

When a vehicle operates almost at the limits of handling–as in the experiment discussed in this chapter whose trajectory is designed to operate X1 at the acceleration of 0.98 μg–driving without any tracking errors already brings the tires close to saturation. Because the total demand calculation by the trajectory tracking control module relies on only tracking errors and their changes and does not consider the vehicle's friction capability, even small perturbations of trajectory tracking can make calculated total demands exceed the range that can be achieved by general axle forces within the tires' friction limits and feasible force regions. In this case, the current algorithm for the optimal tire force allocation cannot find a solution that satisfies the equality constraints (2.1).

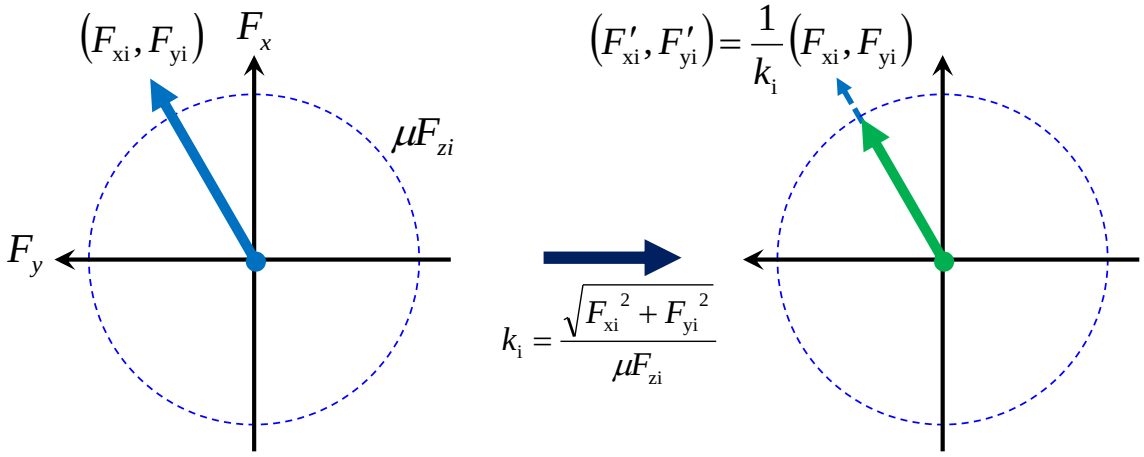

Figure 4.4: Scaling down general axle forces that exceed tire's estimated friction capability

Even in this situation, however, the optimal tire force allocation has to calculate a set of general axle forces to operate the vehicle. One method to handle this problem consists of two parts: First, the optimal tire force allocation assumes that the tires have more friction than originally estimated and finds a set of general axle forces that satisfies the equality constraints (2.1). This is done by relaxing the tires' friction limit constraints, i.e., allowing the initial k_{high} in Algorithm 1 to be larger than 1. Second, the general axle forces that exceed the original estimations of the tires' friction limits are scaled down by being multiplied by their friction usage, as shown in Figure 4.4. This scaling is necessary because the inputs of the actuator command calculation module, which are the general axle forces from the optimal tire force allocation, have to be within the tires' friction limits.

While it is inevitable that some portions of total demands exceeding the vehicle's friction capability cannot be achieved physically, the method proposed above can find a solution to the excessive total demands with only minimal changes of the existing controller structure and the optimization algorithm.

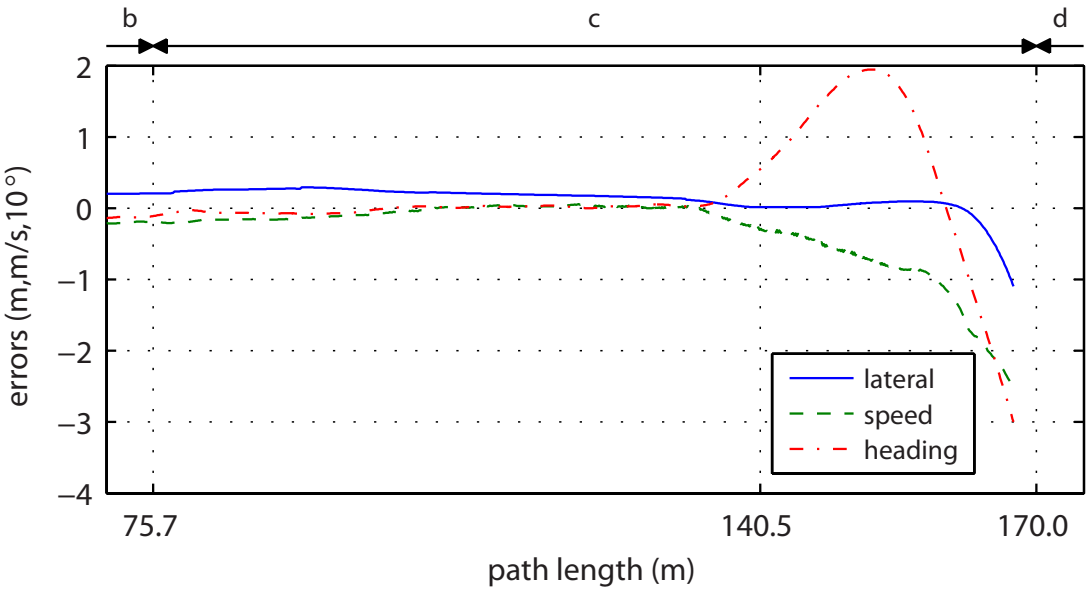

Figure 4.5: Lateral, speed, and heading tracking errors from the force allocation without topographical considerations

4.3.3 Results

For this section, the controller that adopted the force allocation algorithm without topographical considerations is denoted Controller A, and the controller that adopted the force allocation algorithm with topographical considerations is denoted Controller B. Figure 4.5 shows tracking errors along the path segment c (the constant radius curve) from Controller A. As X1 approached the lowest point of the curve, where the path length is 140.5 m, the heading error started to sharply increase. Once the value of the heading error reached 19.5 degrees, it began to decrease. The speed error also started to grow from the point where the heading error began to increase. The lateral error remained near zero for most of the traveled distance but eventually became large, too.

In terms of the vehicle motion, X1 rotated to the inside and then to the outside of the curve. It finally deviated from the desired path to the outside by more than 1 m. At this point, the autonomous driving mode was turned off according to the

driver's judgment. As a result, X1 with Controller A was not able to complete a turn. Because the objective of minimizing all three tracking errors became invalid as the heading error started to sharply increase, the analysis below for the experimental results from this controller investigates only the region up to the point at which the heading error reached its positive maximum and explains why this deviation from the desired trajectory developed initially.

Tracking errors from both controllers along the path segment c are plotted in Figure 4.6. Both controllers exhibited a similar level of small tracking errors until the point at which the heading error of Controller A began to increase. After this point, however, the two controllers showed very different behaviors. While the heading error of Controller A kept on increasing up to 19.5 degrees as explained above (Figure 4.6a), the heading error of Controller B increased only slightly to 1.5 degrees (Figure 4.6b). As Figure 4.6b also shows, the lateral and speed errors were kept almost constant at about 30 cm and 0.2 m/s, respectively, once they reached a steady state. Their maximum magnitudes did not exceed 35 cm and 0.24 m/s, respectively. In other words, while X1 with Controller A rotated to the inside of the curve, X1 with Controller B could successfully track the desired trajectory.

In Figure 4.6a, the lateral and speed errors of Controller A became smaller as X1 approached the lowest point of the curve. This is because the longitudinal and lateral components of the gravitational force directly affected the longitudinal and lateral motions of X1. Because X1 headed downhill and turned left while approaching the lowest point of the curve, the positive longitudinal and negative lateral components of the gravitational force made X1 accelerate forward and to the outside of the curve. These additional accelerations temporarily helped to reduce both tracking errors.

However, the changes of the tracking errors induced by the gravitational force also affected the total demand calculation. For Controller A, the feedforward portion of the total lateral force demand for a constant radius turn is constant. Positive lateral error in a left turn indicates that X1 is inside of the desired curve, and the trajectory tracking control module commands negative lateral force for the proportional feedback portion of the lateral error tracking control. If the positive lateral error of Controller A gets close to zero, the proportional feedback lateral force also gets close to zero.

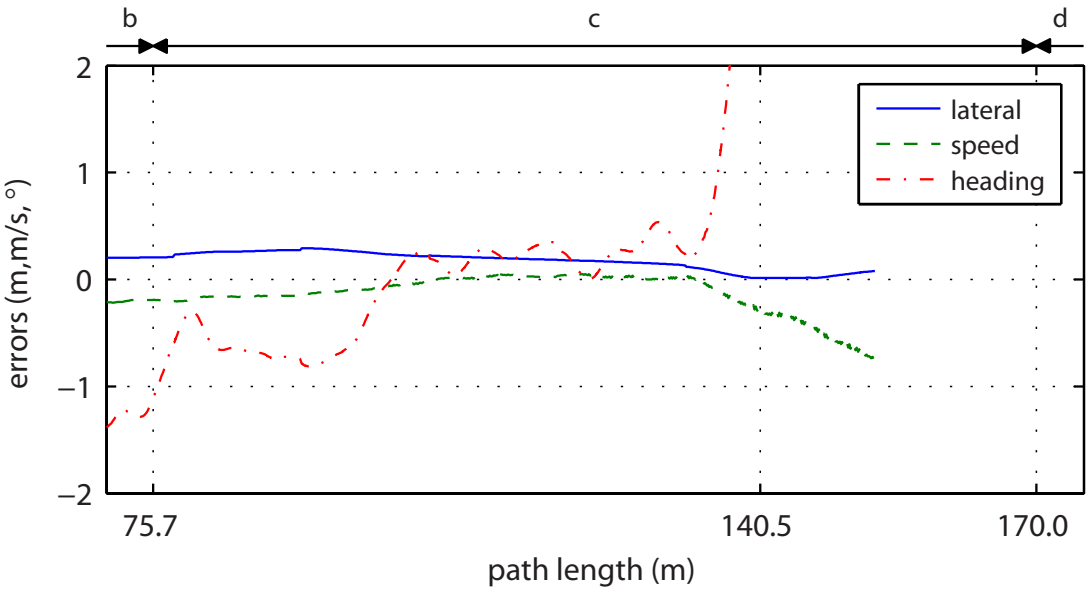

(a)

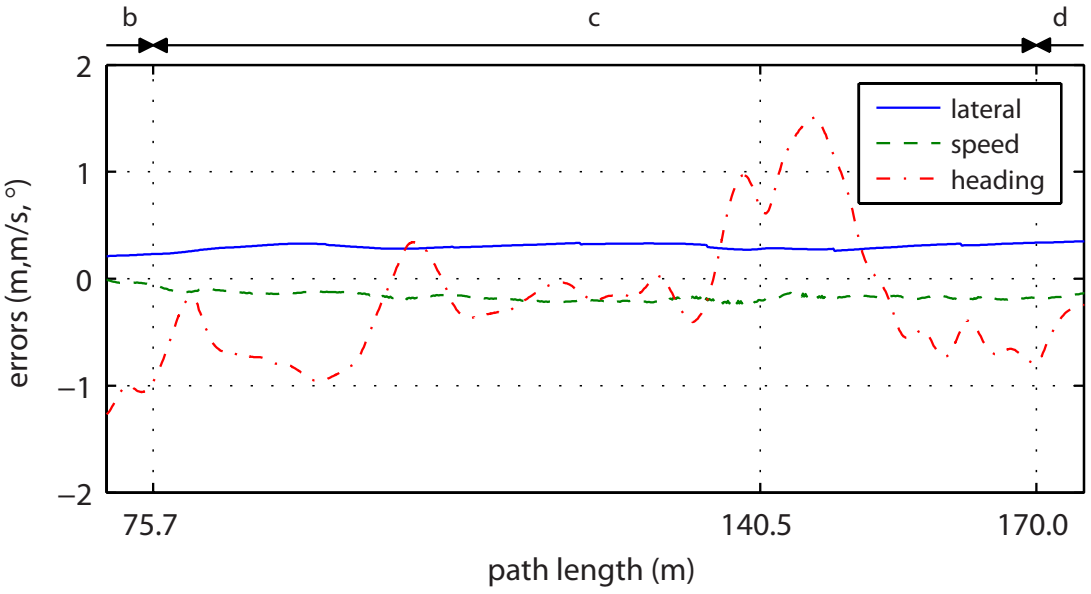

(b)

Figure 4.6: Lateral, speed, and heading tracking errors. (a) From the force allocation without topographical considerations. (b) From the force allocation with topographical considerations.

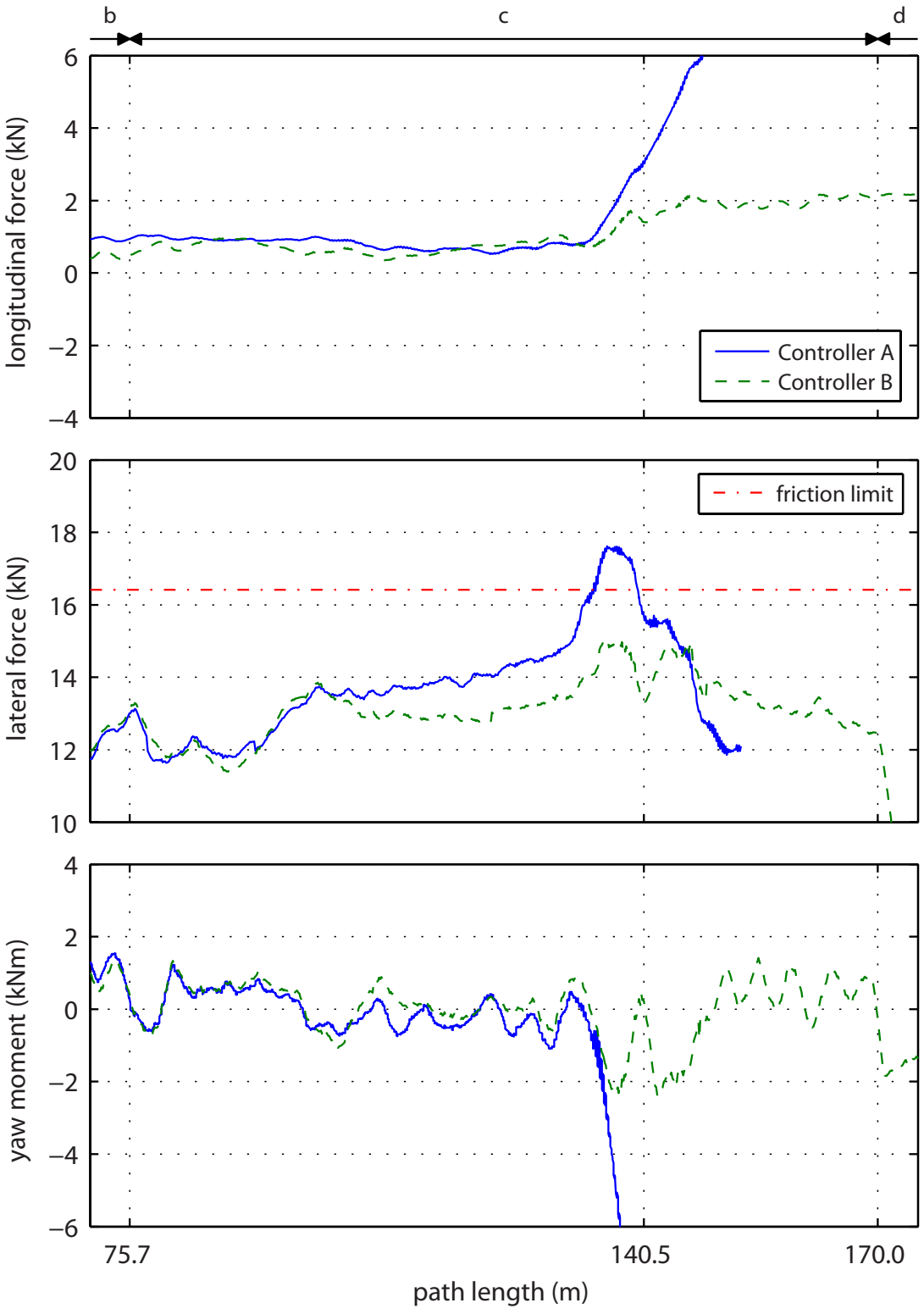

Figure 4.7: Total force and moment demands from the two different force allocations, one without and one with topographical considerations.

At the same time, the trajectory tracking control module tries to resist the negative derivative of the lateral error, or the tendency for X1 to slide outside of the turn by commanding positive lateral force for the derivative feedback portion of the lateral error tracking control. As these feedback portions are added to the positive constant feedforward lateral force for a left turn, the total lateral force demand is expected to keep increasing if the positive lateral error decreases.

Figure 4.7 shows total force and yaw moment demands from both controllers. The total lateral force demand of Controller A actually kept increasing as X1 approached the lowest point of the turn and as the positive lateral error decreased. Eventually, the total lateral force demand exceeded X1's available total friction.

The total lateral force demand for Controller B also increased as X1 approached the lowest point. However, the total lateral force demand of Controller B was always lower than that of Controller A and X1's friction capability. This is because the lateral error of Controller B stayed almost always at a constant positive value, and the feedback portions of the total lateral demand remained constant accordingly. The slight increase was due to the gravitational force compensation, and this compensation prevented the components of the gravitational force from affecting the motion of X1 and made the lateral error stay constant.

Because X1 cannot generate tire forces more than its friction limit, the total demands that exceeded X1's friction limit saturated some tires. The excessive total demands of Controller A generated the tire force commands that exceed the rear tires' friction limits, and those tire force commands were scaled down as explained in Section 4.3.2. Accordingly, the friction usages of the rear wheels reached 1 at around the lowest point of the curve, as shown in Figure 4.8, which means that they fully consumed their estimated friction capability. As a result, the rear wheels could not achieve some longitudinal and lateral forces commanded. These missing tire forces resulted in a portion of the total yaw moment demand from the rear wheels not being realized, and made X1 lose the moment balance between the front and rear axles and start to rotate rapidly.

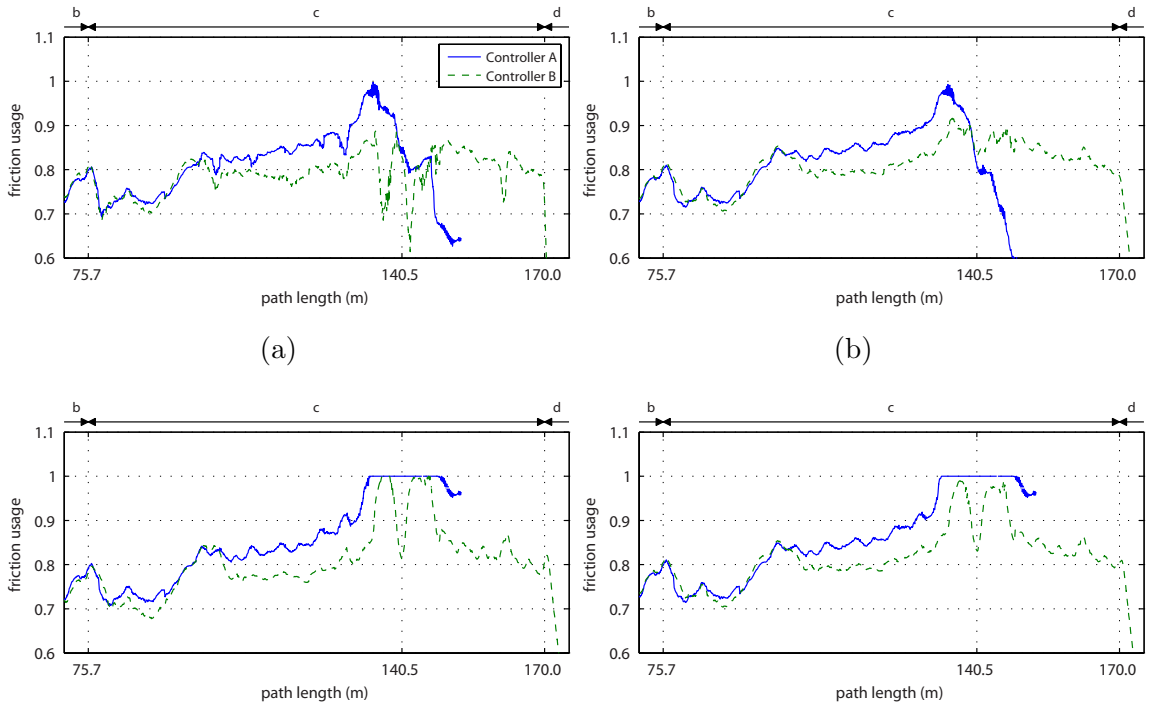

Figure 4.8: Friction usages from the two different force allocations, one without and one with topographical considerations. (a) Front left tire. (b) Front right tire. (c) Rear left tire. (d) Rear right tire.

Chapter 5

Conclusion

Ensuring safety is a primary concern for all automobiles. One measure to address this concern is to increase maneuverability of a vehicle near the limits of handling. As the vehicle gains more maneuverability, it can avoid adverse driving conditions or execute emergency maneuvers more safely. The developments of actuating technology enable many active safety systems to improve automobile maneuverability near the limits of handling by managing the traction of the four tires efficiently.

This dissertation presents an approach to optimally allocate tire forces for an over-actuated vehicle that has four-wheel independent steering, driving, and braking actuators. This abundant actuating capability gives the vehicle the authority to generate any sets of tire forces within the tires' friction limits. The optimal tire force allocation in this dissertation achieves two basic objectives: to keep the friction usages of the four tires equal and to minimize that common friction usage as much as possible. The mathematical algorithm for solving this optimization is formulated as a convex optimization problem (not a non-convex optimization problem with a complex cost function) by constructing the algorithm from the convex feasibility problem and the bisection method. This approach for the optimal tire force allocation prevents understeer and oversteer near the limits of handling by utilizing the tires' friction capabilities only to the extent necessary.

The basic framework of the optimal tire force allocation can handle real-world situations with slight modifications. Implementing all three actuators at all four

wheels is technically challenging and costly, and therefore even a research vehicle used in this dissertation has some limitations on actuation. This limited actuation affects the feasible tire force region that is achievable by a given actuation layout. A simple ellipse approximation can successfully describe the boundary of the feasible tire force region for a tire with steering and braking actuators only, even without having advance knowledge of steering angles, and can be easily adopted as an additional constraint for the convex optimization formulation of the optimal tire force allocation. The resulting solution from the optimization gives a set of tire forces that can be actually generated by the given actuation layout. Because real-world roads are not perfectly flat, the optimal tire force allocation also needs to handle topographical effects on the vehicle dynamics. This is done by accounting for the effects of the components of the gravitational force on total demand and normal force calculations. Experimental results for trajectory tracking on a slanted road demonstrates the performance of the optimal tire force allocation with topographical considerations.

The optimal tire force allocation can serve as a module for controllers with any vehicle control objectives. Because the main inputs of the optimal tire force allocation are general control force and moment at and around the center of gravity of the vehicle, a specific vehicle control objective can be achieved by applying the control force and moment that regulate vehicle motion in a desired way. In this dissertation, the vehicle control objective is autonomous trajectory tracking. The trajectory tracking module calculates the control force and moment for trajectory tracking that consist of feedfoward and feedback portions, which are derived from desired trajectory information and measured tracking errors, respectively. The controller that adopts this trajectory tracking module and the optimal tire force allocation module demonstrates its performance by tracking a trajectory successfully near the limits of handling.

5.1 Future work

The framework of the optimal tire force allocation presented in this dissertation can be extended in several interesting directions.

5.1.1 Solving the optimization problem in real time

In this dissertation, most of the control parameters are assumed to be known and constant, and the vehicle operating conditions are also assumed to remain constant. And these assumptions justify the interpolation using a map that replaces the on-line optimization. However, there exist situations in which these assumptions do not hold: the road surface condition can change significantly in a short period of time, and a sudden failure of one of the actuators can happen. To handle these situation, it would be greatly beneficial to solve the optimal tire force allocation in real time with adjusted control parameters and constraints that reflect new operating conditions.

5.1.2 Identifying each tire's friction limit in real time

The friction usage of each wheel, which is defined as the ratio of actual tire force usage to maximum available friction capability, is the most important variable for the optimal tire force allocation. Therefore, it is essential to calculate or estimate the value of this variable accurately. While the actual tire force usage is easily identified because it is the amount demanded by the controller, the maximum available friction capability is not easily identified.

In this dissertation, it is assumed that the friction coefficient is constant for all four wheels and the normal tire forces are calculated from the static roll model. And the maximum available friction capability was calculated by multiplying these values. These assumptions are valid for the experiments in this dissertation owing to the static nature of the given trajectory and the tests on a well-paved dry asphalt. However, these conditions will not be valid in many situations such as μ-split and wet surface conditions. Therefore, it is necessary to estimate these parameters in real time. Combined with the on-line optimization implementation, the accurate estimation of the maximum friction capability will greatly improve the performance of the optimal tire force allocation.

5.2 Outlook

Even in an era of autonomous driving, vehicles still have certain physical limits and will encounter situations in which the vehicles must be operated near the limits of handling. Increased capability for actuators, sensors, and computing power that can execute intelligent integrated chassis control algorithms will keep expanding the boundary of vehicle safety and maneuverability, thereby saving lives.

Bibliography

[1] M Abe and O Mokhiamar. An integration of vehicle motion controls for full drive-by-wire vehicle. *Proceedings of the Institution of Mechanical Engineers, Part K: Journal of Multi-body Dynamics*, 221(1):117–127, 2007.

[2] Acura. Precision All-Wheel Steer (P-AWS®) and Agile Handling Assist Systems, 2017.

[3] Johan Andreasson. *On Generic Road Vehicle Motion Modelling and Control*. PhD thesis, KTH, 2006.

[4] Audi AG. Technology: quattro, 2017.

[5] Nicolas Bouton, Roland Lenain, Benoit Thuilot, and Jean Christophe Fauroux. A rollover indicator based on the prediction of the load transfer in presence of sliding: Application to an all terrain vehicle. *Proceedings - IEEE International Conference on Robotics and Automation*, (April):1158–1163, 2007.

[6] Stefano Di Cairano, Hongtei Eric Tseng, Daniele Bernardini, and Alberto Bemporad. Vehicle Yaw Stability Control by Coordinated Active Front Steering and Differential Braking in the Tire Sideslip Angles Domain. *IEEE Transactions on Control Systems Technology*, 21(4):1236–1248, 2013.

[7] Christopher R Carlson and J Christian Gerdes. Optimal rollover prevention with steer by wire and differential braking. In *ASME 2003 International Mechanical Engineering Congress and Exposition*, pages 345–354, 2003.

[8] William H Crouse and Donald L Anglin. *Automotive mechanics*. Macmillan/Mc Graw-Hill Co, New York, USA, 10th edition, 1997.

[9] Yifan Dai, Yugong Luo, Wenbo Chu, and Keqiang Li. Optimum tyre force distribution for four-wheel-independent drive electric vehicle with active front steering. *International Journal of Vehicle Design*, 65(4):336–359, 2014.

[10] Leonardo De Novellis, Aldo Sorniotti, and Patrick Gruber. Wheel torque distribution criteria for electric vehicles with torque-vectoring differentials. *IEEE Transactions on Vehicular Technology*, 63(4):1593–1602, 2014.

[11] M.a Doumiati, A.a Victorino, A.a Charara, and D.b Lechner. Lateral load transfer and normal forces estimation for vehicle safety: Experimental test. *Vehicle System Dynamics*, 47(12):1511–1533, 2009.

[12] Howard Dugoff, P. S. Fancher, and Leonard Segel. An Analysis of Tire Traction Properties and Their Influence on Vehicle Dynamic Performance. *SAE Paper 700377*, pages 1219–1243, 1970.

[13] Paolo Falcone, Francesco Borrelli, Jahan Asgari, H. Eric Tseng, and Davor Hrovat. A model predictive control approach for combined braking and steering in autonomous vehicles. In *2007 Mediterranean Conference on Control & Automation*, pages 1–6. IEEE, jun 2007.

[14] Alborz Fallah. What is understeer and oversteer?, 2006.

[15] E. Fiala. Leteral forces on rolling pneumatic tires. *Zeitschrift VDI*, 96(29):973–979, 1954.

[16] Thomas D Gillespie. *Fundamentals of Vehicle Dynamics*. 1992.

[17] GKN Automotive. GKN reveals breakthrough hybrid electric torque vectoring system, 2016.

[18] Michael Grant and Stephen Boyd. Graph implementations for nonsmooth convex programs. In *Recent Advances in Learning and Control*, pages 95–110. Springer-Verlag Limited, 2008.

[19] Michael Grant and Stephen Boyd. CVX: Matlab Software for Disciplined Convex Programming, version 2.1, 2014.

[20] Jonathan Hall, Michael Bassett, Stephen Borman, Tom Lucas, and Andrew Whitehead. Through-the-Road Parallel Hybrid with In-Wheel Motors. Technical report, SAE Technical Paper, 2016.

[21] Ola Härkegård and S. Torkel Glad. Resolving actuator redundancy - Optimal control vs. control allocation. *Automatica*, 41(1):137–144, 2005.

[22] Rami Y Hindiyeh, Kirstin L R Talvala, and J Christian Gerdes. Lanekeeping at the Handling Limits. *Proceedings of the International Symposium on Advanced Vehicle Control 2008*, pages 1–8, 2008.

[23] Tor A Johansen and Thor I Fossen. Automatica Control allocation A survey. *Automatica*, 49(5):1087–1103, 2013.

[24] M. Jonasson, J. Andreasson, B. Jacobson, and a. S. Trigell. Global force potential of over-actuated vehicles. *Vehicle System Dynamics*, 48(9):983–998, sep 2010.

[25] Mats Jonasson, Johan Andreasson, Stefan Solyom, Bengt Jacobson, and Annika Stensson Trigell. Utilization of Actuators to Improve Vehicle Stability at the Limit: From Hydraulic Brakes Toward Electric Propulsion. *Journal of Dynamic Systems, Measurement, and Control*, 133(5):051003, 2011.

[26] Yung Hsiang Judy Hsu, Shad M. Laws, and J. Christian Gerdes. Estimation of tire slip angle and friction limits using steering torque. *IEEE Transactions on Control Systems Technology*, 18(4):896–907, 2010.

[27] Juyong Kang, Jinho Yoo, and Kyongsu Yi. Driving Control Algorithm for Maneuverability , Lateral Stability , and Rollover Prevention of 4WD Electric Vehicles With Independently Driven Front and Rear Wheels. *IEEE Transactions on vehicular technology*, 60(7):2987–3001, 2011.

[28] Alexander Katriniok, Jan P Maschuw, Frederic Christen, Lutz Eckstein, and Dirk Abel. Optimal Vehicle Dynamics Control for Combined Longitudinal and

Lateral Autonomous Vehicle Guidance. In *Control Conference (ECC), 2013 European*, pages 974–979, 2013.

[29] W Kim, K Yi, and J Lee. An optimal traction , braking , and steering coordination strategy for stability and manoeuvrability of a six-wheel drive and six-wheel steer vehicle. *Proceedings of the Institution of Mechanical Engineers, Part D: Journal of automobile engineering*, 226(1):3–22, 2012.

[30] Krisada Kritayakirana and J. Christian Gerdes. Autonomous vehicle control at the limits of handling. *International Journal of Vehicle Autonomous Systems*, 10(4):271–296, 2012.

[31] Horace Lai and DAVID MADÅS. *Test Vehicle for Regenerative Braking Emulation*. PhD thesis, CHALMERS UNIVERSITY OF TECHNOLOGY, 2011.

[32] Sittikorn Lapapong and Sean N Brennan. Terrain-Aware Rollover Prediction for Ground Vehicles Using the Zero-Moment Point Method. In *American Control Conference (ACC), 2010*, pages 1501–1507, 2010.

[33] Bin Li, Avesta Goodarzi, Amir Khajepour, Shih-ken Chen, and Baktiar Litkouhi. An optimal torque distribution control strategy for four-independent wheel drive electric vehicles. *Vehicle System Dynamics*, 53(8):1172–1189, 2015.

[34] E K Liebemann, K Meder, J Schuh, and G Nenninger. Safety and Performance Enhancement: The Bosch Electronic Stability Control (ESP). *SAE Convergence International Congress & Exposition On Transportation Electronics*, 2004.

[35] Yugong Luo, Kun Cao, and Keqiang Li. Coordinated Control of Longitudinal / Lateral / Vertical Tire Forces for Distributed Electric Vehicles. In *American Control Conference (ACC), 2014*, pages 3905–3910, 2014.

[36] Jim McCraw. Torque Vectoring: The Hyper-Smart, Fuel-Efficient Future of All-Wheel Drive, 2009.

[37] Mercedes-Benz. 4MATIC All-wheel Drive, 2017.

[38] Laurence Meredith. *Audi Quattro: The Complete Story*. The Crowood Press UK, 2001.

[39] Paul Mitiguy. *Advanced Dynamics & Motion Simulation*. 2009.

[40] Mitsubishi Motors. Automobile Technology: S-AWC, 2017.

[41] Ossama Mokhiamar and Masato Abe. Simultaneous Optimal Distribution of Lateral and Longitudinal Tire Forces for the Model Following Control. *Journal of Dynamic Systems, Measurement, and Control*, 126(4):753, 2004.

[42] Ossama Mokhiamar and Masato Abe. How the four wheels should share forces in an optimum cooperative chassis control. *Control engineering practice*, 14(3):295–304, 2006.

[43] Kanghyun Nam, Hiroshi Fujimoto, and Yoichi Hori. Lateral Stability Control of In-Wheel-Motor-Driven Electric Vehicles Based on Sideslip Angle Estimation Using Lateral Tire Force Sensors. *IEEE Transactions on Vehicular Technology*, 61(5):1972–1985, 2012.

[44] M Naraghi, A Roshanbin, and A Tavasoli. Vehicle stability enhancement an adaptive optimal approach to the distribution of tyre forces. *Proceedings of the Institution of Mechanical Engineers, Part D: Journal of Automobile Engineering*, 224(4):443–453, 2010.

[45] E. Ono, Y. Hattori, Y. Muragishi, and K. Koibuchi. Vehicle dynamics integrated control for four-wheel-distributed steering and four-wheel-distributed traction/braking systems. *Vehicle System Dynamics*, 44(2):139–151, feb 2006.

[46] Hans B. Pacejka. *Tire and Vehicle Dynamics*. Butterworth-Heinemann, 2012.

[47] Hans B. Pacejka and Egbert Bakker. The Magic Formula Tyre Model. *Vehicle System Dynamics*, 21:1–18, 1992.

[48] Tejas Parge and Siddharth Kshirsagar. Sensotronic Brake Control System Accelerating New Technology. *International Journal of Engineering Technology, Management and Applied Sciences*, 2(3):114–122, 2014.

[49] Heui Peng, Rahman Sabahi, Shih-Ken Chen, and Nikolai Moshchuk. Integrated Vehicle Control Based on Tire Force Reserve Optimization Concept. In *ASME 2011 International Mechanical Engineering Congress and Exposition*, pages 327–335, 2011.

[50] Porsche Cars. Porsche Torque Vectoring (PTV), 2017.

[51] Ali Roshanbin and Mahyar Naraghi. Vehicle Integrated Control-An Adaptive Optimal Approach to Distribution of Tire Forces. In *Networking, Sensing and Control, 2008. ICNSC 2008. IEEE International Conference on*, pages 885–890, 2008.

[52] Jeha Ryu, Ho-Soo Kim, and Jong-Hyup Kim. An emergency obstacle avoidance control strategy for automated highway vehicles. *Vehicle System Dynamics*, 38(5):319–339, 2002.

[53] Jihan Ryu and J Christian Gerdes. Estimation of Vehicle Roll and Road Bank Angle. In *American Control Conference, 2004. Proceedings of the 2004*, pages 2110–2115, 2004.

[54] Brad Schofield. *Vehicle Dynamics Control for Rollover Prevention*. PhD thesis, Lund University, 2006.

[55] Brad Schofield and Tore Hagglund. Optimal control allocation in vehicle dynamics control for rollover mitigation. In *2008 American Control Conference*, pages 3231–3236. Ieee, jun 2008.

[56] Marshall Schuon. About cars; honda is first on the block to flaunt 4-wheel steering, 1987.

[57] Robert Sivinski. Crash prevention effectiveness of light-vehicle electronic stability control: an update of the 2007 NHTSA Evaluation. Technical Report Report no. DOT HS-811-486, U.S. Department of Transportation, Washington, DC, 2011.

[58] Dirk E Smith and John M Starkey. Effects of model complexity on the performance of automated vehicle steering controllers: controller development and evaluation. *Vehicle System Dynamics*, 23(1):627–645, 1994.

[59] Pan Song, Masayoshi Tomizuka, and Changfu Zong. A novel integrated chassis controller for full drive- by-wire vehicles. *Vehicle System Dynamics*, 53(2):215–236, 2015.

[60] Marc Starnes. Estimating Lives Saved by Electronic Stability Control, 2008-2012. Technical Report Report No. DOT HS 812 042, National Highway Traffic Safety Administration, Washington, DC, 2014.

[61] Jason S Stine, Bridget C Hamblin, Sean N Brennan, and Eric T Donnell. Analyzing the influence of median cross-section design on highway safety using vehicle dynamics simulations. *Accident Analysis and Prevention*, 42(6):1769–1777, 2010.

[62] JB Straubel. Tesla All Wheel Drive (Dual Motor) Power and Torque Specifications, 2015.

[63] John Subosits and J. Christian Gerdes. Autonomous vehicle control for emergency maneuvers: The effect of topography. *Proceedings of the American Control Conference*, 2015-July:1405–1410, 2015.

[64] Yuta Suzuki, Yoshio Kano, and Masato Abe. A study on tyre force distribution controls for full drive-by-wire electric vehicle. *Vehicle System Dynamics*, 52(sup1):235–250, 2014.

[65] Ali Tavasoli, Mahyar Naraghi, and Heman Shakeri. Optimized coordination of brakes and active steering for a 4WS passenger car. *ISA Transactions*, 51(5):573–583, 2012.

[66] M. Thommyppillai, S. Evangelou, and R. S. Sharp. Car driving at the limit by adaptive linear optimal preview control. *Vehicle System Dynamics*, 47(12):1535–1550, 2009.

[67] HE Tseng, Behrouz Ashrafi, Dinu Madau, Todd Allen Brown, and Darrel Recker. The development of vehicle stability control at Ford. *IEEE/ASME Transactions on Mechatronics*, 4(3):223–234, 1999.

[68] Tejas Varunjikar, Pramod Vemulapalli, and Sean N Brennan. Multi-Body Vehicle Dynamics Simulation Based On Measured 3D Terrain Data. In *3rd International Conference on Road Safety and Simulation*, 2011.

[69] Jing-Shiam Wang. Effectiveness of stability control systems for truck tractors. Technical Report Report no. DOT HS-811-437, U.S. Department of Transportation, Washington, DC, 2011.

[70] Rongrong Wang, Chuan Hu, Zejiang Wang, Fengjun Yan, and Nan Chen. Integrated optimal dynamics control of 4WD4WS electric ground vehicle with tire-road frictional coefficient estimation. *Mechanical Systems and Signal Processing*, 60:727–741, 2015.

[71] Paul Weissler. Brembo brake-by-wire will be production-ready before 2020, 2016.